PONTIFICIA UNIVERSIDAD CATOLICA DE CHILE

ESCUELA DE INGENIERIA

STRUCTURAL CHARACTERIZATION OF LIQUID FOOD FOAMS STABILIZED BY PROTEINS

JUAN C. GERMAIN

Thesis submitted to the Office of Research and Graduate Studies in partial fulfillment of the requirements for the Degree of Doctor in Engineering Sciences

Advisor:

JOSÉ MIGUEL AGUILERA R

Santiago de Chile, January, 2013

PONTIFICIA UNIVERSIDAD CATOLICA DE CHILE
ESCUELA DE INGENIERIA

STRUCTURAL CHARACTERIZATION OF LIQUID FOOD FOAMS STABILIZED BY PROTEINS

JUAN CARLOS GERMAIN GUZMÁN

Members of the Committee:

JOSÉ MIGUEL AGUILERA R.

FRANCO PREDESCHI P.

DOMINGO MERY Q.

PEDRO BOUCHON A.

HUGO GLORIA-HERNÁNDEZ

CRISTIÁN VIAL E.

Thesis submitted to the Office of Research and Graduate Studies in partial fulfillment of the requirements for the Degree of Doctor in Engineering Sciences

Santiago de Chile, January, 2013

Dedicated to my four women, Beatriz, Valeria, Paulina and Sofía, and the memory of my beloved father, Juan Armando

AKNOWLEDGMENTS

Even though this thesis bears the name of just one person, achieving this work would not have been possible without the help and support of a number of people. Therefore, I would like to take this opportunity to acknowledge all those who in a way or another have been part of this journey. Due to my lousy memory, I apologize in advance to those that I might have forgotten to mention in these lines but that are present in my memories.

First of all I would like to thank my parents, Beatriz and Juan, for their unconditional support and encouragement during my so many years of university studies. Thanks a lot for all the love that you have given me and the education that not without effort you have provided me. Thank you for all your sacrifices, everything I am, I owe you. Dear father, although you had to leave us along the way, I know you have been looking after and guiding me all this time from above.

I would like to express my deepest acknowledgment to my advisor, Dr. José Miguel Aguilera. Thank you very much JM for your continuous guidance, your unconditional support and for your friendship. I apologize because this work took much longer than what I expected, and I thank you for never abandoning me and always being there when needed. But above all I would like to thank you for giving the opportunity to embark in this adventure that changed my life and that has opened me the doors to live experiences that otherwise I would have never lived.

I would like to express my thanks to all my colleagues at Chemical Engineering Department and particularly to my friends of Dr. Aguilera's group. Thanks Javier, Wenceslao, Olivier, Rommy, Elizabeth, Ross Mery, Cristián, Guillermo and Loreto for all those good moments spent together. I would like to give special thanks to Loreto for her support in completing this thesis. Thanks Lore for your words, encouragement and for being there whenever I needed. Thank you also Clarita for your friendship and for having the patience to withstand all of us daily.

I would like also to thank the students I work with during my research. Thanks María de los Angeles, Verena and Patricia for your valuable contribution to this thesis; it was a pleasure to work with you.

I am very grateful also to the Nestlé Research Center for co-funding this research and allowing me to do part of my work at their facilities. My thanks to all NRC scientists who shared with me their precious knowledge.

I would like to express my most sincere acknowledgments to my dearest and lovely wife Pauli. Thanks Pauli for your support, your understanding, your confidence in me, your sincere love, and for making me a happy person sharing every moment of our lives. Thank you for being my support and pillar in all those moments when things seemed too difficult to endure.

Last and not least, thank you Sofia for coming to my life and fill it with a joy I could have never imagined. Your little smile makes me feel that everything is possible.

Research has been funded by CONICYT's doctoral fellowship

GENERAL INDEX

Page

TABLE INDEX

Page

FIGURE INDEX

Page

PONTIFICIA UNIVERSIDAD CATOLICA DE CHILE
ESCUELA DE INGENIERIA

CARACTERIZACIÓN DE LA ESTRUCTURA DE LAS ESPUMAS LÍQUIDAS ESTABILIZADAS POR PROTEÍNAS

Tesis enviada a la Dirección de Investigación y Postgrado en cumplimiento parcial de los requisitos para el grado de Doctor en Ciencias de la Ingeniería.

JUAN CARLOS GERMAIN GUZMÁN

RESUMEN

El trabajo desarrollado en esta tesis se ha enfocado en un elemento reconocido hoy como un ingrediente esencial en innumerables alimentos: burbujas. Las burbujas son elementos estructurales fundamentales en varios productos, y durante los últimos años hemos sido testigos de un creciente interés académico e industrial para estudiar burbujas y su influencia en alimentos. Las espumas son sistemas muy complejos que entremezclan una amplia gama de escalas, que van desde el molecular hasta el nivel macroscópico, pasando por las películas líquidas y las burbujas mismas. Es por tanto necesario desarrollar conocimientos y herramientas que puedan ayudar a entenderlas para controlas y utilizarlas para nuestro beneficio. El objetivo general de esta tesis fue estudiar los atributos de espumas estabilizada por proteínas a diferentes escalas y proporcionar una visión más amplia de estos sumamente complejos sistemas. Los distintos capítulos de este documento describen los esfuerzos realizados en este sentido. Un primer estudio sobre los cambios en las propiedades interfaciales y espumantes inducidos de caseinato de sodio al ser modificado químicamente mediante conjugación con polisacáridos, demostró que este proceso mejoró la funcionalidad de la proteína. La mejora en las propiedades espumantes fue explicada parcialmente por los mayores módulos dilatacionales superficiales mostrados por las burbujas estabilizadas por la molécula conjugada en comparación con aquellas formadas a partir de la proteína nativa. Un segundo análisis de la estructura de espumas basado en la llamada característica de Euler mostró la importancia de incorporar información sobre disposiciones espaciales de

burbujas para describir las “arquitecturas” de espumas. Se demostró que información esencial (complementaria a los tamaños de burbuja) se obtiene a través de mediciones espaciales. Un análisis final de estructura de espumas basado en múltiples técnicas de análisis de imagen indicó que grupos de tres parámetros estructurales (entre los 57 calculados) podían identificar correctamente estructuras de espumas con características diferentes, pero lamentablemente ningún único conjunto de características pudo utilizarse ubicuamente. Los métodos y análisis realizados en esta tesis pueden ayudar en la camino de dilucidar la compleja naturaleza de las espumas. Un mayor y más profundo conocimiento es necesario para poder diseñar mejores productos, a medida que las burbujas ganan importancia como una forma directa de influir en la textura de los alimentos.

Miembros de la Comisión de Tesis Doctoral

José Miguel Aguilera R.
Franco Predeschi P.
Domingo Mery Q.
Pedro Bouchon A.
Hugo Gloria-Hernández
Cristián Vial E.

Santiago, Enero, 2013

PONTIFICIA UNIVERSIDAD CATOLICA DE CHILE
ESCUELA DE INGENIERIA

STRUCTURAL CHARACTERIZATION OF LIQUID FOOD FOAMS STABILIZED BY PROTEINS

Thesis submitted to the Office of Research and Graduate Studies in partial fulfillment of the requirements for the Degree of Doctor in Engineering Sciences by

JUAN C. GERMAIN

ABSTRACT

The work developed in this thesis is committed to an element acknowledged nowadays as an essential ingredient in countless foods: bubbles. Bubbles are fundamental structural elements in several products, and during the last years it have been witnessed an increasing academic and industrial interest to study bubbles and their influence food foams and aerated foods. Foams are highly complex systems that intermingle a wide range of scales, going from the molecular to the macroscopic level, passing through the liquid film and bubble cell levels. It is therefore necessary to develop knowledge and tools that can help understand them to control and use them for our benefit. The general objective of this thesis was to study the attributes of protein-stabilized foams at different scales and to provide a more comprehensive view of these immensely complex systems. The different chapters of this document describe the efforts done in this sense. A first study of the changes induced on the interfacial and foaming properties sodium caseinate when chemically modified by conjugation with polysaccharides, demonstrated that this process improved protein functionality. The better foaming properties were partially explained by the larger surface dilational modules showed by the bubbles stabilized by the conjugated molecule compared to those formed by the native protein. A second analysis of foam structures based on so-called Euler characteristic showed the importance of incorporating information on spatial arrangements of bubbles to describe foam “architectures”. It was demonstrated that essential information (complementary to bubble sizes) is obtained through spatial

measurements. A final analysis of foam structures based on multiple image analysis techniques indicated that groups of three structural parameters (among the 57 calculated) could successfully identify foam structures with different characteristics, but no single set of features could be used ubiquitously. The methods and analyses done in thesis can help on the route of elucidating the complex nature of foams. More and deeper knowledge is required to be able to design better products as bubbles gain importance as a way to influence food product textures.

Members of the Doctoral Thesis Committee:

José Miguel Aguilera R.
Franco Predeschi P.
Domingo Mery Q.
Pedro Bouchon A.
Hugo Gloria-Hernández
Cristián Vial E.

Santiago, January, 2013

1. GENERAL INTRODUCTION - MULTIPLE FOAM SCALES

1.1. Introduction and objectives of the thesis

Labels in supermarket products include lists with innumerable ingredients used in their manufacture. This encompasses simple compounds as sugar, flour and oils to more elaborated (many times synthetic) emulsifiers and preservatives. In those lists however it is not possible to find an element acknowledged nowadays as an essential ingredient in countless food products: bubbles. Plenty food products containing different but significant levels of a gas fraction can be found and few examples are soufflés, whipped cream, mousses, beer, ice cream, popcorn, bread, cakes, biscuits, waffles, pancakes, aerated chocolate bars, meringues, marshmallow, carbonated soft drinks, cornflakes, milkshakes, etc. Key point is that most of them will not exist if it was not for the bubbles present in their structures.

Increasing academic and industrial interest to study food foams and aerated food product comes from the attributes provided by bubbles. Campbell and Mougeot (1999) had listed that some properties bubbles impart are density reductions, rheology and texture changes, appearance and mouthfeel modifications, surface area increments, digestibility and shelf-life alterations due to increased porosity, and flavour intensity modulations. But above all, renewed interest relies on that we use and eat bubbles in our foods ubiquitously and companies recognize that consumer's preference is driven by the unique characteristics of foamed products.

During the last decade it has become clearer to food scientists that structure is critical for understanding food behaviour (Aguilera, 2005). This applies in particular to food foams. Bubbles give novel textures and attractive structures to food products and although simple techniques are routinely used to analyze foams and aerated food products it is necessary to obtain specific and quantitative data on their structure. Efforts are focused to linking structural information to physical properties of foods, and there is a need for quantitative methods that can characterize cellular structures and help

establishing relationships between structure and properties (Lim and Barigou, 2004). More fundament understanding of food foam systems is required to fill this gap.

Liquid foams are colloidal systems in which large numbers of air bubbles (or more generally speaking gas bubbles) are surrounded by an aqueous continuous phase. They are essentially lyophobic colloidal dispersions (continuous phase is thermodynamically driven not to wet the dispersed phase) characterized by the presence of an interfacial (or surface) tension (γ) produced between the 2 phases (Damodaran, 2005). Interfacial tension is the energy supplied to form a unit of interfacial area (A) (de Gennes *et al.*, 2004). Dispersing gas bubbles into a liquid significantly increases A inducing changes in the surface free energy (G_{surf}) of the system (Walstra and Smulders, 1997):

$$\Delta G_{surf} = \gamma \Delta A + A \Delta \gamma \tag{1.1}$$

As all systems should attain their minimum free energy state at equilibrium, thermodynamics dictates that foams will separate into 2 phases after they are formed to minimize A and therefore G_{surf}. Formation and persistence of stable liquid foams is consequence of surface active agents (surfactants), molecules with amphiphilic properties that locate at interfaces forming layers separating both phases (Weaire and Hutzler, 1999). Amphiphilic molecules can accommodate at interfaces because their molecular structure is composed by hydrophilic and hydrophobic regions. The term surfactant is applied to molecules of diverse nature. It can refer to simple small molecules formed by a polar head joined to an aliphatic chain (like a low molecular weight molecule such as a phospholipid) or to more complex and larger synthetic or biological macromolecules such as proteins.

Many food foams owe their existence to presence of proteins (Russo, 2000; Damodaran, 2005). These macromolecules play a major role in food foam stabilization because their amphiphilic nature allows them to accommodate at bubble interfaces. Bubble interfaces are stabilized against rupture by rheological properties proteins confer

to the thin film layers (Lucassen-Reynders, 1993). Proteins form viscoelastic networks sometimes referred to as a two-dimensional gel that stabilize interfacial layers kinetically (Golding and Sein, 2004; Gunning *et al.*, 2004; Carrera Sánchez *et al.*, 2005).

Scheme in Figure 1.1 shows that study of protein-stabilized foams can be done at different levels, each one characterized by length scales relevant to structural elements and phenomena involved. The lowest and probably most relevant is the molecular level. Molecular properties of proteins influence all higher scales and give the unique interfacial and foaming-inducing characteristics to these macromolecules. The following level corresponds to gas/liquid interfaces and liquid films separating bubbles. Protein adsorption processes and protein interfacial properties are of particular interest at this level. The third level corresponds to the actual foam structure and at this scale focus is mainly on bubble sizes, shapes and spatial organizations. Interest is on foam architectures which affect appearance and quality of foamed products. A higher level is finally to consider foams as a macroscopic material. At this level products physics, described mainly by mechanical and rheological properties, is the most relevant aspect.

The purpose of this work has been to provide a more comprehensive view on the study of foams that can help better understand these immensely complex systems. The fundamental hypothesis of this thesis is that the use of different foaming agents (proteins in the specific case of this work) and foaming conditions will produce foams with different characteristics in terms of their physical properties and structure. Therefore, the overall objective was to study the attributes of protein-stabilized foams at the different levels described in Figure 1.1 and try to understand the possible relations between them. In order to achieve this target, specific objectives were established throughout the individual works developed in this thesis:

- Evaluate and compare the changes induced on the interfacial and foaming properties sodium caseinate when chemically modified by conjugation with polysaccharides (Chapter 2).

- Develop a method to quantify bubble spatial distributions on foams structures and show importance of this structural parameter that provides complementary information to bubble size distributions (Chapter 3).
- Identify quantitative parameters that can be used to further describe/differentiate the structural properties of foamed systems (Chapter 4)

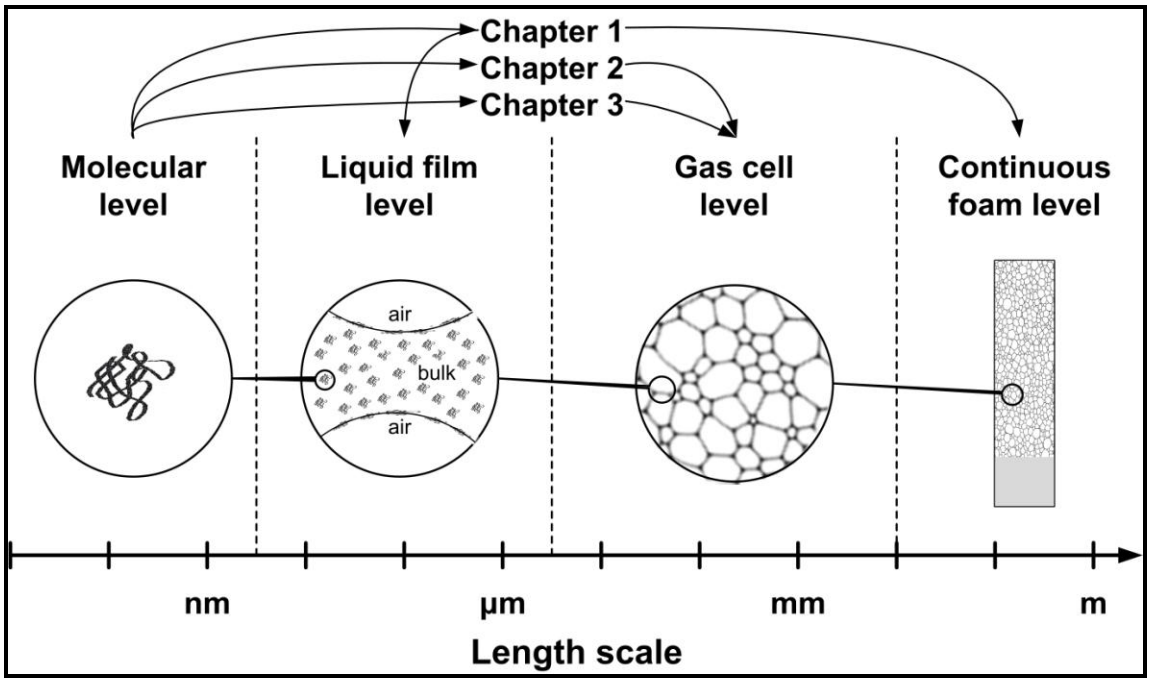

Figure 1.1: Graphical representation of 4 levels in foams analysis. Molecular, liquid film, gas cell, and continuous foam size levels are all characterized by specific lengths. Study of protein stabilized foams focuses at each particular level and addresses aspects relevant at the different length scales. Their relation to the different chapters in this thesis is also depicted.

What follows in this introduction chapter is a general description of the different scales depicted in Figure 1.1. Relevant literature dealing with foam investigations at each level is cited and linked with the results of this thesis.

1.2. Molecular and liquid film levels

1.2.1. Proteins as surface active compounds

The lowest length-scale in the scheme presented in Figure 1.1 is the protein molecular size level. Proteins are a large collection of macromolecules widely present in nature affecting functions of virtually all living organisms (Creighton, 1993). Presence of proteins ranges from their active role in cells and plasma, forming part of cell membranes, antibodies, enzymes, hormones, etc., to their structural functions in hair, nails, tendons, muscles, etc. Nonetheless, they are a relatively homogenous group despite their diverse functionalities. All proteins are linear polymers built by combinations of 20 amino acids. Amino acids are grouped into 3 families, those with strictly hydrophobic side chains, those charged, and those with polar side chains (Branden and Tooze, 1991). Differences in the chemical nature of amino acids give proteins their singular amphiphilic nature and surface activity. But not all proteins types display surface activity. To act as surfactants, proteins should be able to diffuse and adsorb at interfaces, unfold and form cohesive films via molecular interactions (Damodaran, 2005).

Proteins interface stabilization is far more complex than for small surfactant molecules and therefore not as well understood. In contrast to small surfactant molecules such as monoglycerides and phospholipids with identifiable hydrophilic heads and hydrophobic tails, proteins have randomly distributed hydrophobic and hydrophilic groups. Even more, in folded tertiary structures only a small fraction of hydrophobic residues are exposed to the gas phase leaving most of the protein molecule immersed (at least initially) into the aqueous phase (Damodaran, 2005). Large three-dimensional structures of proteins must therefore reconfigure when faced to interfaces to increasingly expose hidden hydrophobic regions. Ability to undergo rapid conformation changes when transferred from one environment to another (molecular flexibility) is consequently a critical property of surface active proteins (Razumovsky and Damodaran, 1999). Timescales and extent of protein conformational changes strongly depends on inter- and intramolecular forces (Prins *et al.*, 1998). Cleavage of intermolecular disulfide

bonds (Yu and Damodaran, 1991) and partial heat denaturation (Zhu and Damodaran, 1994) generally improves protein surface activity because of enhanced molecular flexibility. Proteins foaming capacities are also positively correlated with average molecule hydrophobicity (Kato *et al.*, 1983). Average hydrophobicity is the average free energy change as a consequence of transferring amino acid side chains from non-polar solvents to water. Surface hydrophobic patches facilitate initial protein interfacial anchoring driven by lowering the surface free energy of the system.

Surface and foaming properties of proteins are modified by different methods that involve physical, chemical, enzymatic or genetic processes. Physical modifications involve partial denaturation or unfolding by controlled heat (Bals and Kulozik, 2003) or shearing (Onwulata *et al*., 2003). Chemical modifications alter secondary, tertiary, and quaternary structures and affect hydrophobic-hydrophilic balance. It has been speculated that protein chemical modification via conjugation with polysaccharides improves surface properties, especially at low pH as iso-electric point and solubility are altered and molecular integrity maintained (Morris *et al*., 2004). Enzymatic modification of proteins is mainly carried out by hydrolysis and polymerization reactions. For example, controlled protein polymerization using transglutaminase has shown to affect functional properties (Liu and Damodaran, 1999). Genetic modification is successfully employed nowadays to improve protein thermostability, alter temperature and pH optima, and change substrate specificity of enzymes. However, there are limited examples on specifically improving their functional properties (Utsumi *et al.*, 2002; Adachi *et al.*, 2004).

This particular level of foam length scales is treated in Chapter 2. Surface active and foaming properties of a modified protein were evaluated in comparison to the native protein. Protein modification was done by a chemical reaction to produce a conjugate with maltodextrin. Alteration of protein molecular characteristics had a remarkable effect on functional properties.

1.2.2. Film forming ability of proteins at gas/liquid interfaces

Bubble gas/liquid interfaces and thin lamellas separating them defines a second scale level in the scheme proposed in Figure 1.1. Relevant information at this stage is protein absorption kinetics and equilibrium conditions, interfacial rheological properties, and bubble film permeability characteristics.

Quantifying protein adsorption

The process of protein adsorption at gas/liquid interfaces has been described as involving a number of steps (Maldonado-Valderrama *et al.*, 2005; de Jongh, 2007). These steps are shown schematically in Figure 1.2. Proteins diffuse from the bulk of the continuous phase to the interface, phenomena controlled by molecular size and viscosity. Once close to interfaces proteins adsorb. Net protein adsorption (adsorption minus desorption) is controlled by kinetic energy barriers determining the ratio between sticking and bouncing molecules. Adsorbed proteins then undergo conformational changes to expose their hidden hydrophobic groups to the gas phase. Unfolding kinetics are controlled by activation energy required to disrupt protein intramolecular interactions. Finally, proteins aggregate within the interfacial layer forming a network, step controlled by chemical reactivity and physical-chemical activity of side chains.

Quantification of equilibrium conditions during interfacial protein adsorption together with adsorption dynamics are both subjects of practical importance on foam stability. Several studies have been done to develop theoretical models to accurately describe this process. Protein adsorption shows a sharp increase in surface pressure ($\Pi=\gamma_0-\gamma$, where γ_0 is the surface tension of the pure solvent) with concentration until a certain protein adsorption threshold. Over this threshold Π remains almost constant while adsorption layer thickness still increases significantly (Miller *et al.*, 2004a). Additionally, proteins unfold due to surface denaturation, thus individual protein molecules have variable surface coverage.

Various thermodynamic models describing equilibrium conditions during polymer adsorption have been used to describe protein adsorption (Douillard *et al.*, 2003). Fainerman *et al.* (2003) proposed a theoretical model taking into consideration the particular protein characteristics. This model has proved successful in describing measured protein adsorption and surface pressure isotherms. It corresponds to an extension of previous works (Joos and Serrien, 1991) assuming that protein molecules can adopt multiple states with different molar areas. Fainerman's thermodynamic equilibrium model set the basis for determining protein adsorption kinetics. Miller *et al.* (2004) developed a dynamic interfacial protein adsorption description based on the Ward and Tordai (1946) equation providing a relationship between dynamic adsorption and subsurface protein concentration $c(0,t)$ for fresh and non-deformed surfaces:

$$\Gamma(t) = 2\sqrt{\frac{D}{\pi}}\left[c_0\sqrt{t} - \int_0^{\sqrt{t}} c(0, t-t')d\left(\sqrt{t'}\right)\right] \tag{1.2}$$

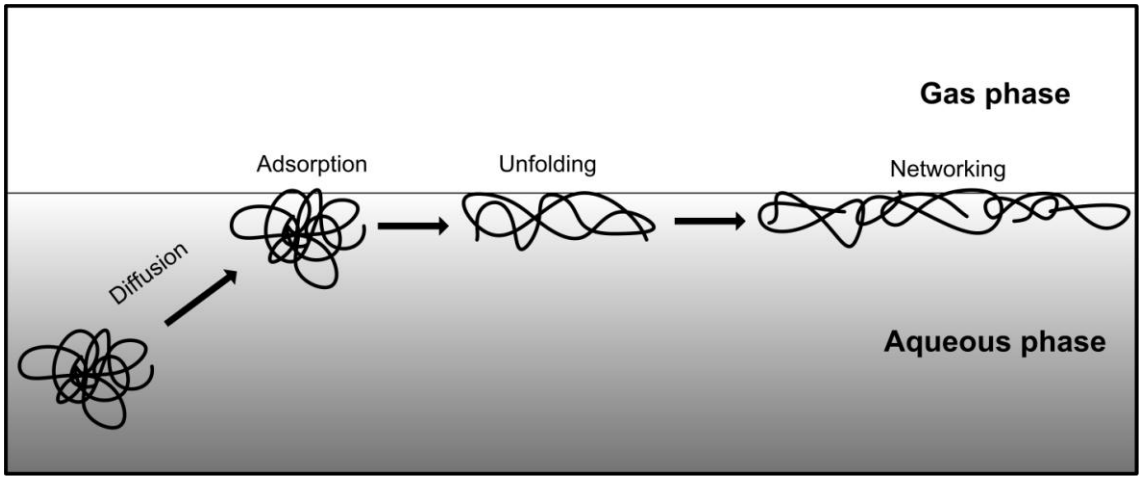

Figure 1.2: Schematic description of the protein adsorption process at gas/liquid interfaces. Native folded proteins diffuse towards the interface where they are adsorbed and undergo denaturation and networking with other proteins through molecular interactions.

Experimentally, measuring protein absorption kinetics is a difficult technical problem commonly accomplished using radiotracer techniques (Xu and Damodaran, 1993) and ellipsometry (Grigoriev *et al.*, 2002). However, dynamic surface tension experiments are technically much simpler to perform and models described above can be employed to represent experimental measurements and unveil adsorption mechanisms (Miller *et al.*, 2004; Maldonado-Valderrama *et al.*, 2005). Various tensiometry techniques are available to determine dynamic surface tensions (Miller *et al.*, 2000). Among them, pendant drop tensiometry has proved a standard and reliable method for elucidating adsorption kinetics (Möbius and Miller, 1998). Pendant drop tensiometry is a non-invasive technique for measuring γ as a function of time based on force mechanical equilibrium on drops or bubbles. At mechanical equilibrium curvature is adjusted to balance pressure difference between the two phases by capillary pressures. Force equilibrium leads to the fundamental Laplace equation (not to be confused with Laplace's Law; Eq. 1.8) describing mathematically the drop (or bubble) interface profile (Eq. 1.3). Physics literature described years ago the theoretical basis of surface tension evaluation using this equation (Andreas *et al.*, 1938; Stauffer, 1965).

$$\frac{1}{x}\frac{d}{dx}\left(x\sin\theta\right)=\frac{2}{b}-cz \tag{1.3}$$

Major drawback of this approach was the cumbersome and lengthy processing time, but nowadays increasing computational capacities and emergence of digital video cameras allows fast real time measurements (Cagna *et al.*, 1992; Labourdenne *et al.*, 1996). Coupled with appropriate software tools this method helps interpreting experimental data in relation to thermodynamics and kinetics models (Aksenenko, 2001).

In Chapter 2 pendant drop tensiometry was used to measure adsorption kinetics of sodium caseinate and its conjugate. Using a simplified semi-quantitave approach, apparent adsorption rates were derived from dynamic surface tension data.

Quantifying film rheology

Foam stability cannot be explained solely by interfacial tension reduction provoked by protein adsorption but also by rheological properties these molecules confer to interfaces. Protein-covered interfaces behave as two-dimensional entities with elasticity and viscosity. Protein presence leads to interfacial tension gradients enabling interfaces to resist tangential stresses providing them with mechanisms for dynamic stabilization (Lucassen-Reyders, 1993).

Interfacial rheology analysis is achieved by compression deformation or shearing motion of surfaces. Surface shear viscosities contribute to long term foams stability. For short term stability interfacial rheology in compression and expansion is more relevant. Interfaces undergo compression and expansion rather than shearing during foaming. High shear viscosities found for interfaces cannot build up in the time scales (<1s) associated with formation of new interfaces (Benjamins and Lucassen-Reynders, 1998). Interface rheological characteristics during compression and expansion are described by the surface dilatational modulus (ε) estimated from the expression originally proposed by Gibbs (Logley and Van Name, 1928):

$$\varepsilon = \frac{d\lambda}{d\ln A} \tag{1.4}$$

Interfacial viscoelastic properties during compression and expansion are extensively investigated by dynamic drop tensiometry (Benjamins *et al.*, 1996) based on the instrument originally developed by Cagna *et al.* (1992). The modified equipment version allows varying drop/bubble area sinusoidally and changes in γ and A are recorded simultaneously through image analysis to determine ε. When films are purely elastic plotting $d\gamma$ against $d\ln A$ produces a straight line. However, deviations occur when relaxation processes in or near the interface affect γ within measuring times. Modulus ε becomes a surface viscoelasticity with elastic (ε') and viscous (ε'') components accounting for energy stored and loss per cycle, respectively. Plotting $d\gamma$ against $d\ln A$ in these cases gives an ellipse (Lucassen and van den Tempel, 1972). Experimentally,

imaginary contribution is represented by a phase angle (ϕ) between stress and strain responses.

$$\varepsilon' = \varepsilon \cos\phi \tag{1.5}$$

$$\varepsilon'' = \varepsilon \sin\phi \tag{1.6}$$

Interfacial rheological properties of surfactants and proteins have been extensively reviewed by Bos and van Vliet (2001). Under the framework of the thermodynamic equilibrium protein adsorption model mentioned before (Fainerman *et al.*, 2003), dependence of limiting Gibbs' elasticity (ε_0) for protein monolayers (defined as ε measured at frequencies where no relaxation processes affect γ in area oscillations time scales) on Γ has been proposed (Lucassen-Reynders *et al.* 2004). Experimental values of ε_0 have been described satisfactorily by Eq. 1.7 and the thermodynamic model.

$$\varepsilon_0 = \frac{RT}{\omega_0}\omega\Gamma\left(\frac{1}{1-\omega\Gamma} - 2a\omega\Gamma - 1\right) \tag{1.7}$$

It has been shown that for low viscosity systems such as liquid foams, interfacial rheological properties of protein films have important effects on Ostwald ripening. As protein films build during adoption, increments on ε reduce disproportionation rates (Damodaran, 2005). Theoretical work done by Kloek *et al.* (2001) has evidenced that presence of viscoelastic interfaces with relevant viscosities larger than a critical value or either completely elastic interfaces can retard or even stop bubble shrinkage. Adapting Kloek's theory, Dickinson *et al.* (2002) tested bubble stabilization mechanisms of proteins and concluded that surface rheology cannot completely stabilize bubble, but introducing modest dilatational elastic contributions into the model gave good agreement between experimental measurements and predictions.

Due to the importance of surface viscoelastic properties on foam stability, Chapter 2 shows measurement and comparison of viscoelastic modules obtained from bubble surfaces stabilized by sodium caseinate and its conjugate. It was shown that conjugation increased surface viscoelasticity, particularly the elastic component, partially explaining the enhanced foaming behaviour of conjugates.

Quantifying film permeability

Ostwald ripening (referred also as disproportionation) occurs because bubble walls are permeable to gas diffusion. Process origin is explained by Laplace's law (Eq. 1.8) which expresses the pressure difference balance (ΔP) across gas/liquid interfaces. For spherical bubbles of radius (R) it becomes:

$$\Delta P = \frac{2\gamma}{R} \tag{1.8}$$

This expression indicates that small bubbles have internal pressures higher than larger ones. Pressure differences between neighbouring bubbles results in concentration gradients that drives diffusion. Gas diffusion processes through entire foams is a problem of great practical importance but difficult to describe and analyze in real systems due to the complexity of the structure. However, Ostwald ripening of single bubbles can be studied employing the Diminishing Bubble (DB) method proposed by Platikanov *et al*. (1980). DB method consists in forming one small gas bubble at the surface of the surfactant solution. Approach partially imitates the situation of bubbles in foams. The film formed between the bubble and the solution surface is analogous to that formed between two bubbles (Figure 1.3). Outside medium acts as an infinitively big bubble contacted directly with the small bubble. Pressure gradient drives gas out of the bubble and as a result it shrinks. Two variables are measured against time via microscopic observation: R and film radius (r). DB method was initially created for experimental determination of contact angles and tensions along contact lines of Newton black films formed by small surfactant molecules. It is used in particular to estimate film permeability coefficients (K), ability of bubble surfaces to block gas flow related to the

molecular organization at interfaces. Values of K are estimated using the expression proposed by Krustev *et al*. (1996):

$$K = \frac{\frac{P_{atm}}{8\gamma}\left(R_0^4 - R_t^4\right) + \frac{8}{9}\left(R_0^3 - R_t^3\right)}{\int_0^t r^2 dt} \tag{1.9}$$

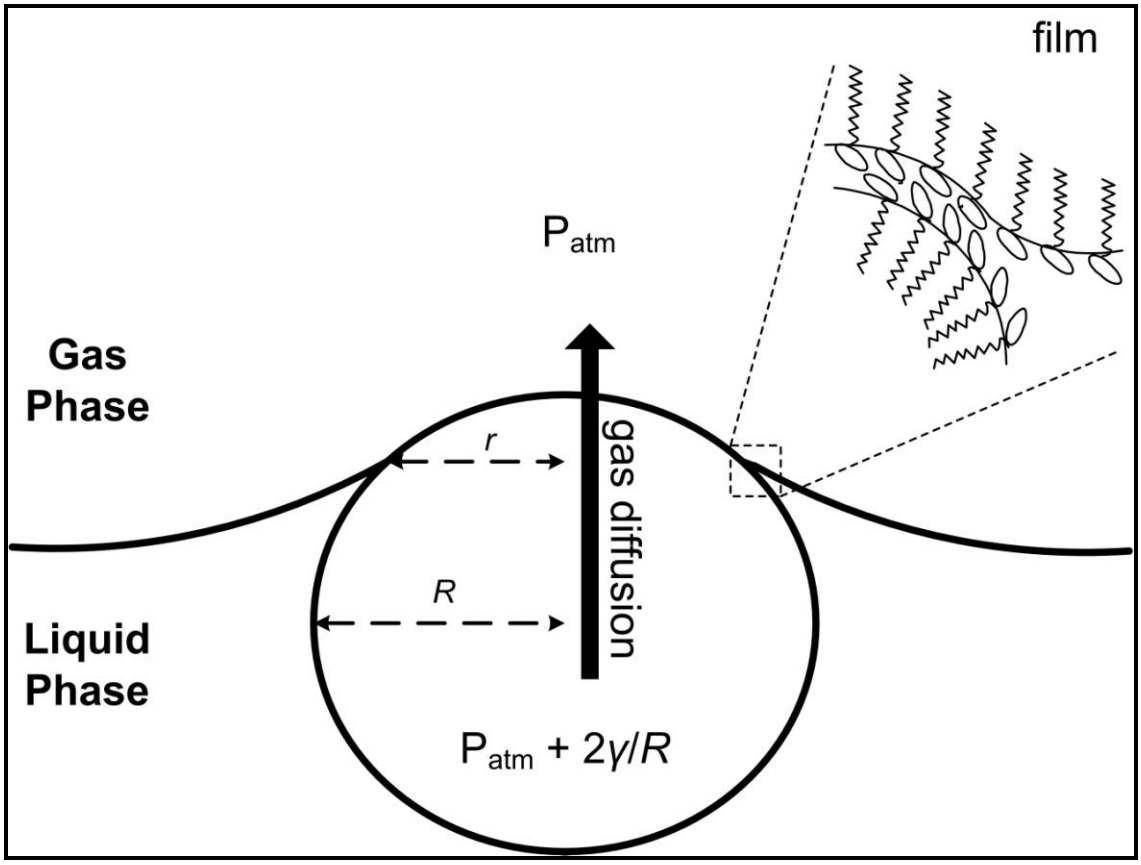

Figure 1.3: Schematic representation of gas diffusion process from a small bubble into the outer medium due to Laplace pressure in the diminishing bubble approach. Film formed at the top of the bubble is a bilayer as those formed in foams.

There is limited literature data of protein film permeabilities. Microscopic films made from *β*-lactoglobulin solutions with different concentrations and pH values were studied by Petkova *et al*. (2003) using DB method. Authors reported values between 0.017-0.022 cm/s, close to permeability values reported for simple surfactants (Nedyalkov *et al.* 1988; Nedyalkov *et al.* 1992) or phospholipid mixtures (Trachant *et al.* 2002). Due to the relatively slow protein adsorption kinetics, *K* values are observed to vary with time. Film structure changes because of protein rearrangements and thinning due to drainage. The phenomenon has been discussed by Schmitt *et al.* (2005) who reported a permeability increase of 20 times for freshly formed films compared to those aged for 24 hrs (0.021 and 0.449 cm/s, respectively).

In Chapter 2, I present and discuss a variation of the DB method implemented in this work to calculate protein film permeabilities. The objective was to simplify the original DB approach avoiding measuring *r* and base calculations solely on *R* values measured automatically by image analysis. Considering that bubble shrinkage results from gas flow through the film into the atmosphere, total mass balance yields the following expression relating the film permeability coefficient with shrinkage kinetics:

$$K = 4\pi \frac{\frac{P_{atm}}{8\gamma}\left(R_0^4 - R_t^4\right) + \frac{2}{9}\left(R_0^3 - R_t^3\right)}{\int_0^t A_f \, dt} \tag{1.10}$$

Eq. 1.10 is analogous to Eq. 1.9 proposed by Krustev *et al.* (1996) but *r* is replaced by the film area (A_f). The change rate of A_f with time is calculated with Eq. 1.11 obtained from the first derivative of the total mass balance.

$$A_f(t) = A_0 \exp \int_0^t \left(\frac{\left(3\frac{P_{atm}}{\gamma}R + \frac{8}{3}\right)\left(\frac{dR}{dt}\right)^2 + R\left(\frac{P_{atm}}{\gamma}R + \frac{4}{3}\right)\frac{d^2R}{dt^2}}{R\left(\left(\frac{P_{atm}}{\gamma}R + \frac{4}{3}\right)\frac{dR}{dt}\right)} \right) dt \tag{1.11}$$

Initial film area (A_0) is estimated by a balance between buoyancy forces and surface tension forces. When using Eqs. 1.10 and 1.11 (and also Eq. 1.9) it is assumed that bubble shrinkage is only caused by gas flow into the atmosphere. Gas diffusion into solutions bulk is neglected. Above equations consider also that bubbles remain spherical and that film area can be approximated to a flat disc. Values of K obtained in this work presented in Chapter 2 were higher compared to those reported in previous studies for protein films. Divergences are attributed to the complexities of protein systems where even low levels of contamination can affect bubble resistances to shrinkage (Dickinson *et al.*, 2002).

1.3. Foam architectures

The third level in the proposed length scale scheme (Figure 1.1) is the bubble size level. Most important at this stage is the ability to produce stable foams and the particular characteristics of bubble structures within foams system.

1.3.1. Equilibrium rules for films and bubbles

First rule that defines equilibrium between liquid films and bubbles is the law of Laplace (Eq. 1.8). Excess pressure that arises to counter balance surface tension explains why bubbles do not shrink until disappearing but equilibrate to form spherical shaped bubbles in three-dimensions or circular discs in two-dimension cross sections. However, within foams only for certain small bubble clusters films remain truly spherical (Weaire and Hutzler, 1999). Work performed by Plateau (1873) may be considered the first scientific study on films, bubbles and foams. Plateau added to the law of Laplace the rules required to define equilibrium for liquid films and bubbles. The laws of Plateau relate to foams in the dry limit but can also apply in more general cases. In dry foams, liquid fractions are very small (<1%) and bubbles adopt polyhedral forms with thin films as their faces, often idealized as single surfaces. Two-dimensional dry foams consist of polygonal cells (Figure 1.4). Plateau stated that for dry foams, films (lines which define cell boundaries in two-dimensions) can intersect only 3 at a time and at angles of 120º (Figure 1.4). Films between gas cells meet in lines forming the edges of

the polyhedral cells in space, and lines meet at vertices. The second law of Plateau states that at vertices no more than 4 intersection lines (or 6 surfaces) may meet, and that this tetrahedral vertex is perfectly symmetric forming an angle equal to $\cos^{-1}(-1/3)$ (~109.5º). Although these rules are concerned mostly with isolated films, bubbles, and their junctions rather than on extended foam structures, they establish the essential laws to define equilibrium configurations. Employed in conjunction with assumptions about gas compressibility, these laws are the basis for foam structure simulations (Weaire and Hutzler, 1999).

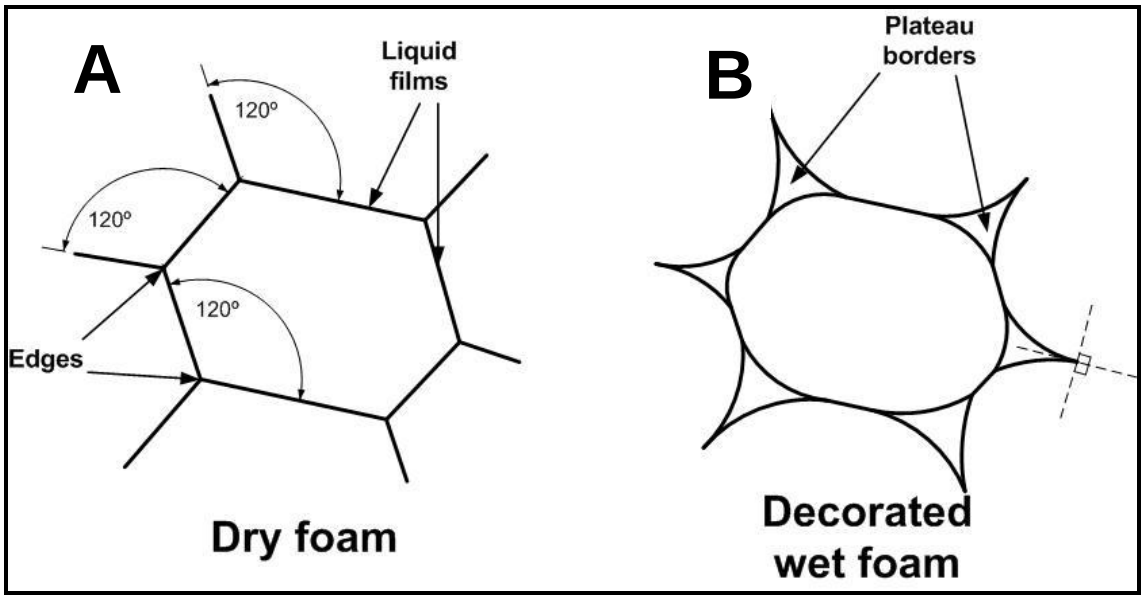

Figure 1.4: Foam structure description. (A) In dry foams bubbles adopt polyhedral forms where Plateau borders can intersect only 3 at a time and at angles of 120º. (B) In wet foams liquid is contained in Plateau borders where they join an adjacent film. Surface normal is the same on both sides of the intersections.

When foam liquid fractions rise over 1%, previous geometrical description does not strictly applies and Plateau laws need to be reconsidered. Liquid is mainly contained in the Plateau borders, finite width channels that replace lines in dry foams (Figure 1.4). Plateau equilibrium rule states that where a Plateau border joins an adjacent

film, the line normal to the surface is the same on both sides of the intersection. However, no general stability rules can be applied to intersection multiplicity at Plateau borders or their own intersection or junctions. It can only be expected to find features exhibited by dry foams in fairly dry foams dressed with Plateau borders. In two-dimensions this idea is given by the decoration theorem (Weaire and Hutzler, 1999): equilibrated wet foams are obtained by the superposition of Plateau borders at each vertex of dry foams in two-dimensions (Figure 1.4B). As liquid fraction further increases, sharp edges of polyhedral (or polygonal) cells are rounded off leading to extreme wet foam limit. At this point cells recover spherical (or circular) shapes and any further liquid increase allows them to come apart. Foam losses all rigidity and becomes a bubbly liquid instead.

1.3.2. Evaluation of foams

Characterization of bubble containing structures is not a simple task because of the very complicated mechanisms associated with formation and stability of such systems. Most direct measurements on fluid foams are related to bulk properties such as foamability (ease with which a foams is formed) and foam stability (Campbell and Mougeot, 1999). Common procedure to determine foamability is to measure time required to form a certain foam volume by sparging gas into a liquid. Foam stability is usually characterized by foam half-life, drainage rates, and conductivity change rates.

Air content of aerated foods is expressed as the void fraction of air or gas hold up ($\emptyset$) (volume fraction of gas based on the dispersion volume). Various experimental approaches are used to determine gas hold-up depending on product characteristics (Niranjan and Silva, 2008). A standard procedure for liquids and pastes with medium to high viscosities is filling and weighing a cup, first with the continuous phase (m_c) and then with the foamed dispersion (m_f). Gas hold up is estimated by density difference (Eq. 1.12). Solid foams like aerated chocolates require different approaches like the flotation method (Haedelt *et al.*, 2005). Instrumental methods based on optical probes (Bispernik *et al*,. 1992) and ultrasound (Fox *et al.*, 2004) have also been developed to measure $\emptyset$ directly.

$$\phi = 100 \times \left(1 - \frac{m_f}{m_c} \right) \tag{1.12}$$

Another parameter used to describe aerated foods is overrun (Eq. 1.13), particularly for systems with very high gas content. It represents the gas fraction based on the volume of the continuous phase, and is related to $\emptyset$ by:

$$overrun = 100 \times \left(\frac{\phi}{100 - \phi} \right) \tag{1.13}$$

Instruments specifically designed to evaluate foaming properties of surface active compounds are available. Foamscan (ITConcept, Longessaigne, France), developed from the work of Guillerme *et al.* (1993), allows direct observation and measurement of volume increase of foams formed by sparging with a controlled gas flow. Foam stability is followed by measuring variation of foam height and drainage rates as functions of time. System consists basically of a glass cylinder were foam is formed under user defined conditions. Foam volume during foam creation and collapse are measured in real time by image processing, whereas liquid fractions and drainage rates are quantified also in real time by resistivity measurements from electrodes located at different heights of the glass tube. Simple parameters that characterize foam properties like foam density, foam expansion coefficient, foaming capability are determined from these experiments. Foamscan, and similar systems based on the idea of Guillerme *et al.* (1993), had been used to study the foaming behaviour of casein (Guillerme *et al.*, 1993; Fains *et al.*, 1997; Rodriguez Patino *et al.*, 1997), *β*-casein (Sarker *et al.*, 1998), sodium caseinate (Carrera Sanchez and Rodriguez Patino, 2005), *β*-lactoglobulin (Sitohy *et al.*, 1995; Schmitt *et al.*, 2005), ovotransferrin (Sarker *et al.*, 1998), acetyled and succinylated pea isolates (Fains *et al.*, 1997), soybean isolate (Guillerme *et al.*, 1993), deamidated gluten (Guillerme *et al.*, 1993; Fains *et al.*, 1997), potato raw proteins (Ralet and Guéguen, 2001), egg-white (Baniel *et al.*, 1997; Hagolle *et al.*, 2000), sodium oleate (Beneventi *et al.*, 2003), bovine serum albumin (Rodriguez

Patino *et al.*, 1997; Sarker *et al.*, 1998), soy globulins (Pizones Ruiz-Henestrosa *et al.*, 2007) and whey protein isolate (Schmitt *et al.*, 2007), among other systems.

Foamscan was used in this thesis to measure foaming properties of sodium caseinate and its conjugate. Results described in Chapter 2 show the remarkable improvement on foaming properties as consequence of protein conjugation.

1.3.3. Image analysis of foams

Digital image analysis has become an important tool in many fields including food science because of the valuable quantitative information and numerical data that can be extracted from images (Aguilera and Stanley, 1999; Russ, 2005). Advances in imaging and computing technologies have make now possible the objective quantification of foams and sponge cell structures (Cauvain, 2003). The general image analysis methodology is usually divided into different consecutive steps which involve image acquisition, pre-processing operations, image segmentation, and feature extraction (Aguilera and Germain, 2007). Figure 1.5A shows grey scale images of fresh protein foam acquired using a CCD camera during work in this thesis. It shows also results of segmenting individual bubbles by thresholding their grey level counterparts. Resulting images can then be further analyzed to measure different attributes. Undoubtedly, the main feature characterizing foam structures is bubble size, but other relevant characteristics/properties can be obtained from images as well.

Bubble sizes

Methods commonly used to determine foam bubble sizes are optical probes, ultrasound sampling probes, and photographic techniques (Niranjan and Silva, 2008). Optical probes consist of fibreglass sensors moved through samples allowing localized determination of bubble size distributions (Bispernik *et al.*, 1992). Ultrasound sampling probes are based on measuring velocities and attenuation spectra of ultrasound waves through samples, information related to bubble sizes (Kulmyrzaev *et al.* 2000). However, these techniques usually require dilute systems and are intrusive. Photographic techniques coupled with image analysis software have been most widely

used in analysis of bubble-containing foods and determination of bubble size distributions (Germain and Aguilera, 2006).

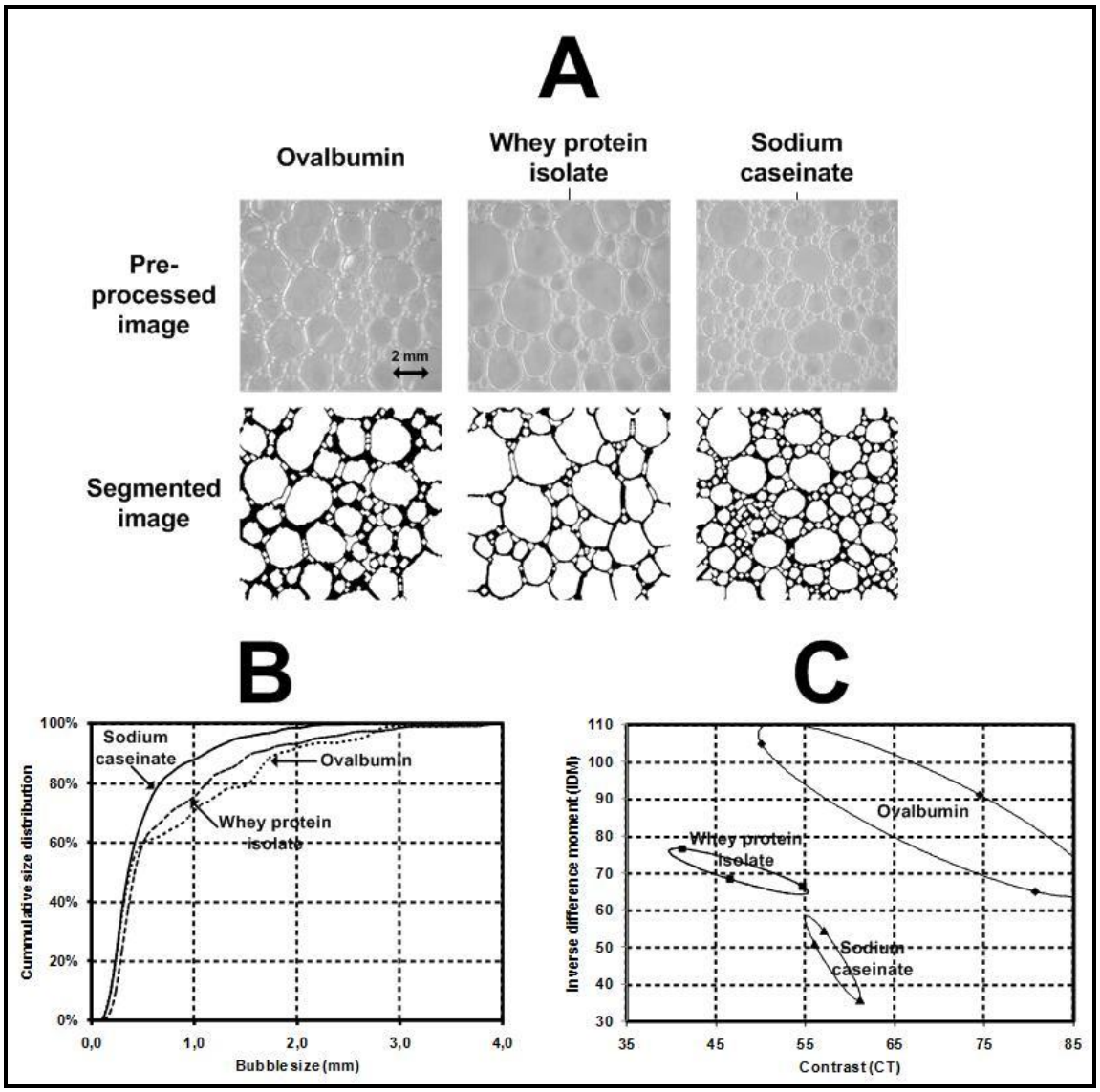

Figure 1.5: (A) Processed grey-level and thresholded images of fresh protein foams. (B) Cumulative bubble sized distributions for the foams in A determined by image analysis. (C) Classification of foams images through texture and discriminant analysis.

Food foams are complex three-dimensional structures generally difficult to observe (Pugh, 2005). The common approach for studying foam structures is therefore using images of two-dimensional foams (e.g., thin foams produced between 2 transparent plates), or two-dimensional images from three-dimensional foam structures. There is a wide range of imaging techniques available and used to characterize foam structures, among them light microscopy (LM), confocal laser scanning (CLSM), scanning electron microscopy (SEM), cryo-SEM, direct use of CCD cameras, and magnetic resonance imaging (MRI). Several literature examples applying these imaging techniques to analyze bubble sizes in foams and aerated products can be found. Bubble size distributions have been determined from LM images by Kulmyrzaev *et al.* (2000) and Bals and Kulozik (2003) for whey protein isolate foams, by Schoonman *et al.* (2001) for maltodextrin/sodium caseinate solid foams, by Chang and Hartel (2002) and Eisner *et al.* (2005) for whipped and ice cream, by Sahi and Alava (2003) and Hicsasmaz *et al.* (2003) for cake batters, and by Jang *et al.* (2005) for gelatine solutions and food emulsions, among others. In a similar way, bubble size distributions have been measured from cake batters and whipped emulsions from fresh milk and whole egg by Richarson *et al.* (2002) and Martinet *et al.* (2005), respectively, using CSLM. SEM has been used by Alavi *et al.* (1999) to determine bubble size distributions in protein-stabilized starch-based supercritical fluid extrudates, and also cryo-SEM has been used by Chang and Hartel (2002) and Eisner *et al.* (2005) in whipped and ice cream for this purpose. Foams from cream, egg white and beer have been analyzed by MRI and signal intensities contributed by aqueous protons recorded over foam lifetime to measure densities, drainage and structure collapse (German and McCarthy, 1989). Duce *et al.* (1995) analyzed a selection of foamed dairy products non-invasively by three different MRI methods.

Most recently, X-ray tomography has risen as a suitable imaging technology to non-invasively generate views of cellular material structures (Trater *et al.* 2005). X-rays are used to obtain series of images at different sample depths. X-rays have proved very useful in analyzing cellular structures because they penetrate materials giving sample image with minimal preparation and non-invasively. Technique has been used by

Lim and Barigou (2004) for investigating cellular structures of aerated chocolate bars, strawberry mousses, honeycomb chocolate bars, chocolate muffins, and marshmallows. It has also been employed by Babin *et al.* (2005, 2006) to analyze bread crumb structures and by Haedelt *et al.* (2005) for macro aerated chocolate. However, application is currently limited for bubble sizes over 50 μm and completely stable food systems.

The disadvantage of 2D images analysis is that actual food foams are 3D objects. Richardson *et al.* (2002) indicated that, although bubble size distributions measured for cake batter are good enough for comparison and performance evaluation purposes, these were not real distributions. Real bubble size distributions can be extracted from 2D data by stereology if required. Stereology is a group of mathematical methods that allow estimating parameters of three-dimensional structures by measuring two-dimensional sections. Schoonman *et al.* (2001) used stereological techniques to unfold true bubble size distributions in foamed maltodextrin/sodium caseinate powders from light microscopy images. Lim and Barigou (2004) measured real size distribution of different food samples from 2D images obtained by X-rays.

Figure 1.5B shows cumulative bubble size distributions calculated from corresponding binary images in Figure 1.5A. Bubble sizes correspond to equivalent diameter determined from projected bubble areas. These distributions do not correspond to real sample bubble size distributions; however, they serve for comparison because in the three cases images were acquired at identical conditions.

Image texture analysis

Image texture analysis (ITA) is another technique progressively gaining popularity in digital image analysis (Aguilera and Germain, 2007). Image texture (not be confused with sensorial texture defined for foods by mechanical instrumental measurements) is used as a way to describe visual perception of irregularities and variations. It relates pixel brightness values with spatial distributions. There are several possibilities for calculating food image textural properties classified in three main

groups: statistical, model-based, and transform-based techniques (Zheng *et al.*, 2006). ITA usefulness is that it can be applied for objective characterization of complex food foams "architectures".

Possibly first published work using ITA to describe images of foam-like structures was the one by Bertrand *et al.* (1992). Textural features were extracted from bread crumb images by a procedure based on the two-dimensional Haar transform and a total of 66 textural features were obtained. A stepwise discriminant analysis allowed identification of 6 texture characteristics which permitted about 81% correct classification of samples into seven specific classes according to the treatments used in bread preparation. Using same mathematical method, Guillerme *et al.* (1993) evaluated image texture of liquid foams formed using three different protein solutions (casein, soybean isolate, deamidated gluten). Foams were formed by sparging and images recorded with a video camera coupled to the foaming apparatus. 81 textural characteristics were extracted from each image and subsequently analyzed using principal components to determine similarities between foam textures. Authors concluded that procedure was well-adapted for comparison and classification of foams, however, it did not adequately describe physical mechanisms of foam formation and destabilization. Following studies by Fains *et al.* (1997), Hagolle *et al.* (2000), and Rahali and Guegen (2000) used the same experimental approach to investigate other protein-based liquid foams. Fains *et al.* (1997) analyzed foaming properties of four protein solutions (casein, acetyled and succinylated pea isolates, and deamidated gluten) indicating that textural features derived from two-dimensional Haar transforms made possible to distinguish different protein foams and to differentiate between stable and unstable systems. Hagolle *et al.* (2000) investigated effects of heating on foaming properties of two egg white proteins (ovalbumin and lysozyme). They concluded that image analysis allowed describing texture evolution with foam aging and also discriminating differences induced by small increments in temperature. Rahali and Guegen (2000) evaluated foamed solutions of bovine *β*-lactoglobulin and enzymatic hydrolysates. ITA allowed identification of three distinctive regions within the principal components map correlated with foam stability measurements. A different approach was

employed by Sarker *et al.* (1998) using a grey level run length method to analyse image texture on liquid foam images obtained with series of model protein, surfactant and protein/surfactant solutions. They concluded also that ITA proved a useful complementary approach to conventional physical measurements in liquid foam analysis. Most recently, Rouillé *et al.* (2005) have used textural techniques based on mathematical morphological treatment to characterize foam-like structures in French bread crumb. Two methods, namely the erosion-dilation method and the closing method, were employed by the authors. Erosion-dilation method characterized both cell and cell wall sizes, whereas the closing method characterized more specifically cell size.

In this thesis, an ITA approach was used that is different from those described above to analyse liquid foam images. Texture was determined using a second order statistical texture method, the gray level co-occurrence matrix (GLCM). The GLCM is a square matrix whose elements correspond to a relative frequency of occurrence $P(i,j,d,\theta)$ of two pixel values (one with intensity i and the other with intensity j) separated by a certain distance d in a given direction θ (Fernández *et al.*, 2005). Matrices present distributions of relative gray levels frequencies that describe how often one gray level will appear in a specified spatial relationship to another gray level. Several GLCM can be built for a particular image depending on parameters d and θ selected. GLCM has the size of the largest pixel value in the image and can be regarded as a 2-D histogram which contains important image texture characteristics. Haralick *et al.* (1973) proposed 14 textural features derived from GLCM, each representing specific image properties. Features are not independent and some represent similar attributes. Most used textural features are energy, contrast, correlation, and inverse difference moment. Energy (or the angular second moment) describes image uniformity. Contrast is a measure of local variations. Correlation is related to brightness values linear dependencies. Figure 1.5C exemplifies results of using this methodology to classify foam images like those shown in Figure 1.5A. Images were analysed to determine different textural features, which were then used to classify foam structures using canonical and Bayesian discriminant analysis. Figure 1.5C shows that images from each of the three proteins become grouped in separate regions according to two textural features (contrast and inverse difference

moment). Results of this analysis on different protein foam architectures are described in detail in Chapter 4.

Spatial distributions

An important limitation of foam characterization studies nowadays is that they do not consider bubbles spatial distribution. Food foams produced by ordinary methods (*e.g.* beating, shaking, sparging, etc.) consist of bubbles randomly mixed and arranged (Weaire and Hutzler, 1999). Determining mean bubble size or even bubble size distributions only describe the elements forming the structure. A higher level of complexity is to specify bubble spatial arrangements (Dickinson, 2007) or the architecture. Consider the three idealized structures built using discs simulating bubbles of two sizes in Figure 1.6A. Images shown share exactly same dimensions and number of elements. Measured bubble size distributions do not differ at all, although structures are completely different just because spatial arrangement variations.

Quantitatively discriminating between different foam architectures is a problem that has not been yet properly addressed and of great importance because of the implications in foam rheological-mechanical responses. A foamed product with evenly distributed gas cells will not behave the same or feel the same in mouth like another formed with unevenly distributed bubbles.

Statistical methods for spatial data analysis commonly employed in geology, geography, and meteorology to describe spatial patterns can prove useful in the analysis of foam architectures. Reed *et al.* (1997) analyzed structure of stable liquid foams formed with a mixture of commercial shaving cream and ethanol from CLSM images in fluorescence mode using second-order stereological methods. Spatial coordinates of foam vertices were determined from images to generate point patterns. Patterns were analyzed with nearest-neighbour distribution functions (*G*-function) and reduced second-moment distribution functions (*K*-function). *G*-functions describe point spatial distributions based on distance measurements from a point to its nearest neighbour and indicate the probability that the distance from a point to its nearest point is less than or

equal to a certain value. *G*-functions are estimated with using Eq. 1.14 (Schabenberger and Gotway, 2005):

$$G(h) = \frac{1}{n}\sum_{i=1}^{n} I(h_i \le h) \tag{1.14}$$

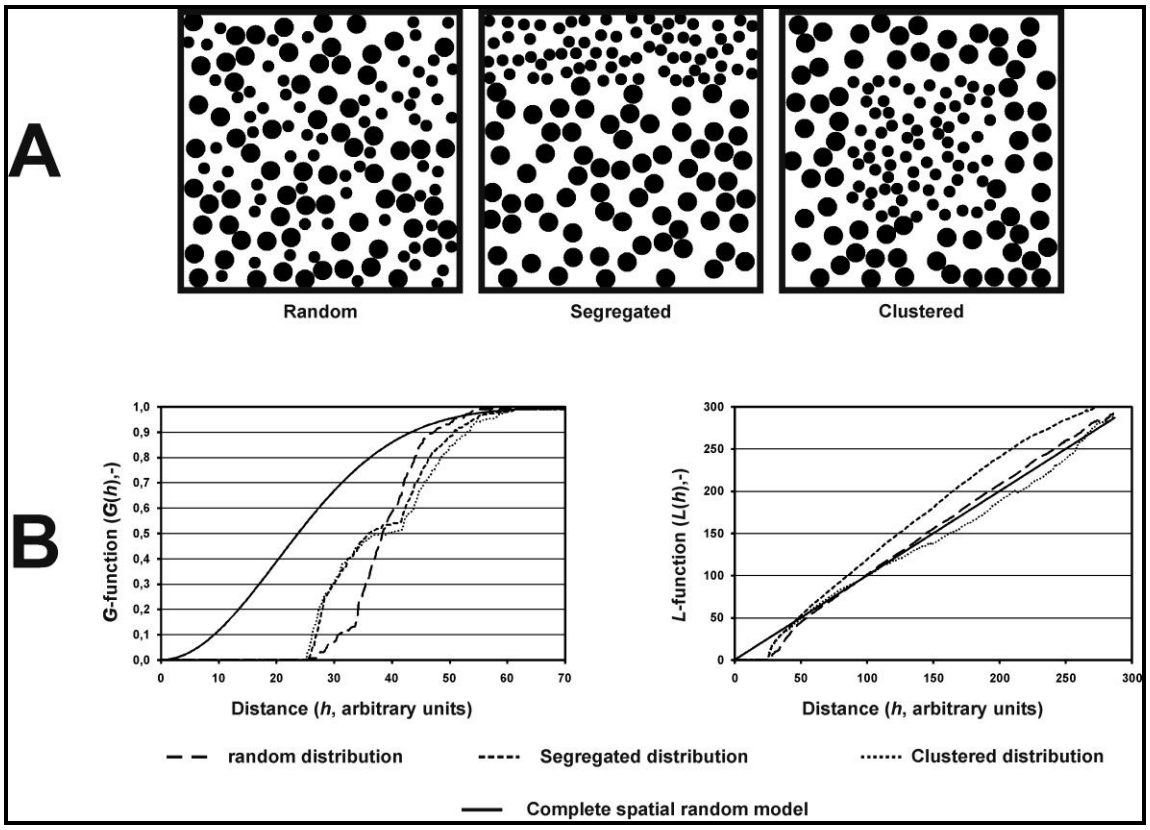

Figure 1.6: (A) Idealized foam structures describing totally different spatial arrangements. Structures are built with discs of two sizes but in one case are randomly distributed, segregated, or clustered. (B) Plots of nearest-neighbour distribution function (*G*-function) and linearized reduced second-moment distribution function (*L*-function) for simulated images like those shown in A, together with the complete spatial random model plots. Each curve corresponds to the average of three simulated images considering either a random, segregated or clustered spatial distribution.

I is an indicator function which returns 1 if $h_i \leq h$. *K*-functions describe points spatial distribution and indicate the mean number of points that lie within a certain radius of a typical point (excluded from the total count). It is estimated by Eq. 1.15 (Schabenberger and Gotway, 2005):

$$K(h) = \frac{1}{n} \sum_{i=1}^{n} \sum_{j \neq i}^{n} I(h_i \leq h) \qquad (1.15)$$

Both calculated empirical functions are compared to a reference model that corresponds to complete spatial randomness (CSR). Point patterns are then classified as being more aggregated or more regular than the reference model. Figure 1.6B shows *G*-functions calculated for simulated images like those shown in Figure 1.6A. Curves shown corresponds to the average of three simulated images considering random, segregated or clustered spatial distributions. Figure 1.6B shows also *L*-functions calculated for simulated images. *L*-functions are linearizations of *K*-functions done to simplify interpretation (Reed *et al.* 1997) where $L(h) = (K(h)/\pi)^{1/2}$. Both distribution functions differ among the simulated distributions.

In this thesis, I used an alternative approach to describe foam architectures. Protein foam images were processed to obtain bubble centroids and centroids patterns were analyzed using geometrical and topological descriptors called Minkowski functionals (Michielsen and De Raedt, 2001). One of these descriptors, the Euler characteristic (χ), represents the number of connected objects minus the number of holes in those objects. Centroids on the images were gradually enlarged, and at each step the value of χ was computed. Curves obtained by plotting χ versus the dilating steps for each image were characterized by four points identified in the curve: maximum and minimum χ, Euler minimum length, and the zero crossing length. Chapter 3 shows that information derived from spatial distribution analysis is complementary to the standard bubble size measurement frequently used to describe foam structures.

1.4. Foam rheology

Last in the length scale levels, foams are considered whole entities with material properties. Main reason to incorporate bubbles into foods is to induce physical changes that in turn provoke desirable sensations. Simple example experienced in kitchens is beating egg whites to obtain meringue. Process begins with a low viscosity fluid and ends with a solid like foam. Liquid foams have the remarkable property of behaving both, as a liquid or a viscoelastic solid depending on the stress value applied when deformed (Hoballah *et al.*, 1997). Figure 1.7 adapted from Weaire *et al.* (1994) accurately accounts this situation. Under small stresses below a yield value, individual bubbles are deformed without significant rearrangements and foams behave as elastic solids. When applied stress is large to surpass a yield stress, irreversible bubble arrangements are triggered and foam flows like a viscous non-Newtonian fluid. Elastic modules (G_0) and yield stress (σ_y) are key parameters that describe rheological behaviour and depend on the foam liquid fraction (Weaire and Hutzler, 1999).

Foam rheological properties have been studied mostly subjecting samples to shear stress (Kampf *et al.*, 2003) under different geometries (cone-plate, plate-plate, and Couette-type). Nevertheless, measuring foam physical properties using standard rheological methods is far from straightforward and needs addressing the particular characteristics of these systems. Measurements reliability depends on samples remaining stable during tests (Niranjan and Silva, 2008). However, foam structures are thermodynamically unstable and change due to Ostwald ripening, liquid drainage, and coalescence. Another problem is wall slip, prevented by roughening contact surfaces (Höler and Cohen-Addad, 2005). Additionally, special care should be taken to ensure homogenous deformation. Misleading measurements are obtained when foams are deformed heterogeneously (Weaire and Hutzler, 1999).

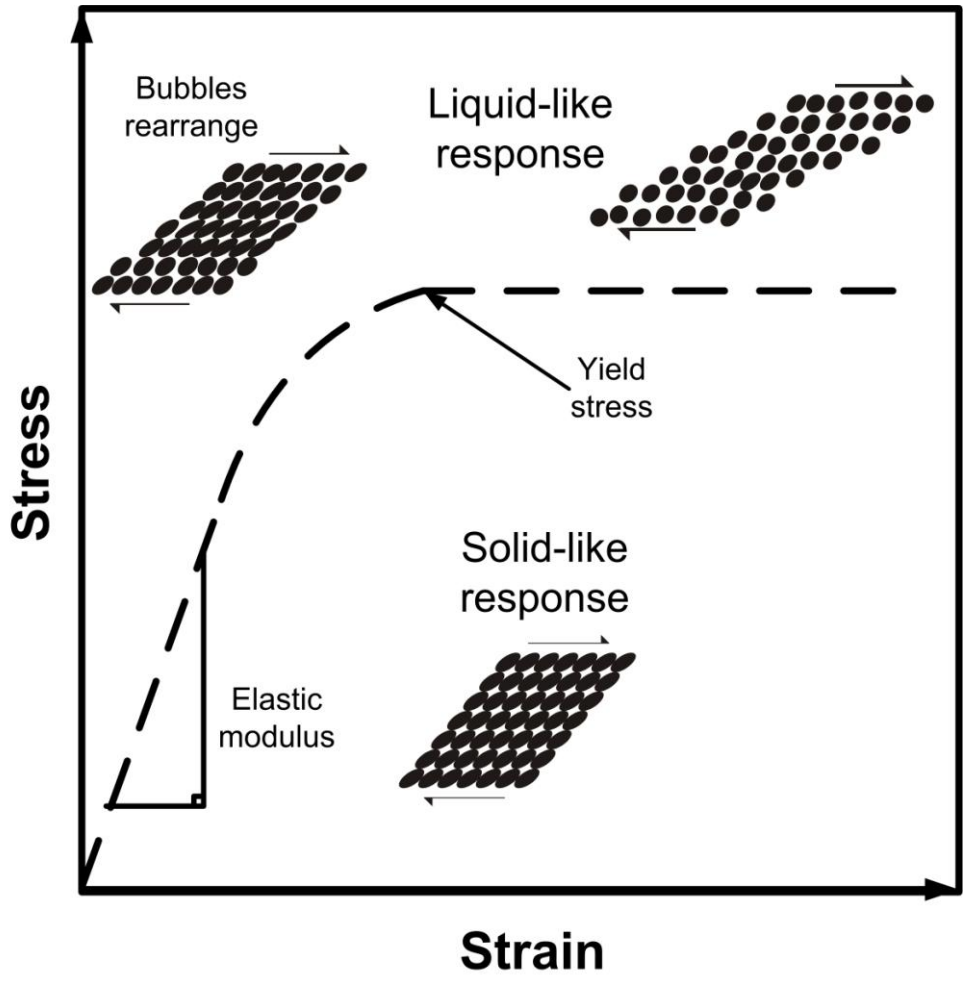

Figure 1.7: Schematic diagram of liquid foams stress-strain response adapted from Weaire *et al*. (1994). Foams behave as elastic solids at low stress-strain values, whereas, over a certain yield stress bubbles begin to come apart as foams flow like viscous non-Newtonian fluids.

1.4.1. Elastic behaviour

Increase in surface area and interfacial energy (*cf*. Eq. 1.1) when foams are subjected to small macroscopic shear stresses gives rise elastic strains. Numerical simulations done on three-dimensional dry random monodispersed and polydispersed foams have determined that G_0 depends on γ and the Sauter mean bubble radius (R_{32}) (Reinelt and Kraynik, 2000):

$$G_0 = 0.51\frac{\gamma}{R_{32}} \tag{1.16}$$

Eq. 1.16 agrees with theoretical predictions, but comparison with real data is not easy because real foams slowly creep and do not settle into truly static equilibrium in response to a step stress. Nevertheless, experimental data extrapolation to the dry limit ($Ø \rightarrow 1$) agrees with Eq. 1.16 (Höler and Cohen-Addad, 2005). Foam elasticity vanishes when $Ø$ reaches values below a critical threshold $Ø_c$ = 0.635 (value for solid spheres closely packed) and that over this G_0 vary according to $Ø(Ø\text{-}Ø_c)$ (Saint-Jalmes and Durian, 1999). Mason *et al.* (1995) proposed the following empirical relation (Eq. 1.17) to describe data on monodispersed emulsion data, which has also been applied to model empirical data on foams (Höler and Cohen-Addad, 2005):

$$G_0 = \alpha\phi(\phi - \phi_c)\frac{\gamma}{\bar{R}} \tag{1.17}$$

Here, α is a dimensionless prefactor usually adopting a value of 1.6 or lower, and $\bar{R}$ the mean bubble diameter.

1.4.2. Viscoelastic behaviour

Foams are not purely elastic solids at small strains but show slow viscoelastic relaxations. Determination of viscoelastic characteristics of soft matter such as foams most commonly involves application of oscillatory shear. Small sinusoidal oscillatory deformations allow measuring the complex shear modulus (G^*):

$$\sigma(t) = G^*(\omega)\varepsilon(t) \tag{1.18}$$

The complex shear modulus accounts for the viscoelastic response of samples and is decomposed in storage (G') and loss (G'') modulus:

$$G^* = G' + iG'' \tag{1.19}$$

Experimental evidence has shown that G^* behaves as if a viscoelastic contribution proportional to $i(\omega)^{1/2}$ were superposed on a constant purely elastic shear modulus in a regime of high angular frequencies (Höler and Cohen-Addad, 2005). At low frequencies, G' presents a plateau value and is almost independent of ω increasing and becoming significantly different from the static elasticity (G_0) only at much higher frequencies. G'' is also virtually frequency independent at low ω values, but extent is smaller. G'' increases with frequency proportional to $\omega^{1/2}$ at values above 1-10 Hz. Conventional linear viscoelasticity theory is not strictly applicable to foams and even small topological arrangements in the structure are sings of plastic deformation (Weaire and Hutzler, 1999). However, oscillatory experiments have showed only a weak dependence of G' and G'' on strain amplitudes for small amplitudes. Additionally, absence of strain induced bubble rearrangements detected through an optical technique (Hoballah *et al.*, 1997), and the relation established between G^* and stress response measured as function of time after application of step stains through the Fourier transform (Gopal and Durian, 2003), have confirmed the existence of a defined linear viscoelastic regime for wet foams.

When drainage and coarsening are negligible and foam structure evolves due purely to disproportionation it has been proposed that G^*evolution can be followed with the empirical scaling law (Cohen-Addad *et al.*, 1998):

$$G^*(\omega,t) = b(t)G^*(\omega a(t),t_0) \tag{1.20}$$

Scaling factors $a(t)$ and $b(t)$ are by definition equal to one at arbitrary reference time t_0 and independent of frequency. The model expressed by Eq. 1.20 has the particular property of grouping rheological experimental data of coarsening foams into a master curve.

1.4.3. Yielding behaviour

Passage from solid-like to liquid-like mechanical behaviour in liquid foams is characterized by the maximum applied stress for which foams will not flow.

Experimental procedures to determine yield stress (σ_y) involve shear start-up experiments with a constant strain rate where σ_y is deduced from maximum stresses (Khan *et al.*, 1988), foam flow over inclined planes (Rouyer *et al.*, 2005), and measuring rheological response to an imposed oscillating stress or strain as a function of amplitude (Saint-Jalmes and Durian, 1999; Rouyer *et al.*, 2005). Values of σ_y obtained from oscillatory experiments are robust quantities (Rouyer *et al.*, 2005). The following expression has been found to roughly agree with σ_y experimental data in aqueous foams and emulsions:

$$\sigma_y = \beta \frac{\gamma}{R} \left(\phi - \phi_c\right)^2 \tag{1.21}$$

However, the sharp σ_y rise with Ø is not described accurately by Eq. 1.21 (Gardiner *et al.*, 1998). Raharitsifa *et al.* (2006) proposed a generalized expression for σ_y of foams as a function of their structural properties to describe experimental data on apple juice foams (Eq. 1.22).

$$\sigma_y = B' \frac{\phi^v}{D_{32}^b} \tag{1.22}$$

1.4.4. Non-Newtonian flow behaviour

Beyond σ_y foams flow like a viscous non-Newtonian fluid. Flow phenomenon is complex and not fully understood (Höler and Cohen-Addad, 2005). Macroscopically, foam steady flow behaviour is described by an effective viscosity (μ_{eff}) defined as the ratio of σ to the effective shear strain rate $(\dot{\varepsilon})$. Llewellin *et al.* (2002) developed a generalized equation to describe the evolution of μ_{eff} with Ø that accounts existence of two different flow regimes based on the extent of bubble distortion:

$$\mu_r = \frac{1}{3}\sqrt{9 - 300 + 250\phi^2 + \frac{\left(450b + 750\right)\phi + \left(225b^2 - 625\right)\phi^2}{25 + 36C_d^2}} \tag{1.23}$$

C_d is a measure of flow steadiness given by the ratio of bubble relaxation time (λ) to the timescale over which the strain rate changes appreciable. Flow curves measured for foams are often fitted using the phenomenological Herschel-Bulkley law (Larson 1999):

$$\begin{aligned} \dot{\varepsilon} &= 0 \qquad\qquad for \quad \sigma \le \sigma_y \\ \sigma &= \sigma_y + \zeta \dot{\varepsilon}^{n} \quad for \quad \sigma \le \sigma_y \end{aligned} \tag{1.24}$$

where ξ and n are empirical parameters. However, flow behaviour of aqueous foams has proved more complex showing that Eq. 1.24 is incapable of capturing all the physics that affects foams flow.

1.5. Outline of the thesis

Work presented in this document has been done keeping in mind the scheme in Figure 1.1. Chapter 2 describes and compares interfacial properties of sodium caseinate and a conjugate produced by the chemical reaction of the protein with a carbohydrate. Differences in interfacial behaviour are discussed in relation to their different foaming properties. Chapter 3 shows results from protein stabilized foams structures based on spatial distributions. It is demonstrated this information complements bubble sizes data in foam structure characterization. Finally Chapter 4 presents different image analysis tools that may be applied to evaluate and discriminate foams produced by proteins according to their particular structural attributes. It is shown that these techniques can be affectively used to discriminate between systems produced from different foaming agents under identical conditions based solely on structural data.

A visual description of how the chapters in this thesis relate between each other at the different scales in foam analysis is depicted in Figure 1.1. Chapter 2 focus on the molecular level and the links with the liquid film size and continuous foam size levels. Chapter 3 and 4 focus also the differences between proteins at the molecular level, but here the impact on the gas cell size level is the main objective.

1.6. References

Adachi, M., Ho, C.Y. and Utsumi, S. (2004). Effects of designed sulfhydryl groups and disulfide bonds into soybean proglycinin on its structural stability and heat induced gelation. *Journal of Agricultural and Food Chemistry*, 52, 5717-5723.

Aguilera J.M. (2006). Seligman Lecture 2005 - Food product engineering: Building the right structures. *Journal of the Science of Food and Agriculture*, 86(8), 1147-1155.

Aguilera, J.M. and Germain, J.C. (2007). Advances in image analysis for the study of food microstructure. In D.J. McClements (Ed.) *Understanding and controlling the microstructure of complex foods*, Woodhead Publishing Limited, Cambridge, England, pp. 261-287.

Aguilera. J.M. and Stanley, D.W. (1999). *Microstructural Principles of Food Processing and Engineering (2nd. Ed.)*, Gaithersburg, MD, Aspen Publishers Inc.

Aksenenko, E.V. (2001). Software tools to interpret the thermodynamics and kinetics of surfactant adsorption. In V.B. Fainerman, D. Möbius and R. Miller (Eds.) *Surfactants: Chemistry, Interfacial Properties, Applications*, Elsevier Science B.V., Amsterdam, The Netherlands, pp. 619-649.

Alavi, S.H., Gogoi, B.K., Khan, M., Bowman, B.J. and Rizvi, S.S.H. (1999). Structural properties of protein-stabilized starch-based supercritical fluid extrudates. *Food Research International*, 32(2), 107-118.

Andreas. J.M., Hauser, E.A. and Tucker, W.B. (1938). Boundary tension by pendant drops. *Journal of Physical Chemistry*, 42, 1001-1019.

Babin, P., Della Valle, G., Chiron, H., Cloetens, P., Hoszowska, J., Pernot, P., Réguerre, A.L., Salvo, L. and Dendievel R. (2006). Fast X-ray tomography analysis of bubble growth and foam setting during bread making. *Journal of Cereal Science*, 43, 393-397.

Babin, P., Della Valle, G., Dendievel, R., Lassoued, N. and Salvo, L. (2005). Mechanical properties of bread crumbs from tomography based Finite Element simulations. *Journal of Materials Science*, 40(22), 5867-5873.

Bals, A. and Kulozik, U. (2003). Effect of pre-heating on the foaming properties of whey protein isolate using a membrane foaming apparatus. *International Dairy Journal*, 13(11), 903-908.

Baniel, A., Fains, A., and Popineau, Y. (1997). Foaming properties of egg albumen with a bubbling apparatus compared with whipping. *Journal of Food Science*, 62, 377-381.

Beneventi, D., Pugh, R.J., Carré, B. and Gandini A. (2003). Surface rheology and foaming properties of sodium oleate and C12(EO)6 aqueous solutions. *Journal of Colloid and Interface Science*, 268, 221-229.

Benjamins, J. and Lucassen-Reynders, E.H. (1998). Surface dilational rheology of proteins adsorbed at air/water and oil/water interfaces. In D. Möbius and R. Miller (Eds.) *Proteins at Liquid Interfaces*. Elsevier Science B.V., Amsterdam, The Netherlands, pp. 341-384.

Benjamins, J., Cagna, A. and Lucassen-Reynders, E.H. (1996). Viscoelastic properties of triacylglycerol/water interfaces covered by proteins. *Colloids and Surfaces A: Physicochemical and Engineering Aspects*, 114, 245-254.

Bertrand, D., Le Guerneve, C., Marion, D., Devaux, M.F. and Robert, P. (1992). Description of the textural appearance of bread crumb by video image analysis. *Cereal Chemistry*, 69, 257-261.

Bisperink, C.G.J. , Akkerman, J.C., Prins, A. and Ronteltap, A.D. (1992). A moving optical fibre technique for structure analysis of heterogeneous products: application to the determination of the bubble-size distribution in liquid foams. *Food Structure*, 11, 101-108.

Bos, M.A. and Van Vliet, T. (2001). Interfacial rheological properties of adsorbed proteins layer and surfactants: a review. *Advances in Colloid Interface Science*, 91, 437-471.

Branden, C. and Tooze, J. (1991). *Introduction to protein structure*. Garland Publishing Inc., New York, USA.

Cagna, A., Esposito, G., Rivière, C., Housset, S. and Verger, R. (1992). *3rd International Conference on the Biochemistry of Lipids*, Lyon.

Campbell, G.M. and Mougeot E. (1999). Creation and characterisation of aerated food products. *Trends in Food Science and Technology*, 10(9), 283-296.

Carrera Sánchez, C. and Rodríguez Patino, J.M. (2005). Interfacial, foaming and emulsifying characteristics of sodium caseinate as influenced by protein concentration in solution. *Food Hydrocolloids*, 19, 407-416.

Carrera Sánchez, C., Rodríguez Niño M.R., Caro, A.L. and Rodríguez Patino, J.M. (2005). Biopolymers and emulsifiers at the air–water interface. Implications in food colloid formulations. *Journal of Food Engineering*, 67, 225-234.

Cauvain, S.P. (2003). Inside the cell structures of bakery products. *The World of Food Ingredients*, 2, 24-28.

Chang, Y. and Hartel, R.W. (2002). Measurement of air cell distributions in dairy foams. *International Dairy Journal*, 12(5), 463-472.

Cohen-Addad, S., Hoballah, H. and Höler, R. (1998). Viscoelastic response of a coarsening foam. *Physical Review E*, 57(6), 6897-6901.

Creighton, T.E. (1993). *Proteins: Structure and Molecular Properties* (2nd edition). W.H. Freeman and Company, New York, USA.

Damodaran, S. (2005). Protein stabilization of emulsions and foams. *Journal of Food Science*, 70(3), R54-R66.

de Gennes, P.-G., Brochard-Wyart, F. and Quéré, D. (2004). *Capillarity and wetting phenomena. Drops, bubbles, pearls, waves*. Springer-Verlag New York, Inc., New York, USA.

de Jongh, H.H.J. (2007). Proteins in food microstructure formation. In D.J. McClements (Ed.) *Understanding and controlling the microstructure of complex foods*, Woodhead Publishing Limited, Cambridge, England, pp. 40-66.

Dickinson, E. (2007). Colloidal systems in foods containing droplets and bubbles. In D. J. McClements (Ed.) *Understanding and controlling the microstructure of complex foods*. Woodhead Publishing Limited, Cambridge, UK, pp. 153-184.

Dickinson, E., Ettelaine, R., Murray, B.S. and Du, Z. (2002). Kinetics of disproportionation of air bubbles beneath the planar air-water interface stabilized by food proteins. *Journal of Colloid and Interface Science*, 252, 202-213.

Douillard, R., Daoud, M. and Aguié-Béghin, V. (2003). Polymer thermodynamics of adsorbed protein layers. *Current Opinion in Colloid and Interface Science*, 8, 380-386.

Duce, S.L., Amin, M.H.G., Horsfield, M.A., Tyszka, M. and Hall, L.D. (1995). Nuclear-magnetic-resonance imaging of dairy-products in 2-dimensions and 3-dimensions. *International Dairy Journal*, 5(4), 311-319.

Eisner, M.D., Wildmoser, H. and Windhab, E.J. (2005). Air cell microstructuring in a high viscous ice cream matrix. *Colloids and Surfaces A-Physicochemical and Engineering Aspects*, 263(1-3), 390-399.

Fainerman, V.B., Lucassen-Reynders, E.H. and Miller, R. (2003). Description of the adsorption behaviour of protein at water/fluid interfaces in the framework of a two-dimensional solution model. *Advances in Colloid Interface Science*, 106, 237-259.

Fains, A., Bertrand, D., Baniel A. and Popineau Y. (1997). Stability and texture of protein foams: a study by video image analysis. *Food Hydrocolloids*, 11(1), 63-69.

Fernández, L., Castillero C. and Aguilera, J.M. (2005). An application of image analysis to dehydration of apple discs. *Journal of Food Engineering*, 67(1-2), 185-193.

Fox, P., Smith, P.P. and Sahi, S. (2004). Ultrasound measurements to monitor the specific gravity of food batters. *Journal of Food Engineering*, 65, 317-324.

Gardiner, B.S., Dlugogorski, B.Z., Jameson, G.J. and Chhabra R.P. (1998). Yield stress measurements of aqueous foams in the dry limit. *Journal of Rheology*, 42, 1437-1450.

Germain, J.C. and Aguilera, J.M. (2008). Quantification of the structural changes in foams stabilized by proteins via image analysis. In G. Campbell, M. Scanlon and L. Pyle (Eds.) *Bubbles in Food 2: Novelty, Health and Luxury*. Eagan Press, St. Paul, USA, pp. 83-87.

German, J.B. and McCarthy, M.J. (1989). Stability of aqueous foams - Analysis using magnetic-resonance imaging. *Journal of Agricultural and Food Chemistry*, 37(5), 1321-1324.

Golding, M. and Sein, A. (2004). Surface rheology of aqueous casein-monoglyceride dispersions. *Food Hydrocolloids*, 18, 451-461.

Gopal, A.D. and Durian, D.J. (2003). Relaxing in foam. *Physical Review Letters*, 91, 2051-2054.

Grigoriev, D.O., Fainerman, V.B., Makievski, A.V., Krägel, J.,Wüstneck, R. and Miller, R. (2002). β-casein bilayer adsorption at the solution/air interface: experimental evidences and theoretical description. *Journal of Colloid and Interface Science*, 253, 257-264.

Guillerme, C., Loisel, W., Bertrand, D. and Popineau, Y. (1993). Study of foam stability by video image analysis: relationship with the quantity of liquid in the foams. *Journal of Texture Studies*, 24, 287-302.

Gunning, P.A., Mackie, A.R., Gunning, A.P., Wilde, P.J., Woodward, N.C. and Morris, V.J. (2004). The effect of surfactant type on protein displacement from the air-water interface. *Food Hydrocolloids*, 18, 509-515.

Haedelt, J., Pyle, D.L., Beckett, S.T. and Niranjan, K. (2005). Vacuum-induced bubble formation in liquid-tempered chocolate. *Journal of Food Science*, 70, E159-E164.

Hagolle, N., Relkin, P., Popineau Y. and Bertrand, D. (2000). Study of the stability of egg white protein-based foams: Effect of heating protein solution. *Journal of the Science of Food and Agriculture*, 80(8), 1245-1252.

Haralick, R.M., Shanmugam, K. and Dinstein, I. (1973). Textural features for image classification. *IEEE Transactions on Systems, Man, and Cybernetics*, 6, 610-621.

Hicsasmaz, Z., Yazgan, Y., Bozoglu, F. and Katnas, Z. (2003). Effect of polydextrose-substitution on the cell structure of the high-ratio cake system. *Lebensmittel-Wissenschaft Und-Technologie-Food Science and Technology*, 36(4), 441-450.

Hoballah, H., Höler, R. and Cohen-Addad, S. (1997). Time evolution of the elastic properties of aqueous foam. *Journal de Physique II*, 7, 1215-1224.

Höler, R. and Cohen-Addad, S. (2005). Rheology of liquid foam. *Journal of Physics: Condensed Matter*, 17, R1041-R1069.

Jang, W., Nikolov, A., Wasan, D.T., Chen, K. and Campbell, B. (2005). Prediction of the bubble size distribution during aeration of food products. *Industrial and Engineering Chemistry Research*, 44(5), 1296-1308.

Joos, P. and Serrien, G.J. (1991). The principle of Braun-Le Châtelier at surfaces. *Journal of Colloid and Interface Science*, 145, 291-294.

Kampf, N., Martinez, C.G., Corradini, M.G. and Peleg, M. (2003). Effect of two gums on the development, rheological properties and stability of egg albumen foams. *Rheologica Acta*, 42(3), 259-268.

Kato, A., Osako, Y., Matsudomi, N. and Kobayashi, K. (1983). Changes in emulsifying and foaming properties of proteins during heat denaturation. *Agricultural and Biological Chemistry*, 47, 33-38.

Khan, S.A., Schnepper, C.A. and Armstrong, R.C. (1988). Foam rheology: III. Measurement of shear flow properties. *Journal of Rheology*, 32, 69-92.

Kloek W., van Vliet T. and Meinders M. (2001). Effect of bulk and interfacial rheological properties on bubble dissolution. *Journal of Colloid and Interface Science*, 237, 158-166.

Krustev, R., Platikanov, D. and Nedyalkov, M. (1996). Temperature dependence of gas permeability of Newton black films. *Langmuir*, 12, 1688-1689.

Kulmyrzaev, A., Cancelliere, C. and McClements, D.J. (2000). Characterization of aerated foods using ultrasonic reflectance spectroscopy. *Journal of Food Engineering*, 46(4), 235-241.

Labourdenne, S., Gaudry-Rolland, N., Letellier, S., Lin, M., Cagna, A., Esposito, G., Verger, R. and Riviere, C. (1996). The oil-drop tensiometer: potential applications for

studying the kinetics of (phospho)lipase action. *Chemistry and Physics of Lipids*, 71, 163-173.

Larson R.G. (1999). *The Structure and Rheology of Complex Fluids*. Oxford University Press, New York, USA.

Lim, K.S. and Barigou, M. (2004). X-ray micro-computed tomography of cellular food products. *Food Research International*, 37(10), 1001-1012.

Liu, M. and Damodaran, S. (1999). Effect of transglutaminase-catalyzed polymerization of β-casein on its emulsifying properties. *Journal of Agricultural and Food Chemistry*, 47, 1514-1519.

Llewellin, E.W., Mader, H.M. and Wilson, S.D.R. (2002). The constitutive equation and flow dynamics of bubbly magmas. *Geophysical Research Letters*, 29(24), 2170.

Logley, W.R. and Van Name, R.G. (1928). *The Collected Works of J. Willard Gibbs, I: Thermodynamics*. Longmans, Green, and Company, New York, USA.

Lucassen, J. and van den Tempel, M. (1972). Dynamic measurements of dilational properties of a liquid interface. *Chemical Engineering Science*, 27, 1283-1291.

Lucassen-Reynders, E.H, Fainerman, V.B. and Miler, R. (2004). Surface dilational modulus or Gibbs' elasticity of protein adsorption layers. *Journal of Physical Chemistry*, 108, 9173-9176.

Lucassen-Reynders, E.H. (1993). Interfacial viscoelasticity in emulsions and foams. *Food Structure*, 12(1), 1-12.

Maldonado-Valderrama, J., Fainerman, V.B., Aksenenko, E.V., Gàlvez-Ruiz, M.J., Cabrerizo-Vílchez, M.A. and Miller, R. (2005). Dynamics of protein adsorption at the

oil–water interface: comparison with a theoretical model. *Colloids and Surfaces A: Physicochemical and Engineering Aspects*, 261, 85-92.

Martinet, V., Valentini, C., Casalinho, J., Schorsch, C., Vaslin, S. and Courthaudon, J.-L. (2005). Composition of interfacial layers in complex food emulsions before and after aeration: effect of egg to milk protein ratio. *Journal of Dairy Science*, 88, 30-39.

Mason, T.G., Bibette, J. and Weitz, D. A. (1995). Elasticity of compressed emulsions. *Physical Review Letters*, 75, 2051-2054.

Michielsen, K. and De Raedt, H. (2001). Integral-geometry morphological image analysis. *Physics Reports*, 347, 461-538.

Miller, R., Fainerman, V.B., Aksenenko, E.V., Leser, M. E. and Michel, M. (2004). Dynamic surface tension and adsorption kinetics of β-casein at the solution/air interface. *Langmuir*, 20, 771-777.

Miller, R., Fainerman, V.B., Makievski, A.V., Krägel, J., Grigoriev, D.O., Kazakov. V.N. and Sinyachenko, O.V. (2000). Dynamics of protein and mixed protein/surfactant adsorption layers at the water/fluid interface. *Advances in Colloid Interface Science*, 86, 39-82.

Möbius, D. and Miller, R. (1998). *Drops and Bubbles in Interfacial Research*, Elsevier, Amsterdam.

Morris, G.A., Sims, I.M., Robertson, A.J. and Furneaux, R.H. (2004). Investigation into the physical and chemical properties of sodium caseinate-maltodextrin glyco-conjugates. *Food Hydrocolloids*, 18, 1007-1014.

Nedyalkov, M., Krustev, R., Kashchiev, D., Platikanov, D. and Exerowa, D. (1988). Permeability of Newtonian black foam films to gas. *Colloid Polymer Science*, 266, 291-296.

Nedyalkov, M., Krustev, R., Stankova, A. and Platikanov, D. (1992). Mechanism of permeation of gas through Newton black films at different temperatures. *Langmuir*, 8, 3142-3144.

Niranjan, K. and Silva, S.F.J. (2008). Bubble-Containing Foods. In J.M. Aguilera and P.J. Lillford (Eds.) *Food Material Science*. Springer Science+Business Media LLC, New York, USA, pp. 281-303.

Onwulata, C.I., Konstance, R.P., Cooke, P.H. and Farrell, H.M.Jr. (2003). Functionality of extrusion-texturized whey proteins. *Journal of Dairy Science*, 86, 3775-3782.

Petkova, V., Sultanem, C., Nedyalkov, M., Benattar, J., Leser, M.E. and Schmitt, C. (2003). Structure of a freestanding film of *β*-lactoglobulin. *Langmuir*, 19, 6942-6949.

Pizones Ruíz-Henestrosa V., Carrera Sánchez, C. and Rodríguez Patino. J.M. (2007). Formulation engineering can improve the interfacial and foaming properties of soy globulins. *Journal of Agricultural and Food Chemistry*, 55, 6339-6348.

Plateau, J.A.F. (1873). *Statique Expérimentale et Théorique des Liquides soumis aux seules Forces Moléculaires*, Gauthier-Villars, Paris, France.

Platikanov, D., Nedyalkov, M. and Nasteva, V. (1980). Line tension of Newton black films II. Determination by the diminishing bubble method. *Journal of Colloid and Interface Science*, 75(2), 620-6289.

Prins, A., Bos, M.A., Boerboom, F.J.G. and Van Kalsbeek, H.K.A.I. (1998). Relation between surface rheology and foaming behaviour. In D. Möbius and R. Miller (Eds.) *Proteins at Liquid Interfaces*. Elsevier Science B.V., Amsterdam, The Netherlands, pp. 221-265.

Pugh, R.J. (2005). Experimental techniques for studying the structure of foams and froths. *Advances in Colloid and Interface Science*, 114, 239-251.

Rahali, V. and Gueguen, J. (2000). Foaming characteristics of chemical and enzymatic hydrolysates of bovine beta-lactoglobulin. *Nahrung*, 44(5), 309-317.

Raharitsifa, N., Genovese, D.B. and Ratti, C. (2006). Characterization of apple juice foams for foam-mat drying prepared with egg white protein and methylcellulose. *Journal of Food Science*, 71(3), E142-E151.

Ralet, M.C. and Guéguen J. (2001). Foaming properties of potato raw proteins and isolated fractions. *Lebensmittel Wissenschaft und Technologie*, 34, 266-269.

Razumovsky, L. and Damodaran, S. (1999). Surface activity-Compressibility relationship of proteins. *Langmuir*, 15, 1392-1399.

Reed, M.G., Howard, C.V. and Shelton, C.G. (1997). Confocal imaging and second-order stereological analysis of liquid foam. *Journal of Microscopy*, 185, 313-320.

Reinelt, D.A. and Kraynik, A.M. (2000). Simple shearing flow of dry soap foams with tetrahedrally close-packed structure. *Journal of Rheology*, 44, 453-471.

Richardson, G., Langton, M., Faldt, P. and Hermansson, A.M. (2002). Microstructure of alpha-crystalline emulsifiers and their influence on air incorporation in cake batter. *Cereal Chemistry*, 79(4), 546-552.

Rodriguez Patino, J.M., Rodríguez Nino, R. and Alvarez Gomez, J.M. (1997). Interfacial and foaming characteristics of protein-lipid systems. *Food Hydrocolloids*, 11(1), 49-58.

Rouillé, J., Della Valle, G., Devaux, M.F., Marion, D. and Dubreil, L. (2005). French bread loaf volume variations and digital image analysis of crumb grain changes induced by the minor components of wheat flour. *Cereal Chemistry*, 82(1), 20-27.

Rouyer, F.R, Cohen-Addad, S. and Höler, R. (2005). Is the yield stress of aqueous foams a well defined quantity? *Colloids and Surfaces A: Physicochemical and Engineering Aspects*, 263, 111-116.

Russ, J.C. (2005). *Image Analysis of Food Microstructure*. Boca Raton, Florida, EE.UU.: CRC Press LLC.

Russo, C. (2000). Food foams. *Industrie Alimentari*, 39(391), 425-443.

Sahi, S.S. and Alava, J.M. (2003). Functionality of emulsifiers in sponge cake production. *Journal of the Science of Food and Agriculture*, 83(14), 1419-1429.

Saint-Jalmes, A. and Durian, D.J. (1999). Vanishing elasticity for wet foams: Equivalence with emulsions and role of polydispersity. *Journal of Rheology*, 43, 1411-1432.

Sarker, D.K., Bertrand, D., Chtioui, Y. and Popineau, Y. (1998). Characterisation of foam properties using image analysis. *Journal of Texture Studies*, 29, 15-42.

Schabenberger, O. and Gotway, C.A. (2005). *Statistical methods for spatial data analysis*. Chapman & Hall/CRC, Boca Raton, Florida, USA.

Schmitt, C., Bovay, C, Rouvet, M., Shojaei-Rami, S., and Kolodziejczyk, E. (2007). Whey protein soluble aggregates from heating with nacl: physicochemical, interfacial, and foaming properties. *Langmuir*, 23, 4155-4166.

Schmitt, C., Palma Da Silva, T., Bovay, C., Rami-Shojaei, S., Frossard, P., Kolodziejczyk, E. and Leser, M.E. (2005). Effect of time on the interfacial and foaming properties of β-lactoglobulin/acacia gum electrostatic complexes and coacervates at pH 4.2. *Langmuir*, 21, 7786-7795.

Schoonman, A., Mayor, G., Dillmann, M.L., Bisperink, C. and Ubbink, J. (2001). The microstructure of foamed maltodextrin/sodium caseinate powders: a comparative study by microscopy and physical techniques. *Food Research International*, 34(10), 913-929.

Sitohy, M., Chobert, J.M., Popineau, Y. and Haertle, T. (1995). Functional properties of *β*-lactoglobulin phosphorylated in the presence of different aliphatic amines. *Lait*, 75, 503-512.

Stauffer, C.E. (1965). The measurement of surface tension by the pendant drop technique. *Journal of Physical Chemistry*, 69, 1933-1938.

Tranchant, J.F., Bonté, F., Leroy, S., Nedyalkov, M., Platikanov, D., Javierre, I. and Jean-Benattar, J.J. (2002). Black foam films from aqueous solutions of a mixture of phospholipids and a permeation enhancer. *Journal of Colloid and Interface Science*, 249, 398-404.

Trater, A.M., Alavi, S. and Rizvi, S.S.H. (2005). Use of non-invasive X-ray microtomography for characterizing microstructure of extruded biopolymer foams. *Food Research International*, 38(6), 709-719.

Utsumi, S., Maruyama, N., Satoh, R. and Adachi, M. (2002). Structure-function relationships of soybean proteins revealed by using recombinant systems. *Enzyme and Microbial Technology*, 30, 284-288.

Walstra, P. and Smulders, I. (1997). Making emulsions and foams: an overview. In E. Dickinson and B. Bergenståhl (Eds.) *Food Colloids – Proteins, Lipids and Polysaccharides*. Woodhead Publishing Limited, Cambridge, UK, pp. 367-381.

Weaire, D. and Hutzler, S. (1999). *The Physics of Foams*. Clarendon Press, Oxford, UK.

Weaire, D., Fortes, M.A. and Portugal, L. (1994). Stress and strain in liquid and solid foams. *Advances in Physics*, 43(6), 685-738.

Xu, S. and Damodaran, S. (1993). Comparative adsorption of native and denatured egg-white, human, and T_4 phage lysozymes at the air/water interface. *Journal of Colloid and Interface Science*, 159, 124-133.

Yu, M.-A. and Damodaran, S. (1991). Kinetics of protein foam destabilization: Evaluation of a method using bovine serum albumin. *Journal of Agricultural and Food Chemistry*, 39, 1555-1562.

Zheng, C.X., Sun, D.W. and Zheng, L.Y. (2006). Recent applications of image texture for evaluation of food qualities - a review. *Trends in Food Science and Technology*, 17(3), 113-128.

Zhu, H. and Damodaran, S. (1994). Heat-induced conformational changes in whey protein isolate and its relation to foaming properties. *Journal of Agricultural and Food Chemistry*, 42, 846-855.

2. CHANGES IN SODIUM CASEINATE INTERFACIAL AND FOAMING PROPERTIES BY CONJUGATION

2.1. Introduction

Liquid foams are two phase systems where a gas is dispersed in a liquid as bubbles. Stabilization of the new interfacial surface produced during foam formation requires the presence of surface active molecules. Amphiphilic molecules (surfactants) adsorb at interfaces forming layers that prevent coalescence of freshly formed bubbles (Prins *et al*., 1998; Russo, 2000; Dukhin *et al*., 1995). The first direct consequence of surfactant adsorption is reduction of surface tension, energy required to produce an additional interface. Lower interfacial tensions make bubbles more deformable and easier to disperse (Wilde, 2000). Stable foam creation requires small bubbles and besides energy input and physical properties of phases, interfacial tension is a key factor controlling bubble size. However, interfacial tension reduction cannot explain foam formation with more than a transient short-lived stability. As argued by Lucassen-Reynders (1993), if this were the case it should be possible to prepare foams directly from pure low-tension liquids in absence of surfactants.

Many foam-based food products owe their existence to proteins (Russo, 2000; Damodaran, 2005). These macromolecules are essential in food foam formation because of their amphiphilic nature. Proteins not only contribute to lowering surface tensions, but also stabilizing bubble surfaces because of specific rheological properties they impart to interfaces (Bos and van Vliet, 2001). Proteins form viscoelastic networks sometimes referred to as two-dimensional gels that stabilize interfacial layers kinetically, in contrast to small surfactant molecules that form adsorbed layers of mobile fluid stabilizing interfaces via the Gibbs–Marangoni effect (Gunning, *et al.* 2004; Golding and Sein, 2004; Carrera Sánchez *et al.*, 2005).

Although proteins significantly contribute to gas cell wall stabilization, foams are unstable and change with time. Stability of aerated systems is affected by three basic mechanisms: drainage, Ostwald ripening, and coalescence (Lau and Dickinson, 2005).

Liquid drains by gravity through channels that are formed between gas bubbles thus, they pack closer together as the liquid fraction decreases. Pressure differences between foam bubbles drive gas diffusion through the films that separate them. Smaller bubbles shrink and disappear while others initially grow because of the Ostwald ripening processes. Finally, foams collapse due to film rupture and bubble coalescence. Many factors can be adducted to account for this such as film thinning because of drainage, inadequate surfactant concentration, presence of impurities or antifoaming agents (Weaire and Hutzler, 1999).

Drainage rate is commonly retarded by increasing the viscosity of the continuous phase (Dutta *et al.*, 2004). Also, the chemical and physical nature of surface active molecules has an important effect on stability. Gas diffusion through bubble walls can be reduced by better molecular packing over interfaces thus limiting permeabillity. Bubble film resistance to rupture can be enhanced by using molecules that link more tightly and resist rupture forces (Dickinson, 1992). Molecules that differ chemically and physically can exhibit different foaming properties during foam formation and/or foam stability.

Proteins pack and link strongly near their isoelectric point because repulsion electric charges are neutralized. However, moving close to isoelectric pH drastically reduces surface active properties because of charge decrease and loss of solubility. It has been speculated that chemical modification of proteins via conjugation with polysaccharides may improve their surface properties, especially at low pH as the iso-electric point and solubility will be altered and molecular integrity maintained (Morris *et al.*, 2004).

The objective of this work was to compare the interfacial behaviour and foaming properties of a common food protein, sodium caseinate, and a conjugate obtained via its chemical reaction with a commercially available polysaccharide used in food industries (Glucidex®21). If conjugation modifies the surface active behaviour of protein, then it may be possible to obtain improved foaming properties using conjugates

rather than proteins, particularly at a pH closer to isoelectric conditions. Analytical techniques used in this work included surface tension measurements using Wilhelmy plate method and dynamic bubble shape analysis, foaming behaviour in an analytic foam characterizing system, analysis of protein adsorption and surface rheology via dynamic bubble shape analysis, and study of film permeability with a variation of the diminishing bubble method.

2.2. Materials and Methods

2.2.1. Samples and preparation

Sodium caseinate was obtained from Emmi Suisse SA (Dagmersellen, Switzerland). Measured solid content was 92.46%. Sodium caseinate was conjugated with Glucidex 21 (Roquette Fréres, Lestrem, France), a low DE dried glucose syrup obtained by starch hydrolysis, as described by Gloria-Hernández (2006). Conjugation reaction was done by incubation for 12 hrs at 70ºC of a sodium caseinate:Glucidex 21 mixture (weight ratio 1:5; 60% total solids). The reaction product was purified via ion-exchange chromatography to remove unreacted macromolecules and freeze dried for storage. Measured solid and protein content of purified conjugate were 86.9% and 75.0%, respectively. Sodium caseinate used in experiments was subjected to the same treatment used for conjugation (12 hrs at 70ºC) to avoid differences due to thermal effects. Protein and conjugate aqueous solutions at different concentrations were prepared by carefully dissolving them in Mili-Q water. pH was adjusted by addition of either 0.1 N HCl or 1 N NaOH when necessary. Protein concentrations of aqueous solutions were calculated considering solid and protein contents.

2.2.2. Interfacial Measurements

Static surface tension measurements were done with the Wilhelmy plate method in a tensiometer model K12 (KRÜSS GmbH, Hamburg, Germany) at a controlled temperature of 25°C. The system was coupled with an automatic Dosimat (automatic burette; Model 665, Metrohm, Switzerland) for adding controlled liquid volumes directly into the measuring glass which was attached also to a magnetic stirrer.

Surface tension as a function of concentration curves were determined for sodium caseinate and conjugate samples by increasing gradually the solution concentration in the measuring glass containing initially pure HPLC water.

Dynamic surface tension measurements were done in a pendant-drop Tracker tensiometer (ITConcept, Longessaigne, France). Description of the system can be found elsewhere (Benjamins *et al.*, 1996). During experiments protein and conjugate solutions were placed inside an optical glass cuvette at controlled temperature (25°C) and a small axisymetric air bubble was created at the tip of a syringe (bubble area set to 16 mm^2). Bubble size was controlled automatically by the software adjusting the position of the syringe plunger connected to an electric motor. Surface tension values were calculated based on the fundamental Laplace equation (Eq. 1.3) in real time from bubble images taken with a CCD camera. Fast sampling rate was used (approximately 3 images per second) during initial stages of adsorption when surface tension drops rapidly. After 10-30 minutes sampling rate was reduced to one measurement every 100 s. Bubble interface dilational viscoelastic modulus were measured when reaching surface tension values close to equilibrium conditions (≥5 hours) by applying a sinusoidal area fluctuation to the system. Area was varied at two frequencies (0.10 and 0.20 Hz) using a 10% deformation to remain within the linear response region. Surface dilational modulus in compression and expansion were calculated from measured changes in surface tension and surface area using Eq. 1.4 proposed by Gibbs (Logley and Van Name, 1928).

2.2.3. Foaming Experiments

An analytic foam characterizing system Foamscan (ITConcept, Longessaigne, France) developed from the work of Guillerme *et al.* (1993) served for studying foaming behaviour of sodium caseinate and conjugate solutions. Foams were formed from 20 mL of protein or conjugate solution placed inside a basin at the base of a column by sparging air through a porous glass plate at a flow rate of 30 or 80 mL/s until the foam reached a volume of 120 mL. Temperature during experiments ranged between 26.5-28.0 ºC. When the foam reached the target volume inside the cylindrical column sparging was

stopped and the evolution (foam volume and liquid drainage) followed for a maximum of 30 min. All experimental conditions were tested at least in duplicate.

2.2.4. Diminishing Bubble Method

Bubble wall permeability was evaluated using a variation of the diminishing bubble (DB) method proposed by Platikanov *et al*. (1980). The original DB method consists in forming a small bubble that floats at the solution surface. During experiments the bubble radius and film radius (formed between bubble and solution surface) are measured against time via microscopic observation and permeability is calculated from time dependencies of these variables (Krustev *et al*., 1996).

A simplified DB approach was implemented that allowed automatic data acquisition during bubble shrinkage and estimation of permeability coefficients only by means of values of bubble radius. The experimental set up consisted of a polystyrene dish (35 mm diameter) as the observation cell with a piece of plastic tube tightly fixed to the base forming an inner chamber (Figure 2.1A). The investigated solution was placed in the inner zone and a single bubble was created with a microsyringe. The outer region was partially filled with water and closed to minimize evaporation (Figure 2.1B). Microscopical observations were done with a Digital Blue Computer Microscope (model QX5, Prime Entertainment, USA) connected to a computer for automatic acquisition of time sequences of images. Radius data were extracted from bubble images using Object Image (Vischer, 2001), a public domain image analysis program.

Considering that bubble shrinkage results only from gas flowing into the atmosphere (diffusion into the solution bulk is neglected), mass balance for the bubble yields Eq. 1.10 relating permeability coefficients with physical and geometrical factors. Variation of the bubble film area is estimated with Eq. 1.11, which is obtained by the derivative of the total mass balance. The initial film area A_0 is estimated by a balance between buoyancy force and surface tension forces. When using Eqs. 1.10 and 1.11 it is assumed that bubbles remain spherical and also that the film area can be approximated to a flat disc.

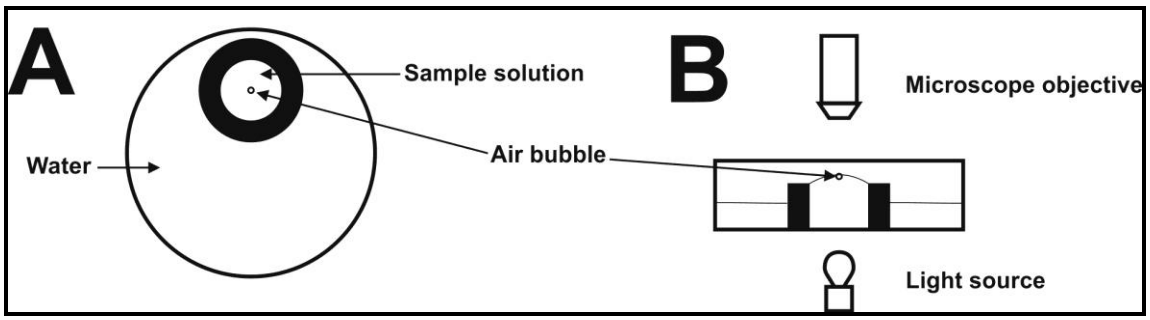

Figure 2.1.: Experimental set up for the Diminishing Bubble method. Observation cell is showed from above (A), and from the side (B).

2.3. Results and Discussion

2.3.1. Surface tension with Wilhelmy Plate

Measured surface tension versus concentration curves using the Wilhelmy plate for thermally treated sodium caseinate and conjugate at pH 7.0 are shown in Figure 2.2. The figure indicates that surface active behaviour of the conjugate differs from that of the original protein. Conjugated sodium caseinate reduced the surface tension of the solution to values below 40 mN/m as concentration increased, whereas sodium caseinate reached equilibrium at higher values near 45 mN/m. Rouimi *et al.* (2005) reported an equilibrium surface tension at air/water interfaces of 46.4 mN/m for sodium caseinate at 1.0 mg/mL using same type of tensiometer. A value of 47 mN/m was reported in the review of Bos and van Vliet (2001) for sodium caseinate at 0.3 mg/mL and pH 6.7. This data agree with our experimental measurements for sodium caseinate. Figure 2.2 shows also the surface tension versus concentration curve for sodium caseinate without heat treatment. Results show that this factor had no important effect on protein surface tension values. The static behaviour of surface tension was also unmodified by changing pH to 5.5 (Figure 2.2).

Another difference between both systems derived from Figure 2.2 is that protein concentrations required to reach surface tension values closer to equilibrium conditions were much larger for the conjugate than for pure protein. For small surfactant

molecules, equilibrium surface tensions are reached at concentrations over the critical micelle concentrations (CMC). CMC is the concentration at which there are enough molecules to cover the entire interface and excess molecules form ordered aggregates (micelles) in the bulk. CMC is commonly estimated by intersecting the 2 linear regions that appear when plotting surface tension curves in semi-log scale. Although, for proteins it is not correct to define a CMC but rather a surface saturation concentration, it was attempted to estimate equilibrium conditions as done for small surfactants. However, proteins samples did not evidenced a well-defined saturation concentration. In this case it was found that values of saturation concentration ranged between 0.16 and 0.36 mg/mL and between 2.5 and 5.0 mg/mL for sodium caseinate and conjugate respectively (Figure 2.3).

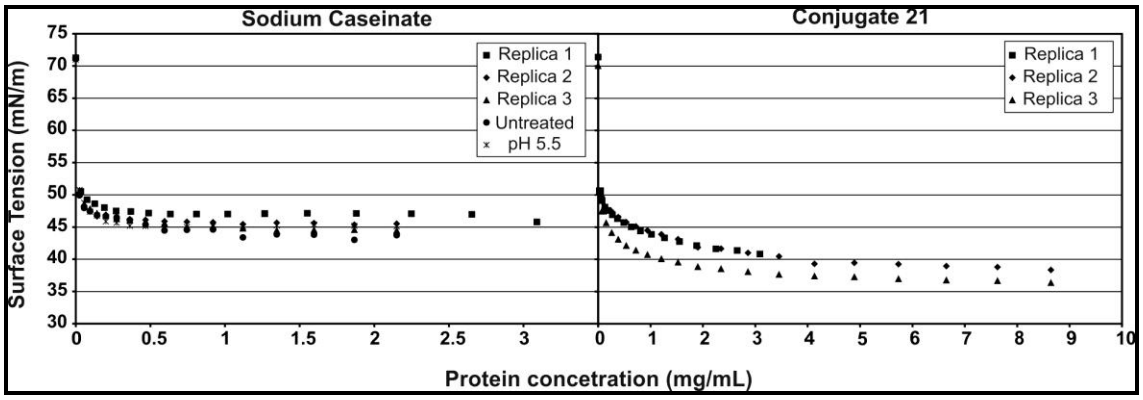

Figure 2.2: Surface tension versus concentrations curves for thermally treated sodium caseinate and conjugate samples at pH 7.0. Additional data are shown to illustrate that the surface tension of sodium caseinate was unaffected by the thermal treatment or pH change.

Measurements of static surface tension verified important changes in surface behaviour of sodium caseinate upon conjugation. Nevertheless, observed also low reproducibility between the replicas and absence of clearly marked surface saturation concentration points. The reasons are that the Wilhelmy plate might not be suitable to analyze the surface active behaviour of proteins because it fails achieving steady-state

adsorption states particularly at high protein concentrations (Krishnan *et al*., 2005). Meniscus stretching with the Wilhelmy plate conspires against adsorption kinetics by inducing protein movement to freshly formed surfaces. Adsorption may not reach equilibrium conditions, as was observed particularly for the conjugate that did not reached a plateau at high concentrations. Besides, increased protein adsorption can occur without changes in surface tension because proteins can form a second layer underneath the adsorption layer (two-dimensional aggregates) (Fainerman and Miller, 1999).

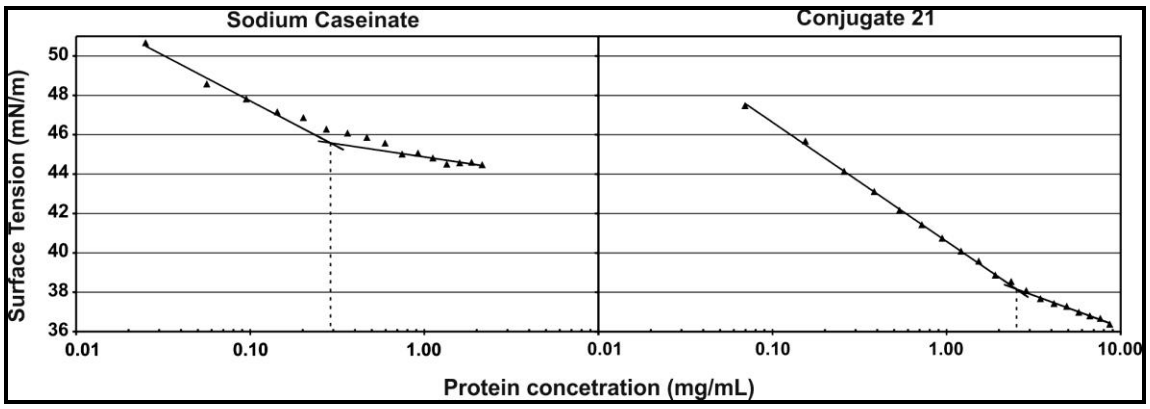

Figure 2.3: Surface tension values plotted against the logarithm of the concentration for sodium caseinate and conjugate. In both cases, curves correspond to replica 3 in Figure 2.2.

2.3.2. Foaming Behaviour

Sodium Caseinate

Foaming properties of sodium caseinate were tested at two pH (5.5 and 7.0) and two concentration (1.0 and 4.0 mg/mL) conditions. All solutions reached the final target foam volume with the exception of 1 mg/mL solutions at pH 5.5. At this condition it was impossible to reach 120 mL of foam either with 30 or 80 mL/min of air. During the first stage of foam formation (when sparging) no important effects of pH, concentration or gas flow were observed. Foams sparged with 80 mL/min formed faster (75-78 s) than foams sparged with 30 mL/min (208-213 s). However, foam capacities

(ratio between foam volume and the gas volume) were similar and ranged between 1.15-1.23. On the contrary, marked effect of all three variables was observed on foam liquid fractions immediately after sparging stopped (Figure 2.4). Liquid fractions increased with increasing pH, protein concentration and sparging flow.

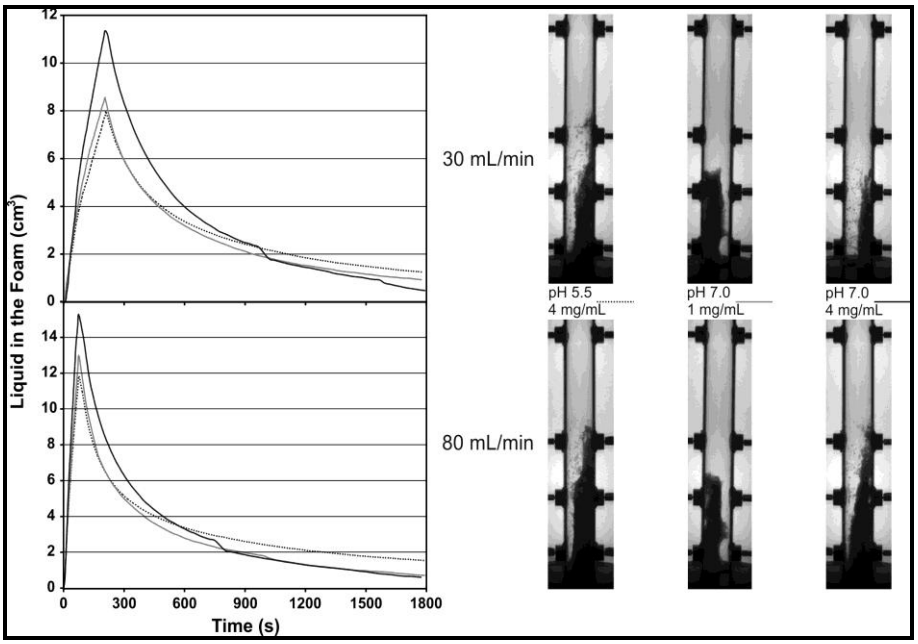

Figure 2.4: Foamscan results for sodium caseinate samples sparged at 30 or 80 mL/min. Curves represent the amount of liquid contained in the foam during formation and drainage. Images describe foam appearances after 30 minutes.

Foam stability after sparging stopped was particularly difficult to analyse quantitatively by following the changes in foam volume because foam collapse occurred heterogeneously. In most cases very irregular collapsing processes were observed because the foam was sticking to the cylinder wall thus, extensively altering foam volume measurements obtained from images by Foamscan. A more reliable indicator of foam stability was in this case liquid drainage. Liquid drained during foam collapse is commonly used to estimate foam stability (Baniel *et al*., 1997; Fains *et al*., 1997; Beneventi *et al*., 2003; Carrera Sanchez and Rodriguez Patino, 2005). However, liquid

drainage cannot be considered a perfect stability indicator. It is reasonable that higher liquid fractions keep bubbles away from each other preventing Ostwald ripening and coalescence, but high liquid fractions is not a necessary condition to have stable foams. To avoid misinterpretations, drainage curves are therefore presented together with foam images describing foam appearance 30 minutes after their formation. Figure 2.4 shows drainage curves together with the corresponding images for sodium caseinate foams. Severe foam collapse occurred in all cases and the liquid fraction reached similar low values. Drainage rates were slightly reduced at pH 5.5 but in general sodium caseinate foams were unstable and collapsed rapidly.

Conjugate

Based on Wilhelmy plate results indicating that conjugate protein required higher surface saturation concentration to achieve complete surface coverage, experiments done in the Foamscan used both pH (5.5 and 7.0) at a single high concentration (4.0 mg/mL). Foam formation results were very similar to the ones observed for sodium caseinate, with foam capacities ranging between 1.13 and 1.25, and increasing liquid fractions with higher gas flow rates and pH (Figure 2.5). Nonetheless, foam images show that foams were more stable at pH 5.5 than at pH 7.0. Curves indicated also that liquid drained more slowly at lower pH. It is generally acknowledged that foams prepared from protein solutions closer to their isoelectric pH tend to be more stable. Protein net charges are smaller and molecules interact and pack more compactly over interfaces. Foam images in Figure 2.5 show also that lower sparging flow also helped improving foam stability. It can be speculated that this result is due to an increased adsorption time when sparging at lower flowrates and also to more regular bubble sizes produced, thus, retarding collapse.

Based on results for mixtures between sodium caseinate and conjugate (next section), it was decided to drastically reduce concentrations used in conjugate foaming experiments. Figure 2.6 shows effects of reducing protein concentration from 0.8 to 0.2 mg/mL on conjugate foam behaviour at pH 5.5. As measured previously, foam capacities did not differ greatly between experiments and ranged between 1.16 and 1.21.

Exceptions were experiments using solutions at 0.2 mg/mL. Target volume could not be reached at 30 mL/min and foam capacity was reduced to 1.02 when using 80 mL/min. Foam stability decreased with deceasing concentration, situation that correlated with higher drainages. Most surprisingly, low concentrations were enough to obtain very stable conjugate foams, a result that contradicted static surface tension measurements.

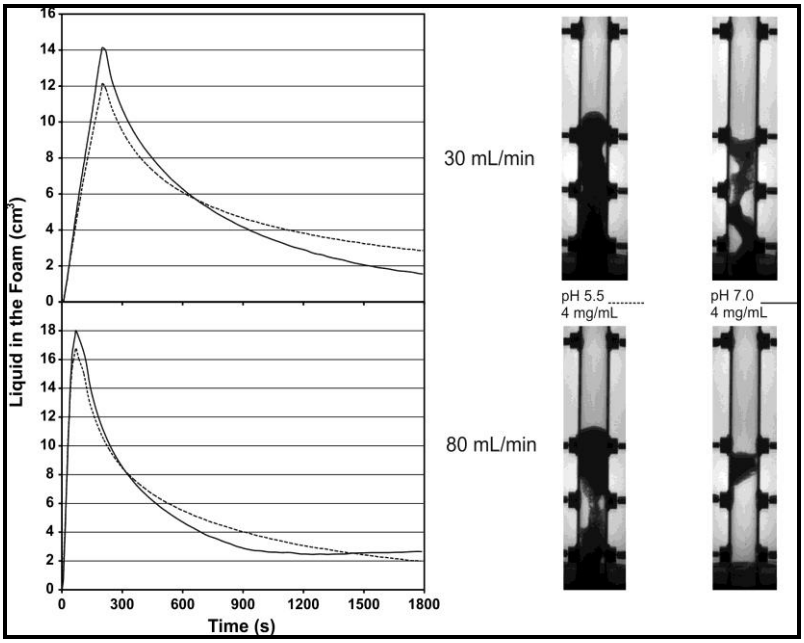

Figure 2.5: Foamscan results for conjugate samples prepared at high concentration and sparged at 30 or 80 mL/min. Curves represent the amount of liquid contained in the foam during formation and drainage. Images describe foam appearances after 30 minutes.

Mixtures

The foaming behaviour of sodium caseinate/conjugate mixtures was also studied. From a practical/industrial standpoint this is sensible because (1) is costly to produce conjugate in large volumes and (2) un-purified conjugation reaction product is a mixture containing conjugate and un-reacted proteins and carbohydrates.

Figure 2.7 shows results of foaming different mixtures at pH 5.5 where only the conjugate concentration was varied keeping sodium caseinate concentration constant at 1.0 mg/mL (or 4.0 mg/mL). Foam capacity varied between 1.22 and 1.27 and contrary to preliminary idea, foam stability improved considerably as conjugate concentration was reduced. At higher concentrations the foam coarsened and collapsed much faster. Process was even faster when increasing sodium caseinate level to 4.0 mg/mL (Figure 2.7). It is interesting to note the differences in drainage curves obtained with these mixtures. In those formed using a gas flow rate 30 mL/min, concentration had a notable effect but all samples drained to very similar final liquid fraction. However, in those formed with air flow rates of 80 mL/min concentration the effect was lost, and all drainage curves overlapped. Comparing these curves with foam images evidences that foam stability was not well described by liquid drainage.

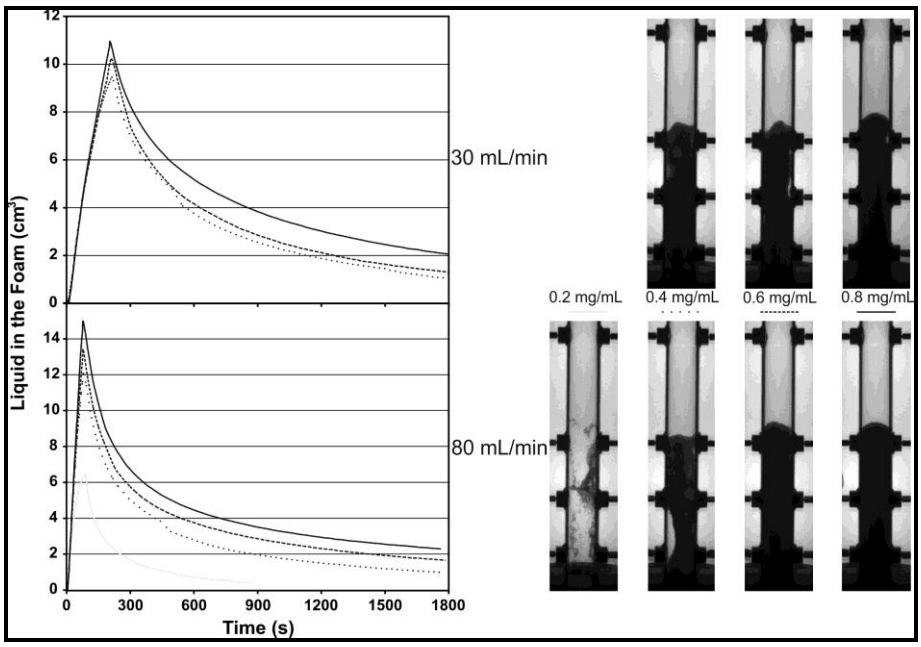

Figure 2.6: Foamscan results for conjugate samples prepared at low concentration, pH 5.5 and sparged at 30 or 80 mL/min. Curves represent the amount of liquid contained in the foam during formation and drainage. Images describe foam appearances after 30 minutes.

A second series experiments with mixtures were carried out considering the good stability showed by conjugate foams when using 0.80 mg/mL solutions at pH 5.5 and the stability loss when going below this concentration shown in Figure 2.6. Therefore, foams were formed from 0.80 mg/mL total concentration solutions containing varying ratios between both molecules (Figure 2.8). It was not possible to foam with the mixture containing only 10% of conjugate and sparged with 30mL/min. In all other cases foam capacities were lower (0.70-1.09) compared to the previous experiments (~1.2). Images in Figure 2.8 show that when the conjugate fraction in the mixture increased the foam became more stable, but stability was not comparable to the one observed using pure conjugate (Figure 2.6).

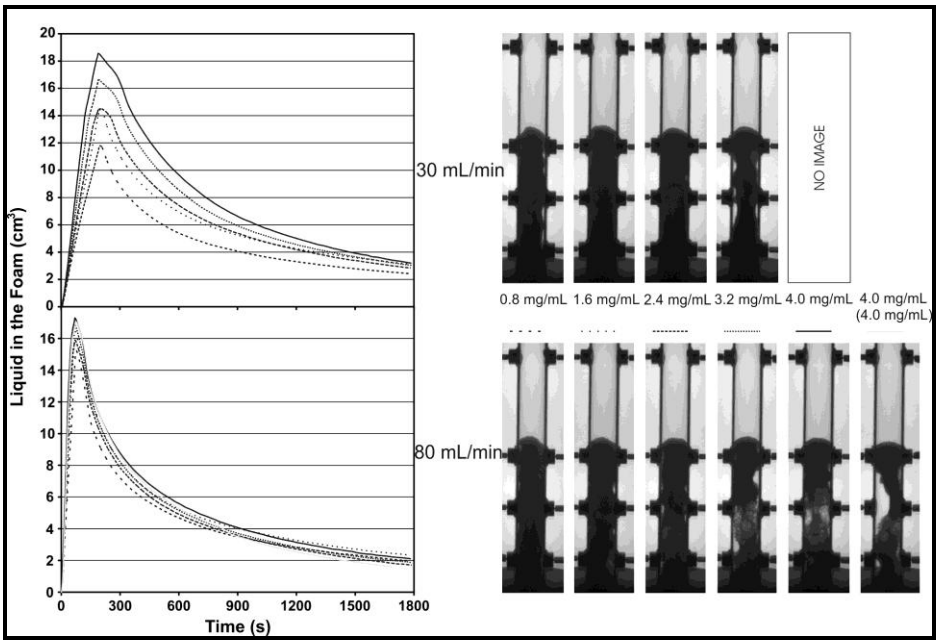

Figure 2.7: Foamscan results for mixtures at pH 5.5 containing increasing concentrations of conjugate at a constant sodium caseinate concentration (1.0 mg/mL or 4.0 mg/mL) and sparged at 30 or 80 mL/min. Curves represent the amount of liquid contained in the foam during formation and drainage. Images describe foam appearances after 30 minutes.

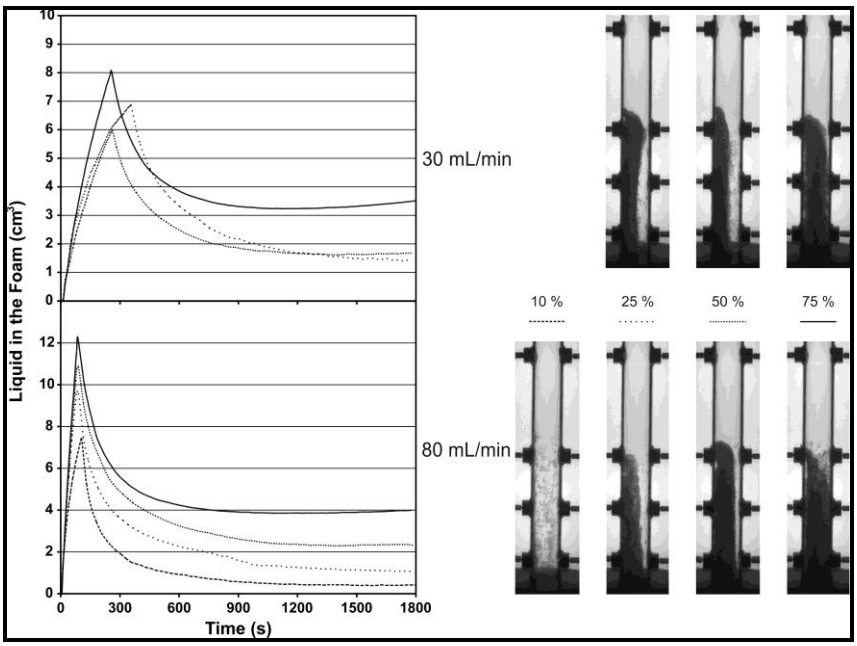

Figure 2.8: Foamscan results for conjugate/sodium caseinate mixtures (0.80 mg/mL total protein concentration) at pH 5.5 and sparged at 30 or 80 mL/min. Percentages represent conjugate mass fraction in the mixture. Curves represent the amount of liquid contained in the foam during formation and drainage. Images describe foam appearances after 30 minutes.

2.3.3. Results of drop/bubble shape analysis

Surface tension experiments

Figure 2.9 shows dynamic surface tension measurements obtained for solutions of sodium caseinate, conjugate, and mixtures prepared at different protein concentration and pH conditions using the pendant-drop Tracker tensiometer. Results obtained for sodium caseinate indicate that for concentrations over 1.0 mg/mL the surface tension reaches equilibrium near 47 mN/m at pH 7.0. This is consistent with values measured using the Wilhelmy Plate method (45 mN/m). Results show also that at a lower protein concentration of 0.3 mg/mL the equilibrium surface tension was higher (50 mN/m) indicating that at this condition there were not enough molecules to fully

saturate the interfacial area. Surface tension values become independent of bulk concentration at 1.0 and 2.0 mg/mL reaching conditions close to surface saturation.

Results obtained for conjugated protein at pH 5.5 shown in Figure 2.9 exhibit an interesting behaviour. Increasing concentration from 0.2 to 0.8 mg/mL decreases the equilibrium surface tension from 44.5 to 39.6 mN/m, respectively. However, increasing the concentration to a higher value of 4.0 mg/mL does not reduce further equilibrium surface tension. This partially explains good foam stability observed at 0.8 mg/mL and pH 5.5 in Foamscan experiments (Figure 2.6). From the results in Figure 2.9 it can be assumed that this concentration is high enough to achieve surface coverage and good bubble stability. This aspect was masked in Wilhelmy plate measurements because absorption kinetics might be too slow to be accurately followed by this method. Measurements carried out at pH of 7.0 showed also that equilibrium surface tension value decreased with increasing protein concentration. However, in these cases reaching equilibrium required longer times even at high protein concentrations. This can be observed by the difference in the equilibrium surface tensions between the experiments at 2.0 and 5.0 mg/mL.

Experimental results for sodium caseinate/conjugate mixtures also shown in Figure 2.9 were all done at pH 7.0. Final equilibrium surface tension appeared to be unchanged (*ca.* 44 mN/m) when increasing total protein concentration from 1.0 to 2.0 mg/mL in 50/50 mixtures. However, reaching this value was slower at lower total concentration. Mixture that included 1.0 mg/mL of both samples should have reached a lower surface tension value than the one measured because of higher conjugate concentration. However, it appears that protein competes with the conjugate over the interface, thus increasing final surface tensions. Increasing conjugate concentration to 5.0 mg/mL with sodium caseinate at 1.0 mg/mL reduced further the surface tension, but again it was observed a higher equilibrium value than the one expected for conjugate alone. When increasing sodium caseinate concentration to 5.0 mg/mL equilibrium value was reached more slowly, evidencing once more competition between both types of molecules.

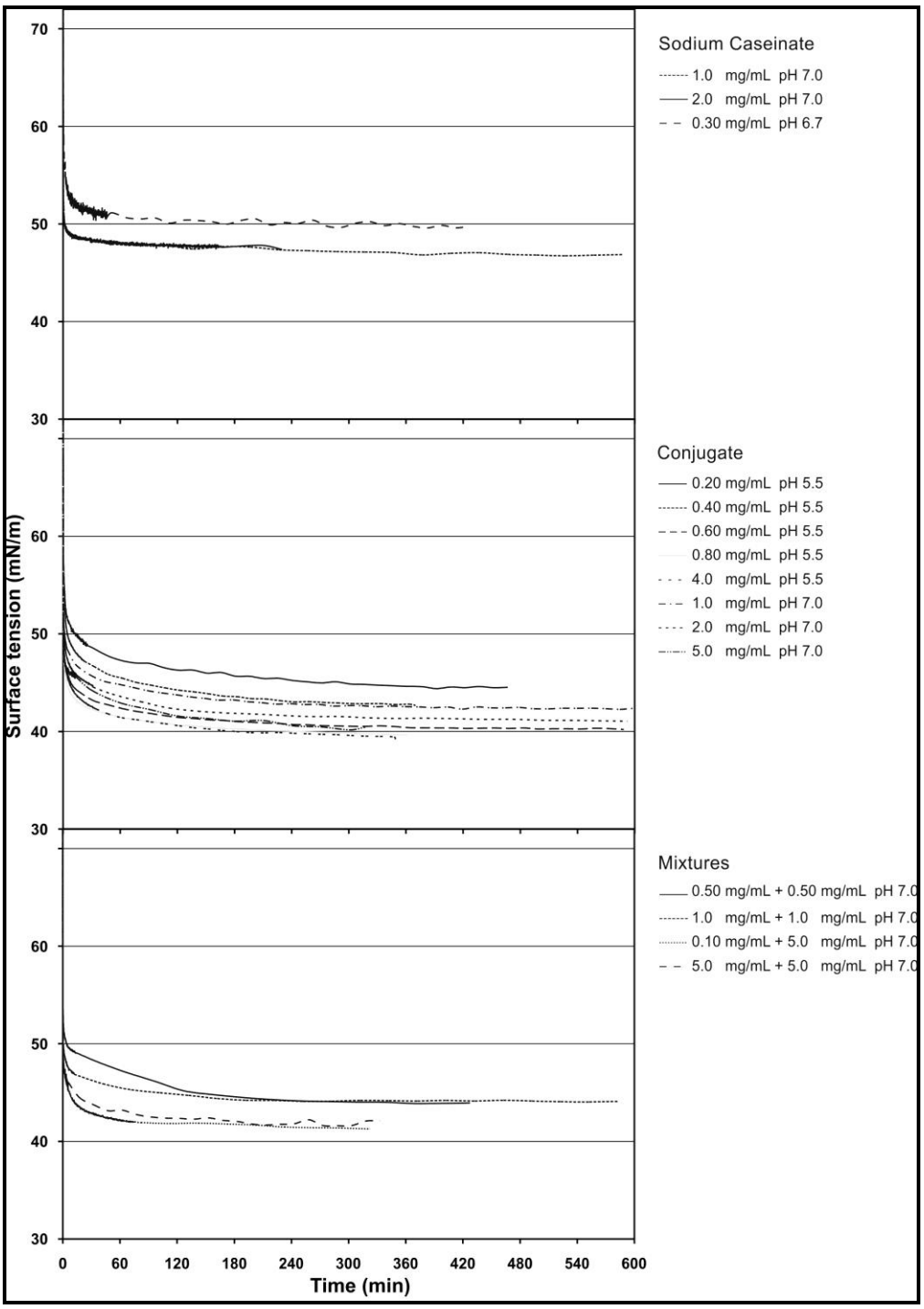

Figure 2.9: Surface tension versus time curves measured using automatic drop/bubble shape analysis for sodium caseinate, conjugate, and mixture solutions prepared at different concentrations and pH conditions.

Protein adsorption kinetics

Protein adsorption process at interfaces is not as fully understood as for small surfactant molecules. Proteins are large three dimensional structures that when adsorbed change their spatial conformation. Timescales and extent of these conformational changes strongly depend on inter- and intramolecular forces (Prins *et al.*, 1998). Protein adsorption follows different steps, generally involving molecular diffusion from bulk to interface, adsorption, unfolding, aggregation at interfacial layer, multilayer formation and even interfacial gelation (Maldonado-Valderrama *et al.*, 2005). Mathematical models have been presented to describe protein adsorption kinetics based on the particular characteristics of these molecules (Fainerman *et al*., 2003; Miller *et al*., 2004). They unfortunately require physical data determined independently describing protein geometrical dimensions and intermediate states during adsorption.

Assuming that the amount of protein adsorbed at an interface is directly related to the decrease in surface tension, a semi-quantitative protein adsorption analysis was performed based on data in Figure 2.9. First, an x-shifted power equation with offset [$y=a(x-b)^c+d$] was fitted to all the experimental curves. This type of equation gave very good fitting results in all cases. From the slopes of these fitted curves, surface tension decreasing rates were calculated. Results of this analysis are shown in Figure 2.10. For sodium caseinate apparent adsorption rates increased with decreasing protein concentrations. This might be related to higher viscosities reducing molecular diffusion and thus retarding mass transfer. A very similar behaviour was observed for conjugate samples, however in this case higher apparent adsorption rates were obtained for concentrations of 0.4 mg/mL rather than for 0.2 mg/mL. When comparing the curves obtained at different pH conditions, it can be concluded that lowering pH increased adsorption rates. This was noticed particularly when comparing absorptions at 1.0 or 2.0 mg/mL and pH 7.0 with those at 4.0 mg/mL and pH 5.5 that are very similar, although at pH 5.5 concentrations were 2-4 times higher. In relation to mixtures, all tested conditions exhibited similar apparent adsorption rates that slightly increased when conjugate concentration was increased to 5.0 mg/mL and sodium caseinate remained

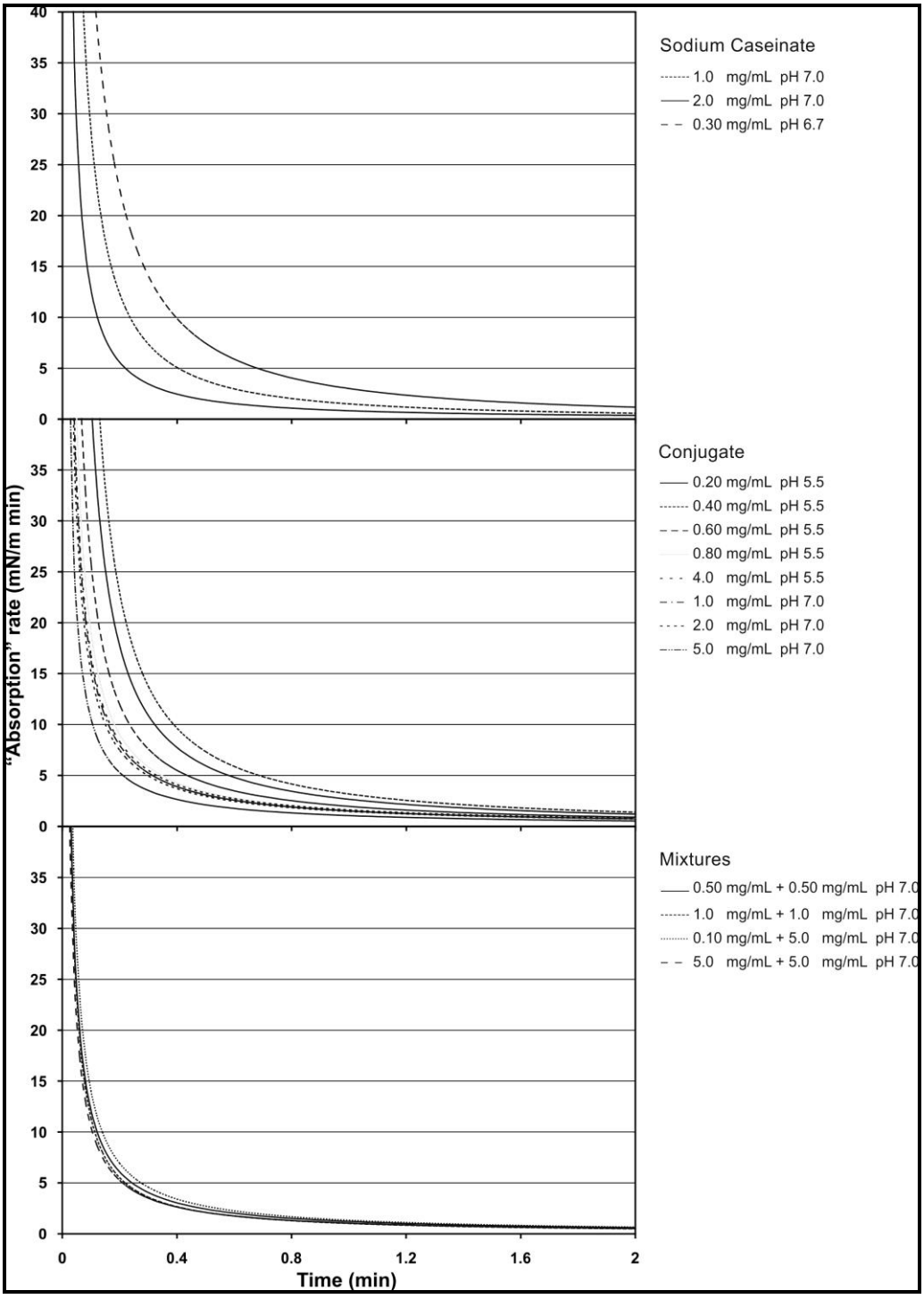

Figure 2.10: Apparent adsorption rates derived from the data in Figure 2.9 as the slope of the surface tension versus time curves.

low (1.0 mg/mL). However, an overall look of Figure 2.10 shows that mixtures had lower apparent adsorption rates than pure samples. When comparing sodium caseinate with conjugate, it is not immediately clear which one adsorbs faster and a conclusion with respect to this aspect is not simple based on this approach.

Viscoelasticity experiments

Interfacial viscoelasticity results obtained with dynamic drop/bubble tensiometer are shown in Figure 2.11. Direct comparison of data between sodium caseinate and conjugate samples analyzed at pH 7.0 shows that surface dilational modulus of conjugate films were 2-3 times higher than those measured for sodium caseiante, while phase angles were approximately 2 times smaller. The higher modulus and elastic component exhibited by conjugate can be related to the better stability showed during the Foamscan experiments (Figures 2.4-6). Figure 2.11 shows also that the modulus increased with decreasing concentration. This can explain also the poor stabilities observed at 4.0 mg/mL (Figure 2.5), while they improved considerably at 0.80 mg/mL (Figure 2.6). Concentrations lower than 0.80 mg/mL gave higher modulus values, however, at these concentrations the surface coverage was not enough and resulting foams were less stable.

Regarding effects the applied frequency on measured rheological interfacial properties, increase in surface dilational with increased modulus frequency is logical. Relaxation phenomena play an important role at high levels of protein adsorption verified experimentally by the appearance of a phase angle. Presence of a viscous component, which is given by the product of viscosity and imposed frequency, results in higher suface dilational modulus when increasing applied frequency.

2.3.4. Diminishing Bubble experiments

Bubble shrinkage

Sample solutions were analyzed using the modified DB method. In all experiments the bubbles formed at the solution surface were imaged at a sampling rate

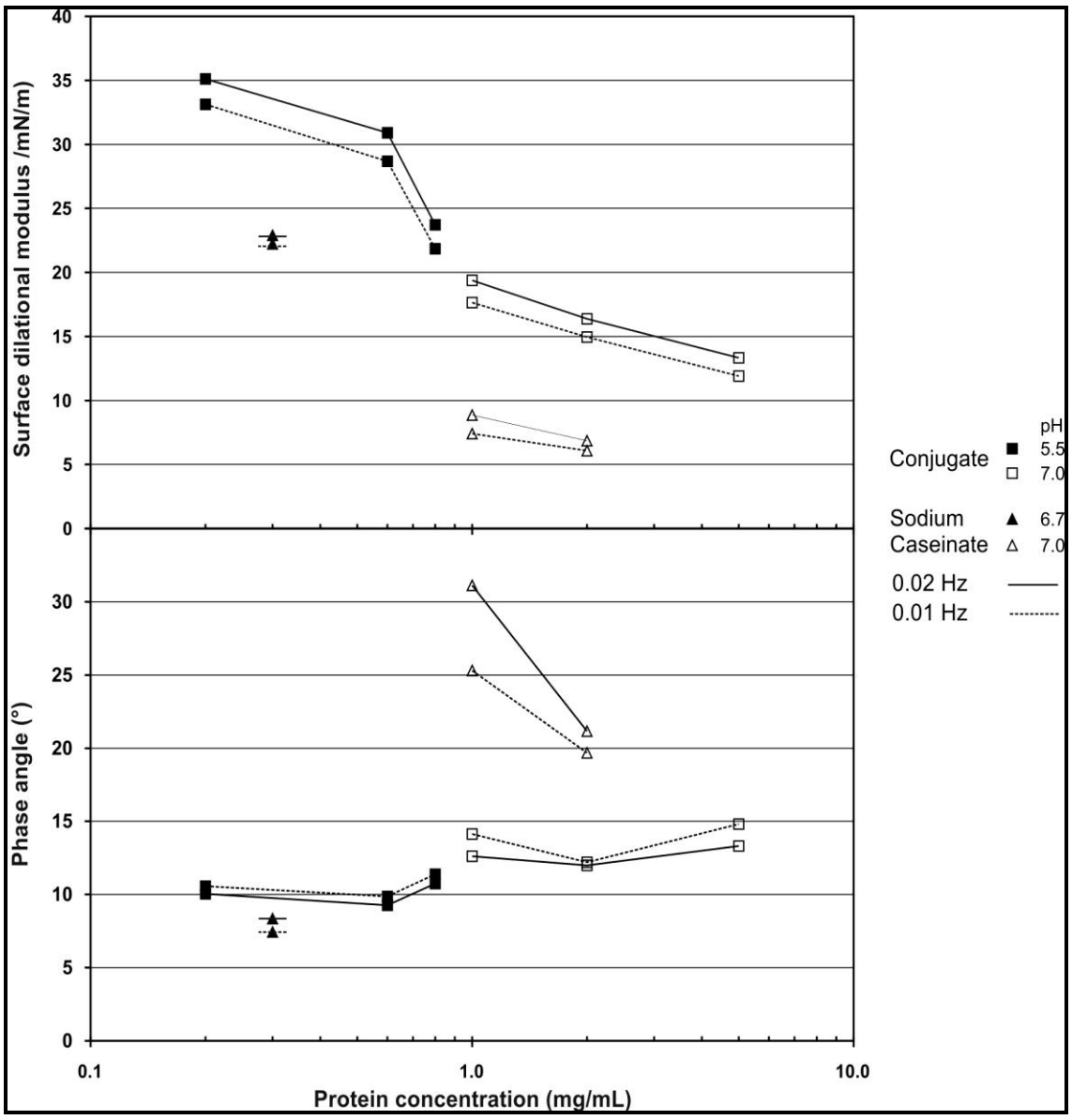

Figure 2.11: Surface dilational modulus and phase angles measured at different concentrations and pH conditions for sodium caseinate and conjugate interfaces.

of one image every two minutes. Image analysis yielded bubble radius versus time curves which are difficult to compare because of differences in initial bubble radius. A better way to compare sample behaviour was to estimate instant bubble shrinking velocities and plot them against radius values. Shrinking rates were estimated from

bubble radius versus time curves as the slopes of fourth or lower-order polynomials fitted to experimental data. In all cases polynomials gave good fits (R^2>0.99).

Figure 2.12 shows the estimated shrinking rates curves for selected samples. From this figure it can be observed that samples show different shrinking rates, being the egg albumen and whey protein samples the ones that showed lowest and more stable shrinking rates, whereas sodium caseinate and conjugate show increasingly larger values. However, it is still difficult from this figure to analyze the effects of the experimental conditions. One could intuitively think that higher protein concentration and pH closer to the isoelectric point of protein should lead to better surface packing over the gas bubbles, and thus yield lower shrinking rates. However, this does not occur particularly for the whey protein where it is possible to observe the shrinking rates are lower for pH 7.0 than for pH 5.5. This phenomena has been noted by Petkova *et al*. (2003), who argued that the reduction of the gas permeability could be explained by stronger interactions between the molecules into the film due to the increase of the film charge at pH 7.0 compared to that at the isoelectric point.

Estimation of the film permeabilities

Film permeability values (*K*) were estimated according to the modified method, using the polynomials fitted to the experimental data. Permeability for egg albumen solution prepared at 0.4 mg/mL and pH 7.0 was 1.71 cm/s. Films formed from whey protein isolate solutions prepared at 0.1 mg/mL and pH 7.0, and 0.4 mg/mL and pH 5.5 or 7.0, presented permeabilities of 2.73, 1.44, and 2.13 cm/s respectively. For conjugate it was obtained a permeability of 2.70 cm/s for solutions prepared at 0.1 mg/ml and pH 5.5, and a permeability of 2.30 cm/s for solutions prepared at 0.4 mg/ml and pH 7.0. Samples solutions of sodium caseinate at 0.1 and 0.4 mg/mL at pH 5.5 showed permeability values of 2.70 and 5.28 cm/s respectively.

Little information is available on gas permeability through protein films using the DB method to compare these findings. Recently, microscopic films made from *β*-lactoglobulin solutions with different concentrations and at different pH values were

studied by Petkova *et al.* (2003) using the DB method. Authors reported values between 0.017-0.022 cm/s, close to permeability values reported for simple surfactants (Nedyalkov *et al.*, 1988; Nedyalkov *et al.*, 1992) or phospholipid mixtures (Trachant *et al.*, 2002). Schmitt *et al.* (2005) reported permeability values for fresh and aged films formed with *β*-lactoglobulin/acacia gum electrostatic complexes. Values estimated by the authors were 0.021 and 0.449 cm/s, respectively. Data obtained in this work seems to be one or two orders of magnitude higher.

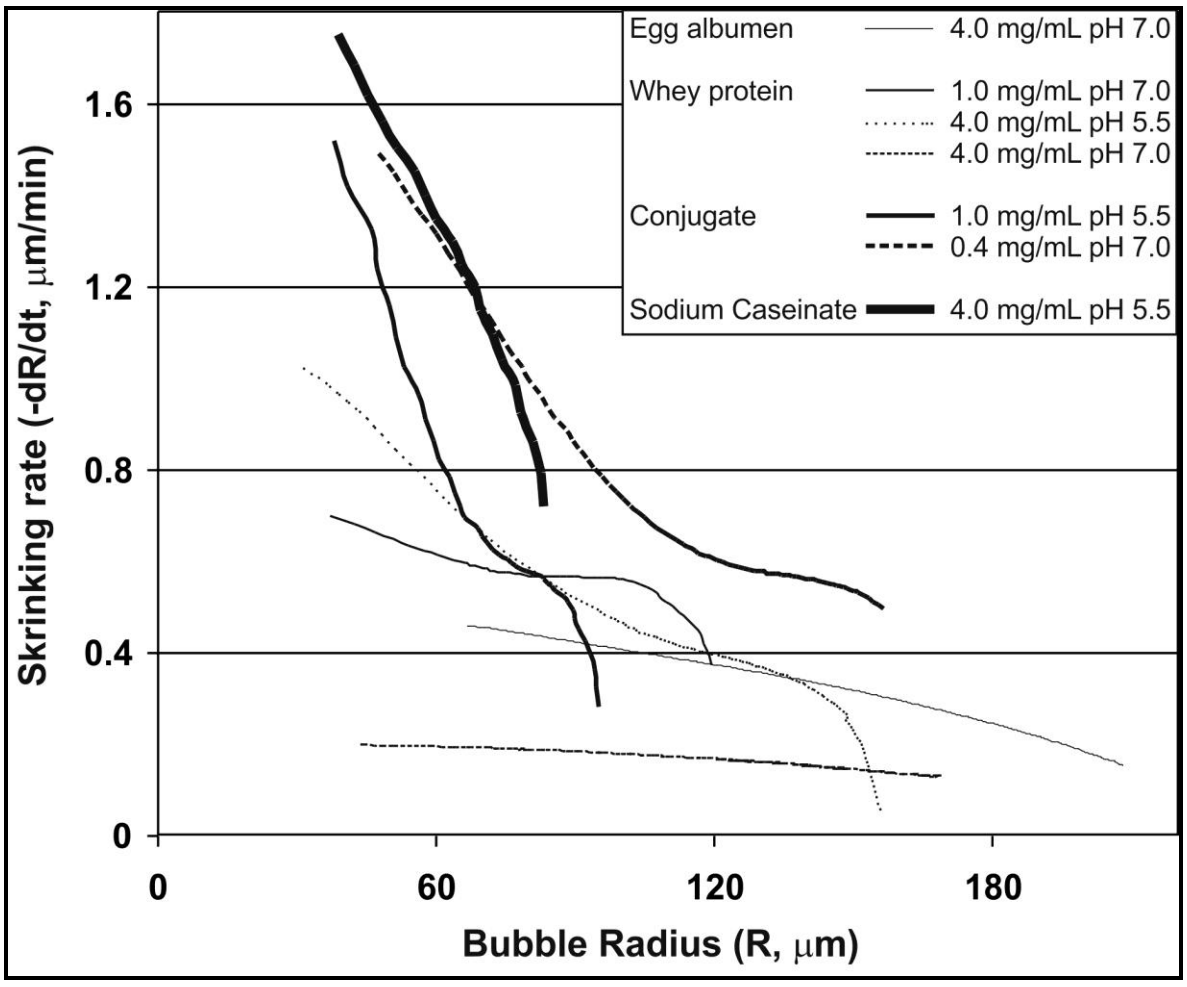

Figure 2.12: Shrinking rate versus bubble radius curves derived from the experimental data for selected samples.

At this point is important to state that DB method was originally proposed for investigating Newtonian Black films of small surfactant molecules. Thinning is much slower for protein films because of their rigid character and stay thicker than Newton Black films. Overestimation of permeability coefficients compared to ones reported in literature can be related to the use of our simplified approach. Some assumptions employed may not sustain, leading to errors particularly in the estimation of the film area, which was not measured as in the original setup (Platikanov *et al.*, 1980). Assumption that air bubbles remain spherical is supported by low values of dimensionless Bond number (Dickinson *et al.*, 2002). However, proteins films are more rigid and irregular, so distortion may occur. In the approach used in this thesis air diffusion into the bulk was neglected because it was considered that mass transfer occurs preferably through the film. Calculations indicate that mass transfer driving force through the film is 50 times higher than that driving mass transfer into the solution. But bubble walls offer less resistance than thicker double protein layers of films though this may not be negligible. It should be noted also that the estimated permeabilities are average values representing all film lifetime. Film structure changes because of protein unfolding and thins because of liquid drainage. This phenomenon has been discussed by Schmitt *et al.* (2005), who reported a permeability increase of 20 times (from 0.021 cm/s to 0.449 cm/s) for freshly formed films of β -lactoglobulin/acacia gum compared to films aged for 24 hrs. Interfacial rheological properties of protein films may also have important effects on the disproportionation kinetics. Theoretical work done by Kloek *et al.* (2001) have evidenced that presence of viscoelastic interfaces can retard or even stop bubble shrinkage. These effects were not explicitly incorporate in the modelling.

2.4. Conclusions

Foam experiment results demonstrated that sodium caseinate conjugation yielded molecules with better foaming properties. Protein modification by formation of covalent bonds with the carbohydrate changed surface active properties and improved foaming behaviour. In contradiction to Wilhelmy plate results, low conjugate concentrations (0.8 mg/mL) were enough to obtain more stable foams, whereas at higher concentrations foams resulted less stable and collapsed faster. Better foaming

performance of conjugate was not related to faster interfacial adsorption kinetics, but to lower surface tensions and higher surface elasticities. Lower surface tensions facilitate generation of surface area and smaller bubbles, and higher elasticities give bubbles dynamic stabilization mechanism against coalescence and Ostwald ripening. Glycation of proteins can have a huge potential for application in food foams because of the improved proprieties compared to proteins alone. Protein conjugation might be a feasible route to produce surface active molecules with tailored and improved foaming properties for the food industry in the near future.

2.5. References

Baniel, A., Fains, A., and Popineau, Y. (1997). Foaming properties of egg albumen with a bubbling apparatus compared with whipping. *Journal of Food Science*, 62, 377-381.

Beneventi, D., Pugh, R.J., Carré, B. and Gandini, A. (2003). Surface rheology and foaming properties of sodium oleate and C12(EO)6 aqueous solutions. *Journal of Colloid and Interface Science*, 268, 221-229.

Benjamins, J., Cagna, A. and Lucassen-Reynders, E.H. (1996). Viscoelastic properties of triacylglycerol/water interfaces covered by proteins. *Colloids and Surfaces A: Physicochemical and Engineering Aspects*, 114, 245-254.

Bos, M.A. and Van Vliet, T. (2001). Interfacial rheological properties of adsorbed proteins layer and surfactants: a review. *Advances in Colloid Interface Science*, 91, 437-471.

Carrera Sánchez, C. and Rodríguez Patino, J.M. (2005). Interfacial, foaming and emulsifying characteristics of sodium caseinate as influenced by protein concentration in solution. *Food Hydrocolloids*, 19, 407-416.

Carrera Sánchez, C., Rodríguez Niño M.R., Caro, A.L. and Rodríguez Patino, J.M. (2005). Biopolymers and emulsifiers at the air–water interface. Implications in food colloid formulations. *Journal of Food Engineering*, 67, 225-234.

Damodaran, S. (2005). Protein stabilization of emulsions and foams. *Journal of Food Science*, 70, R54-66.

Dickinson, E. (1992). *An Introduction to Food Colloids*, Oxford University Press, Oxford, UK.

Dickinson, E., Ettelaine, R., Murray, B.S. and Du, Z. (2002). Kinetics of disproportionation of air bubbles beneath the planar air-water interface stabilized by food proteins. *Journal of Colloid and Interface Science*, 252, 202-213.

Dukhin, S.S., Kretzschmar, G. and Miller, R. (1995). The dynamics of adsorption at liquid interfaces. In D. Möbius and R. Miller (Eds.) *Dynamics of Adsorption at Liquid Interfaces: Theory, Experiment, Application*. Elsevier Science B.V., Amsterdam, The Netherlands, pp 100-139.

Dutta, A., Chengara, A., Nikolov, A., Wasan, D. T., Chen, K., and Campbell, B. (2004). Texture and stability of aerated food emulsions—effects of buoyancy and Ostwald ripening. *Journal of Food Engineering*, 62, 169-175.

Fainerman, V.B. and Miller, R. (1999). Equation of state for concentrated protein surface layers at the water/air interface. *Langmuir*, 15, 1812-1816

Fainerman, V.B., Lucassen-Reynders, E.H. and Miller, R. (2003). Description of the adsorption behaviour of protein at water/fluid interfaces in the framework of a two-dimensional solution model. *Advances in Colloid Interface Science*, 106, 237-259.

Fains, A., Bertrand, D., Baniel A. and Popineau, Y. (1997). Stability and texture of protein foams: a study by video image analysis. *Food Hydrocolloids*, 11(1), 63-69.

Gloria-Hernández, H. (2006). *Formation of protein-polysaccharide conjugates ad study of their physicochemical and functional properties*. Unpublished Doctoral thesis, Universidad Politécnica de Valencia, Valencia, España.

Golding, M. and Sein, A. (2004). Surface rheology of aqueous casein–monoglyceride dispersions. *Food Hydrocolloids*, 18, 451-461.

Guillerme, C., Loisel, W., Bertrand, D. and Popineau, Y. (1993). Study of foam stability by video image analysis: relationship with the quantity of liquid in the foams. *Journal of Texture Studies*, 24, 287-302.

Gunning, P.A., Mackie, A.R., Gunning, A.P., Wilde, P.J., Woodward, N.C. and Morris, V.J (2004). The effect of surfactant type on protein displacement from the air-water interface. *Food Hydrocolloids*, 18, 509-515.

Kloek, W., Van Vliet, T. and Meinders, M. (2001). Effect of bulk and interfacial rheological properties on bubble dissolution. *Journal of Colloid and Interface Science*, 237, 158-166.

Krishnan, A., Wilson, A., Sturgeon J., Siedlecki, C.A. and Vogler, E.A. (2005). Liquid–vapour interfacial tension of blood plasma, serum and purified protein constituents thereof. *Biomaterials*, 26, 3445-3453.

Krustev, R., Platikanov D. and Nedyalkov, M. (1996). Temperature dependence of gas permeability of Newton black films. *Langmuir*, 12, 1688-1689.

Lau, C.K. and Dickinson, E. (2005). Instability and structural change in an aerated system containing egg albumen and invert sugar. *Food Hydrocolloids*, 19, 111-121.

Logley, W.R. and Van Name, R.G. (1928). *The Collected Works of J. Willard Gibbs*, I: Thermodynamics. Longmans, Green, and Company, New York, USA.

Lucassen-Reynders, E.H. (1993). Interfacial viscoelasticity in emulsions and foams. *Food Structure,* 12(1), 1-12.

Maldonado-Valderrama, J., Fainerman, V.B., Aksenenko, E.V., Gàlvez-Ruiz, M.J., Cabrerizo-Vílchez, M.A. and Miller, R. (2005). Dynamics of protein adsorption at the oil–water interface: comparison with a theoretical model. *Colloids and Surfaces A: Physicochemical and Engineering Aspects*, 261, 85-92.

Miller, R., Fainerman, V.B., Aksenenko, E.V., Leser, M.E. and Michel, M. (2004). Dynamic surface tension and adsorption kinetics of β-casein at the solution/air interface. *Langmuir,* 20, 771-777.

Morris, G.A., Sims I.M., Robertson, A.J. and Furneaux, R.H. (2004). Investigation into the physical and chemical properties of sodium caseinate-maltodextrin glyco-conjugates. *Food Hydrocolloids*, 18, 1007-1014.

Nedyalkov, M., Krustev, R., Kashchiev, D., Platikanov, D. and Exerowa, D. (1988). Permeability of Newtonian black foam films to gas. *Colloid Polymer Science*, 266, 291-296.

Nedyalkov, M., Krustev, R., Stankova, A. and Platikanov, D. (1992). Mechanism of permeation of gas through Newton black films at different temperatures. *Langmuir*, 8, 3142-3144.

Petkova, V., Sultanem, C., Nedyalkov, M., Benattar, J., Leser, M.E. and Schmitt, C. (2003). Structure of a freestanding film of β-lactoglobulin. *Langmuir*, 19, 6942-6949.

Platikanov, D., Nedyalkov, M. and Nasteva, V. (1980). Line tension of Newton black films ii. determination by the diminishing bubble method. *Journal of Colloid and Interface Science*, 75(2), 620-6289.

Prins, A., Bos, M.A., Boerboom, F.J.G. and Van Kalsbeek, H.K.A.I. (1998). Relation between surface rheology and foaming behaviour. In D. Möbius and R. Miller (Eds.) *Proteins at Liquid Interfaces*. Elsevier Science B.V., Amsterdam, The Netherlands, pp. 221-265.

Rouimi, S., Schorsch, C., Valentini, C. and Vaslin, S. (2005). Foam stability and interfacial properties of milk protein–surfactant systems. *Food Hydrocolloids*, 19, 467-478.

Russo, C. (2000). Food foams. Industrie Alimentari, 39(391), 425-443.

Schmitt, C., Palma Da Silva, T., Bovay, C, Rami-Shojaei, S., Frossard, P, Kolodziejczyk, E. and Leser, M.E. (2005). Effect of time on the interfacial and foaming properties of β-lactoglobulin/acacia gum electrostatic complexes and coacervates at pH 4.2. *Langmuir*, 21, 7786-7795.

Tranchant, J.F., Bonté, F., Leroy, S., Nedyalkov, M., Platikanov, D., Javierre, I. and Jean-Benattar, J.J. (2002). Black foam films from aqueous solutions of a mixture of phospholipids and a permeation enhancer. *Journal of Colloid and Interface Science,* 249, 398-404.

Vischer, N. (2001). Object Image, version 2.07. Available from: http://simon.bio.uva.nl/object-image.html.

Weaire, D. and Hutzler, S. (1999). *The Physics of Foams*. Clarendon Press, Oxford, UK.

Wilde, P.J. (2000). Interfaces: their role in foam and emulsion behaviour. *Current Opinion in Colloid & Interface Science*, 5,176-181.

3. DESCRIBING BUBBLE SPATIAL DISTRIBUTIONS ON FOAM STRUCTURES

3.1. Introduction

Over the last two decades it has become clearer to food scientists that structure (from macro to micro level) is key for understanding the physical behavior of foods (Aguilera and Stanley, 1999; Aguilera, 2000; Aguilera, 2005; Aguilera, 2006). In particular, specific and objective quantitative data on foam structures (and aerated products in general) is required to improve our current understanding of these systems. Bubbles give novel textures and attractive structures to food products, and consumer perception and acceptance are affected by physical characteristics they convey (Campbell and Mougeot, 1999).

Concise review of scientific literature illustrates that main structural property investigated on foamed food products is bubble size and size distributions. Examples are ubiquitous. Bubble size distributions have been determined from light microscopy images by Kulmyrzaev *et al*. (2000) and Bals and Kulozik (2003) for whey protein isolate foams, by Schoonman *et al*. (2001) for maltodextrin/sodium caseinate solid foams, by Chang and Hartel (2002) and Eisner *et al*. (2005) for whipped and ice cream, by Sahi and Alava (2003) and Hicsasmaz *et al*. (2003) for cake batters, and by Jang *et al*, (2005) for gelatin solutions and food emulsions, among others. Bubble size distributions have been measured from cake batters and whipped emulsions from fresh milk and whole egg by Richarson *et al.* (2002) and Martinet *et al.* (2005), respectively, using confocal scanning laser microscopy. Scanning electron microscopy has been used by Alavi *et al.* (1999) to determine bubble size distributions in protein-stabilized starch-based supercritical fluid extrudates, and also cryo-SEM has been used by Chang and Hartel (2002) and Eisner *et al.* (2005) in whipped and ice cream for this purpose. Most recently, X-ray tomography has risen as a suitable imaging technology to non-invasively generate views of the structure of cellular materials (Trater *et al*., 2005). The technique has been used by Lim and Barigou (2004) on aerated chocolate bars, strawberry mousses, honeycomb chocolate bars, chocolate muffins, and marshmallows. It has also

been employed by Babin *et al.* (2005, 2006) to analyze the structure of bread crumbs, and by Haedelt *et al.* (2005) for macro aerated chocolate.

Disadvantage of bubble sizes and size distributions is that cannot give direct data on the spatial distribution of the bubbles within foams. Food foams produced by ordinary methods (*e.g.* beating, shaking, sparging, etc.) consist of bubbles with a wide distribution of sizes, which are randomly mixed and arranged (Weaire and Hutzler, 1999). Determining mean bubble sizes or even the bubble size distributions describe only the bubbles forming the structure. A higher level of complexity is to specify the spatial arrangement of those bubbles within the structure (Dickinson, 2007) or what I refer to "architecture". This situation is exemplified by the drawings in Figure 3.1. The figure shows three idealized structures built-up using disks simulating bubbles of two sizes. In the structure on the left of Figure 3.1 bubbles are randomly distributed, in the structure in the middle the small bubbles are clustered at the center, and in the structure on the right the small bubbles are segregated at the top. The three sketches share identical dimensions and number of small and large bubbles. Bubble size distributions do not differ between the three structure types, but spatial properties are entirely different.

In this work, I propose using a set of geometrical and topological descriptors called Minkowski functionals (MFs) (Michielsen and De Raedt, 2001) to describe the foam structure. Application of MFs in statistical physics and cosmology are reviewed by Mecke (2000) and Kerscher (2000), respectively. Erosion/dilation techniques combined with additive MFs have been successfully applied in many areas, including condensed matter physics (Mecke, 2000), geology (Arns *et al*., 2001a,b), and digital image analysis (Serra, 1982, 1988). Use of the method has been reported by Liang *et al*. (2006) to describe microstructure of model lipid systems.

The main objective of this work is to show the importance of taking into account the spatial distribution of bubbles within foam structures and to introduce a value that can be employed for this purpose, the so called Euler characteristic derived

from Minkowski analysis. This has been done by analyzing the physical meaning of the Euler characteristic on model foam structures and also by measuring bubble spatial properties on real liquid foam samples.

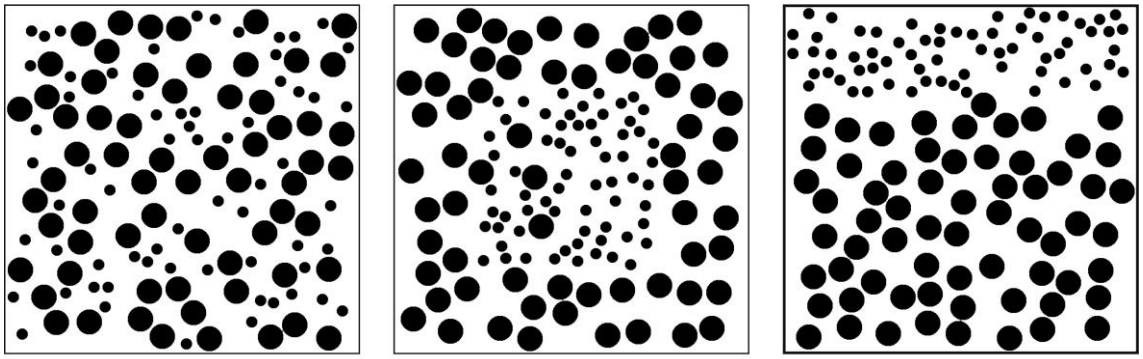

Figure 3.1: Simulated model foam structures with identical size distributions but different spatial arrangements. The three simulated structures share equal dimensions and number of small and large bubbles, but in (A) bubbles are randomly distributed, in (B) small bubbles are clustered at the center, and in (C) small bubbles are segregated at the top.

3.2. Materials and Methods

3.2.1. Samples and solution preparation

Commercially available protein sources were used to prepare the foam samples. Sodium caseinate (SCN) was obtained from Sigma-Aldrich (Saint Louis, USA), lot 84H478, and contained 87.5 % dry matter (d.m.) Whey protein isolate (WPI) from Davisco Foods International (Minnesota, USA), lot 057-4-420, and contained 85.7 % d.m. Ovalbumin (OVB) from Fluka BioChemica (Buchs, Switzerland), lot 1143891, and contained 84.4 % d.m. A conjugated protein (CJG) was also included in the study. The CJG was the result of the chemical reaction between sodium caseinate (Emmi Suisse SA, Dagmersellen, Switzerland) and Glucidex 21 (Roquette Fréres, Lestrem, France), a dried glucose syrup obtained by starch hydrolysis with a dextrose equivalent

of 20-23. Conjugation process is described by Gloria-Hernández (2006). Measured solid and protein content of purified conjugates were 86.9% and 75.0 % d.m., respectively.

Solutions used in foaming experiments were prepared by carefully dispersing the proteins and the conjugate in distilled water. Protein concentrations were adjusted to low (0.1 wt%) and high (0.4 wt%) levels, except for the conjugate, which was only analyzed at 0.1 wt%. pH was adjusted by the addition of either 0.1 N HCl or 1 N NaOH when necessary to low (5.5) and neutral (7.0) values.

3.2.2. Experimental sep-up for foam formation

Foaming experiments were done on a bench-top foaming apparatus implemented in the laboratory that is based on the description of Guillerme *et al*. (1993). The simplified scheme in Figure 3.2 describes this set-up that allows controlled formation of foam samples and recording of structures through time. System works with a flow of compressed air coming from a cylinder that is controlled with a gas flowmeter. Air flow sparges through the solution placed over a porous glass frit. Foam produced during sparging process is formed inside an acrylic column with rectangular cross section (37x37) mm. Column is illuminated using neon tubes, two vertically placed on the column sides, and a third illuminating from top.

All foaming experiments were done under the same conditions. A fixed volume (20 mL) of either protein or conjugate solution was placed inside foaming device at the base of the column. Gas was sparged into the solution at a rate of 50 mL/min through the porous fritt. Sparging continued until the foam produced within the column reached 120 mL, representing a theoretical gas fraction of 83.3 %. In certain cases the final total volume achievable was lower than 120 mL because of low foamability of the solution, particularly those containing proteins at low concentration and neutral pH. Once sparging was stopped, evolution of the foam structure was followed for a maximum of 29 min. Experiments for the three proteins and conjugate solutions, at both concentration and pH conditions, were performed in triplicate, except for 0.1 wt% CNJ at pH 7.0 which was only studied in duplicate.

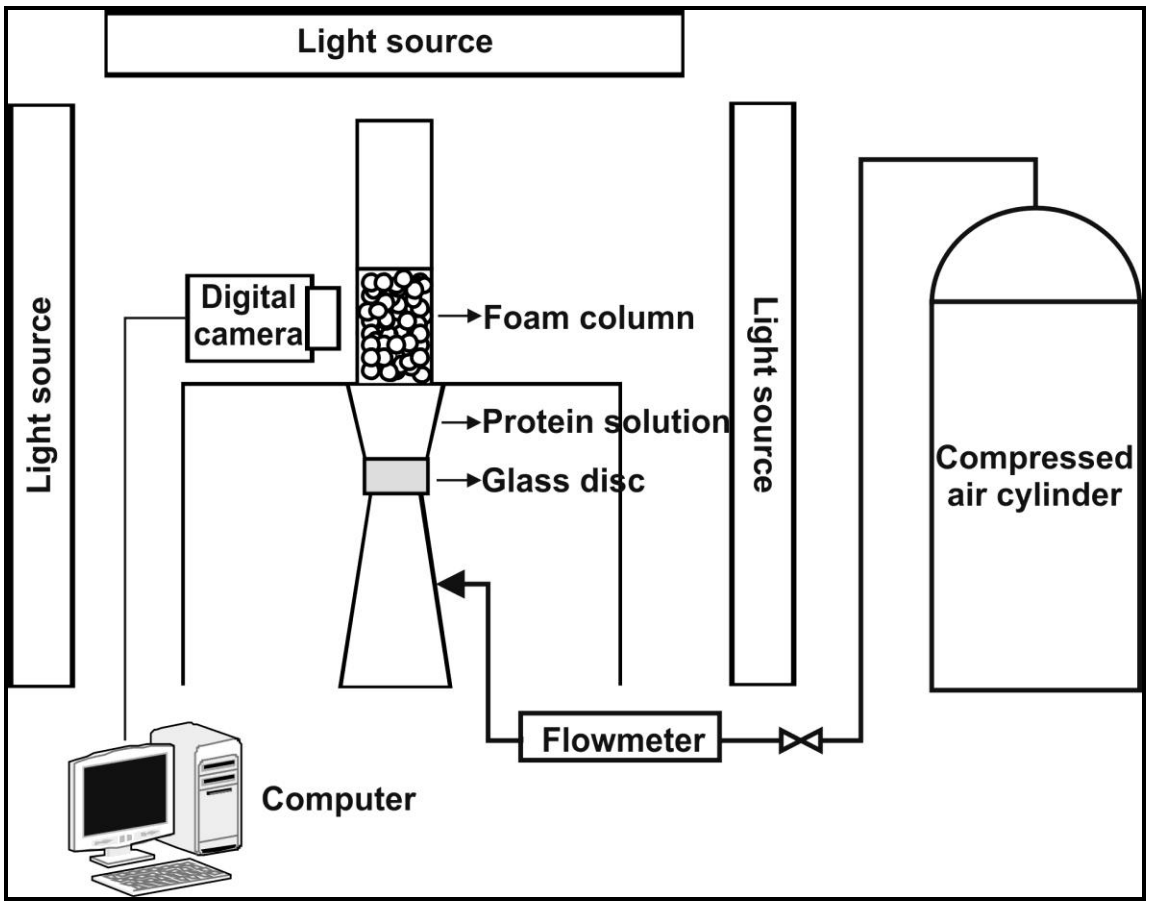

Figure 3.2: Scheme of the experimental apparatus used for the controlled formation and structural analysis of foams.

3.2.3. Image acquisition, processing and analysis

Image acquisition was done using a CoolSnap Pro digital camera (Media Cybernetics, Silver Spring, USA) coupled with a 16 mm Topica lens. As depicted in Figure 3.2, the camera was positioned facing one side of the square column. The camera was placed between the light sources in way no shadow was projected on the column wall. The recorded structure images corresponded therefore to two-dimensional slices of foam facing directly the surface of the column. It ought to be mentioned that bubble faces on the surface might be geometrically distinct from those in the interior, but since the objective is to describe bubble spatial distributions this does not imposes a restriction. Distance between the edge of the lens and the column face was set to 45 mm.

Height measured from the central part of the lens to the base of the foam column fixed to 50 mm. Acquisition was started immediately after sparging was stopped.

Original raw data was acquired as uncompressed TIFF color image series with frame size of 1392x1040 pixels of and calibration of 17 pixels per mm. Bubble segmentation process was done in a semi-automatic mode. Fully automatic protocol could not be developed because operator evaluation and manual input was required to account specific differences between samples. Processing operations were made in Image Pro-Plus software (Media Cybernetics, Silver Spring, USA). Processing steps consisted in selecting and cutting the center zone of images, where illumination was more homogeneous, to produce images of 657x 624 pixels. Converting color images to grey scale maps and enhance constant between foreground and background through histogram equalization followed by highpass and sharpen filtering. Separating touching bubbles through morphological watershed filtering and binarization by global thresholding. An opening filter was used at the end to remove some of remaining noise. Segmentation errors remaining at the end of the processing protocol were corrected manually by filing operations. Figure 3.3 compares the results of the processing protocol with the respective grey scale unprocessed images in selected cases.

3.2.4. Bubble size determination

Bubble size values were determined from the processed binary images using an in-house image analysis code implemented in MATLAB 7.10 (MathWorks, Massachusetts, USA). The program loads a complete time sequence of images and identifies all individual bubbles contained in each frame. The total area of each single bubble is calculated from the number of pixels and information is translated into equivalent bubble diameters (D_{eq}) value using:

$$D_{eq} = \sqrt{\frac{4}{\pi} area} \tag{3.1}$$

Bubble sizes raw data was exported into Excel files for further analysis. Mean D_{eq} values and statistical errors were computed using the data from all replicas for each system investigated.

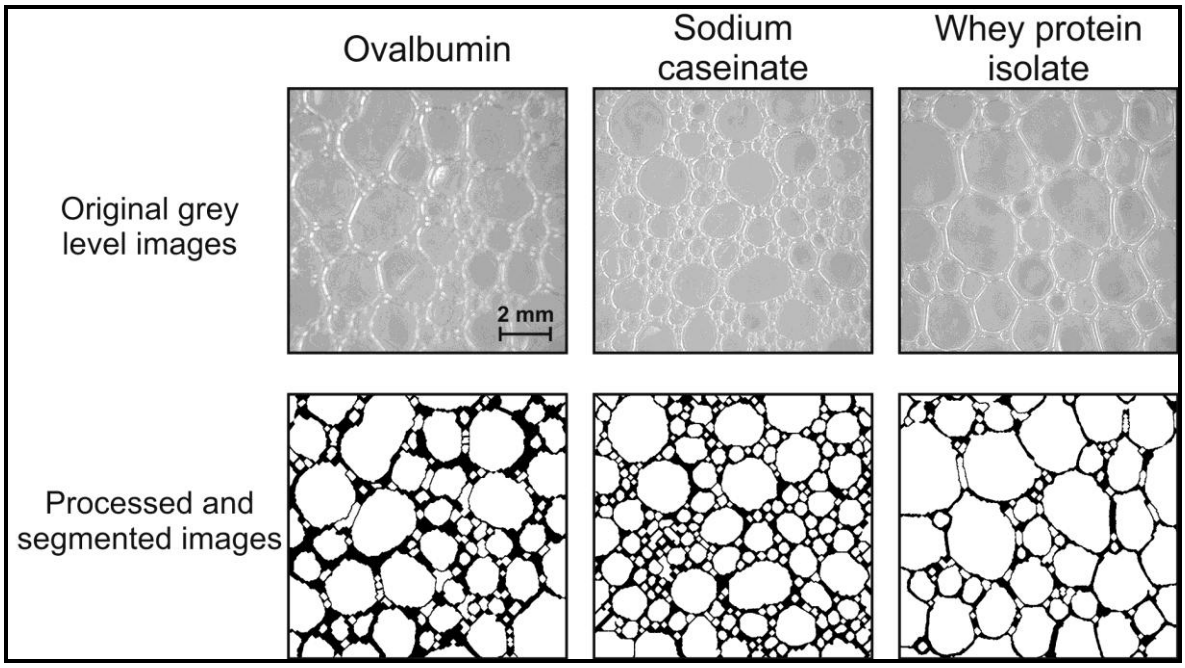

Figure 3.3: Original grey level images recorded during foaming experiments and processing and binarization results. Frames showed correspond to those immediately after sparging was stopped. Conditions in all cases are 0.1 wt% protein and pH 5.5.

3.2.5. Determination of spatial distributions by Minkowski analysis

Spatial distributions of bubbles in foams were analysed using a family of topological and geometrical descriptors belonging to the methods of integral geometry. These descriptors are known in digital image analysis and mathematical morphology as Minkowski functionals (MFs) (Michielsen and De Raedt, 2001). These functionals allow quantitative characterization of the morphology (time evolution of content, shape, and connectivity) of spatial patterns (Mecke and Sofonea, 1997). They embody information from every order of the point correlation functions, are numerically robust even for

small samples, and yield global as well as local morphological information (Kerscher *et al*., 2001).

In a *d*-dimensional space, *d*+1 MFs describe the morphological content of a spatial pattern. Although theoretically Minkowski analysis can be applied to a space of any dimension, the discussion is limited only to the two-dimensional case where three MFs can be determined. These MFs are the area (*A*) (or surface coverage), the perimeter (*U*) (or boundary length), and the Euler characteristic (χ). Regardless of the complex mathematics underlying the theory, MFs have the particular advantage of being easily calculated from digital images. MFs for entire images are calculated as the sum of the MFs for each pixel in the image (additive property). Consider for example that we want to characterize the geometry and topology using MFs of a pattern formed by black pixels representing the disk shown Figure 3.4. Each black pixel is decomposed into 4 vertices, 4 edges and the interior of the pixel. After counting the total number of black squares (n_s), edges (n_e), and vertices (n_v), the three MFs are calculated from:

$$\begin{aligned} A &= n_s \\ U &= -4n_s + 2n_e \\ \chi &= n_s - n_e + n_v \end{aligned} \tag{3.2}$$

For the example shown in Figure 3.4 we find $A = 13$, $U = 20$ and $\chi = 1$.

Among these three MFs that can be calculated in two dimensions the most sensitive parameter to changes in spatial distributions is χ. The Euler characteristic describes the connectivity (topology) of spatial patterns using number and positions as the basis for characterization and this functional is used for the analysis of foam structures in this work. The complete procedure for characterizing two-dimensional spatial patters using χ has been previously described by Liang *et al*. (2006), who applied the method to analyse the distribution of fat crystals and crystal flocks in model lipids systems from CLSM images. In this study the analysis begins determining the centroids of all bubbles within a foam digital image. The resulting list of (*x*,*y*) coordinates for all

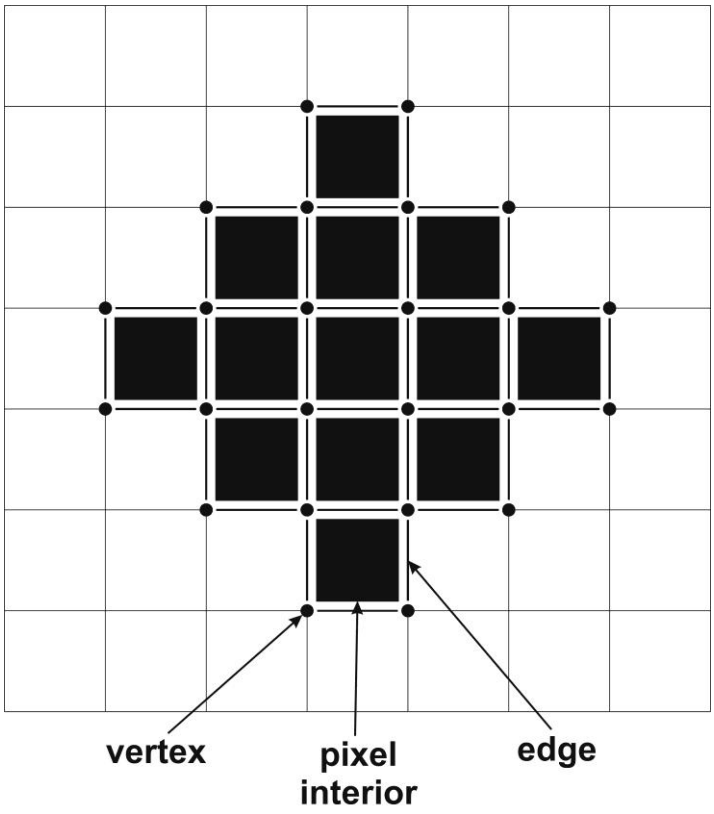

Figure 3.4: Decomposition of the black and white pattern representing a disk into squares, edges and vertices. For this example: number of squares n_s = 13, number of edges n_e = 36, and number of vertices n_v = 24.

bubble centroids defines the bubbles spatial distribution in two dimensions. The next step in the analysis is then to draw a disk of radius r around each coordinate and calculate χ for the set of disks as described above. Disks were used in this work because of bubble geometry but shape selection is arbitrary. Drawing of disks on digital images was done using a dilating technique based on the Euclidean distance map which has the advantage of being isotropic (Russ, 2005). The quantitative description of the bubble spatial distribution within the foam is given by the changes of χ as a function of r. The curve resulting from the plot of χ versus r is characterized by four values: maximum (χ_{max}) and minimum Euler characteristic (χ_{min}), Euler minimum length (l_{min}), and zero crossing length (l_0) (Liang *et al.*, 2006). Figure 3.5 shows a typical plot of χ versus r that results in this particular case from the analysis of the simulated random foam structure

shown in Figure 3.1A. Figure 3.5 indicates the four representative curve values (χ_{max}, χ_{min}, l_{min} and l_0) and shows also graphically the process of drawing increasingly larger disks over the initial bubble spatial distribution. Initially, when the disks are small and do not overlap, χ reaches its maximum equal to the number on bubbles. Values of χ then start to decrease as r increases and disks overlap eventually reaching negative magnitudes. As the disks growing process continues, χ reaches its minimum and finally begins to increase again until an end value of 1 when the entire image is covered by the disks.

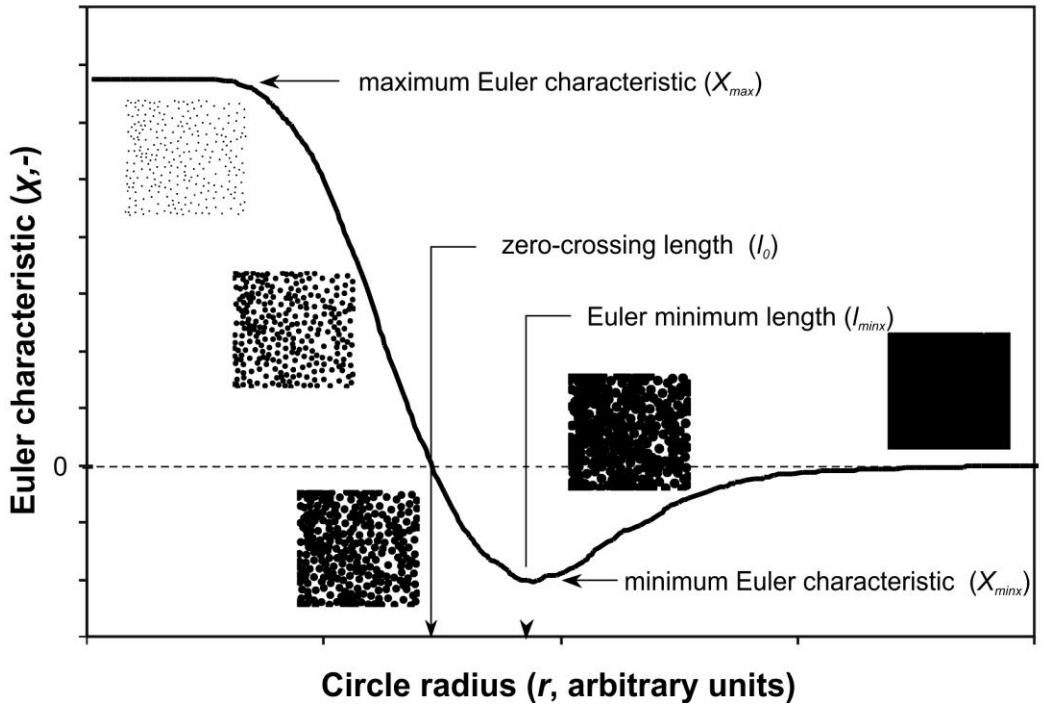

Figure 3.5: Typical plot of the Euler characteristics versus increasing disk radius resulting from the analysis of the simulated random foam structure shown in Figure 3.1A. Arrows indicate the four representative curve values. Figures along the plot exemplify graphically the disk growing process from the bubble centroids spatial distribution.

Plots describing the variation χ as a function of r for simulated foam structures and images of real foams obtained during the sparging experiments were determined with an in-house code implemented in MATLAB 7.10 (MathWorks, Massachusetts, USA). Each of these plots were then analysed to extract their respective χmax, χ_{min}, l_{min} and l_0 values.

3.3. Results and Discussion

3.3.1. Physical interpretation of Euler characteristic values

Before starting investigating foam structures using Minkowski analysis, it is necessary to get a better understanding of the information given by the four values extracted from the Euler characteristic plot. The simplified diagrams presented in Figure 3.6, where disks are used once more to represent two-dimensional bubble cuts, give an intuitive idea of the physical meaning of each value by comparing a base case (1) with four other situations (2-5). Representations 2-5 in Figure 5 were designed to differ only in one of the four parameters with the base case, while the other three remain identical between both situations.

The physical interpretation of χ_{max} is given by comparison of cases 1 and 2. The value of χ_{max} is equal to the number of bubbles. It is hence direct that χ_{max} in the base case has a larger magnitude than in case 2. Graphically, case 2 represents a more packed arrangement than case 1, although nearest neighbour distances between bubbles remain unmodified. This indicates that the maximum Euler characteristic yields information that is related to compactness degree of the arrangement in structure.

Comparison between cases 1 and 3 illustrates the physical interpretation of l_0. The magnitude l_0 is larger for case 1 than for case 3. Relative positions of the bubbles between both cases are similar; however distances in case 3 between adjacent bubbles are on average shorter. Thus, the zero-crossing length is a measure of distance with a direct connection to the separations between adjacent bubbles of the structure.

The information contained in the value of by χ_{min} can be understood by comparing cases 1 and 4. The base case represents a situation where the value of χ_{min} is lower than case 4. The only structural difference between both cases is that in the latter one bubble is displaced from the bottom to the top row. This change in position implies a reduction in total number of interconnections that can be established between the bubbles of the structure. The bubble that has been moved can no longer see the same number of neighbors as before. This give rise to the idea of connectivity, defined as the number of links a bubble in the structure can establish simultaneously with the immediate neighbors. Therefore, the minimum Euler characteristic gives information that is related to the degree of connectivity within the structure.

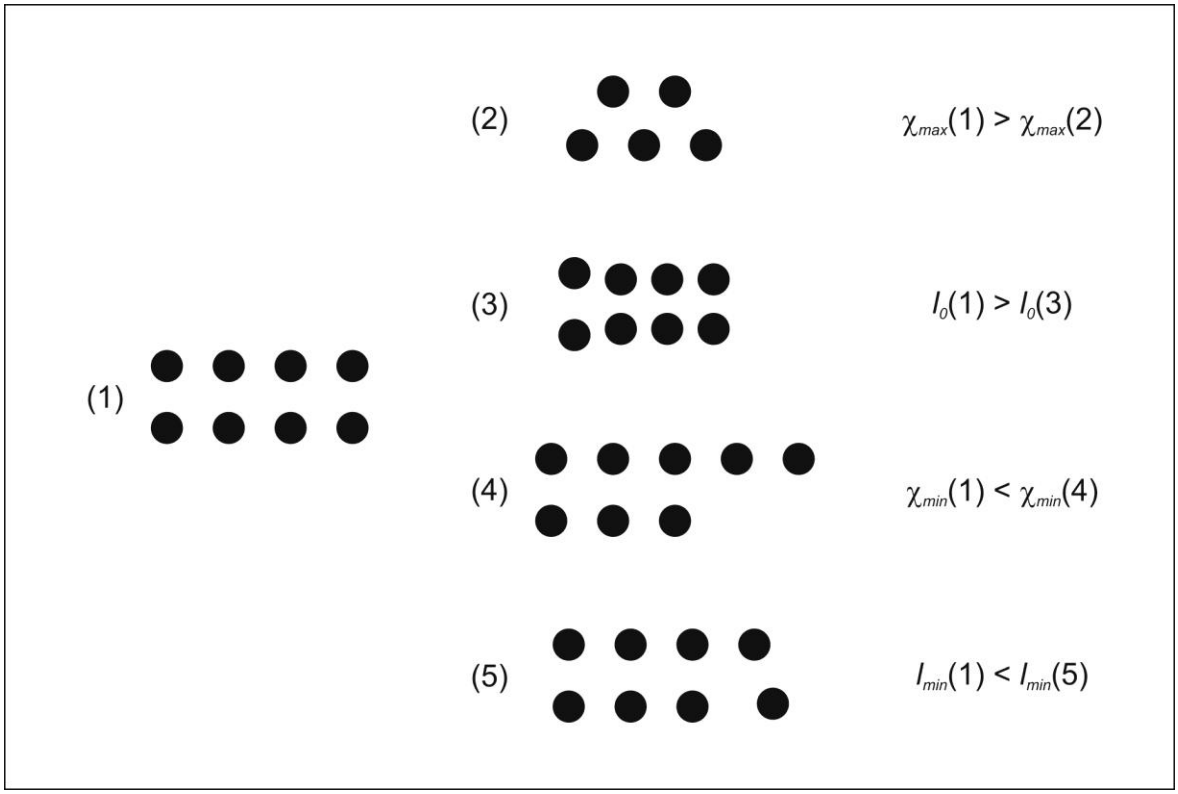

Figure 3.6: Physical interpretation of the Euler characteristic values. Diagrams compare situation where only one Euler characteristic value is modified, while the other three remain equal.

Finally, the physical meaning of l_{min} is illustrated by cases 1 and 5. Both cases differ only that in the second one a bubble has been slightly displaced up and to the right. This modification translates into and increment in the magnitude of l_{min}. Average distance between adjacent bubbles remains the same for both cases (value of l_0 remains equal), also the degree of connectivity (same value of χ_{min}), but the average distance necessary to connect the bubbles has increased. Consequently, the Euler minimum length can be regarded as a measure of the connectivity distance of the structure.

3.3.2. Size and spatial measurements on model bubble structures

The Minkowski analysis was applied to model bubble structures as those depicted in Figure 3.1. The objective is to illustrate the additional information provided by the Euler characteristic parameters in a simplified case. Table 3.1 summarizes the results obtained for the mean bubble sizes expressed as average D_{eq} and spatial distributions measurements from Euler characteristic analysis. The values reported in the table correspond to mean values calculated from ten simulations of each structure type shown in Figure 3.1. Simulations of model bubble structures were customized in MATLAB 7.10 (MathWorks, Massachusetts, USA). Each simulated structure consisted in 65 small and 65 large disks (9 and 21 pixels in diameter respectively) distributed over a 600x600 pixels^2 grid in either random, clustered or segregated organization. The surface covered by disks was fixed to 32% of the total area. An additional rule that disks should not overlap each other nor the edges of the grid was also imposed during simulations.

Values in Table 3.1 indicate that the three model structure types share identical values for the average D_{eq} and χ_{max}. These results are straightforward based on the manner the structures were simulated described above. Measurements of the other three Euler characteristics values nonetheless, show that the three model systems have different spatial properties. Based on the previous analysis, the higher value of l_0 in the segregated structure expresses that in this case adjacent disks are on average further away than disks in the random and clustered structures. Furthermore, the degree of connectivity of the disks in the random case is higher than for the segregated, which in

turn is higher than for the clustered, evinced by the increase observed in the values of χ_{min}.The connectivity distances between the structures also increase, being the random structure the one with shorter distances, followed by the clustered structure and finally the segregated structure, as shown by the differences in the values of l_{min}. These observations are direct result of the purely spatial constraints imposed to the positions of the disks on the simplified systems simulated. Nevertheless, this model example shows the complementary information on the foam structure that can be gained by incorporating measures of spatial properties on the analysis.

Table 3.1: Results of the image analysis of idealized foam structures

Average structural parameters[a]	Structure type		
	random	clustered	segregated
D_{eq}	31.3 ± 0.3	31.3 ± 0.3	31.3 ± 0.3
χ_{max}	130.0 ± 0.0	130.0 ± 0.0	130.0 ± 0.0
l_0	23.2 ± 0.1	23.8 ± 0.4	25.1 ± 0.3
χ_{min}	-70.8 ± 2.5	-47.4 ± 1.7	-51.8 ± 2.1
l_{min}	31.2 ± 0.6	33.4 ± 1.2	36.5 ± 0.6

[a]Values correspond to the average of 10 simulations. Means are reported with standard errors. Units of D_{eq}, l_0 and l_{min} are in pixels.

3.3.3. Size and spatial measurements on real foams

The Euler characteristic method was finally applied to real foam structures. The series of pictures in Figure 3.7 give a summary overview of the range of different foam “architectures” produced through sparging by changing the stabilizing molecule, the solution concentration and pH as described in the Methods section. Figure 3.7 illustrates graphically and to some extent the diversity and complexity embodied by real

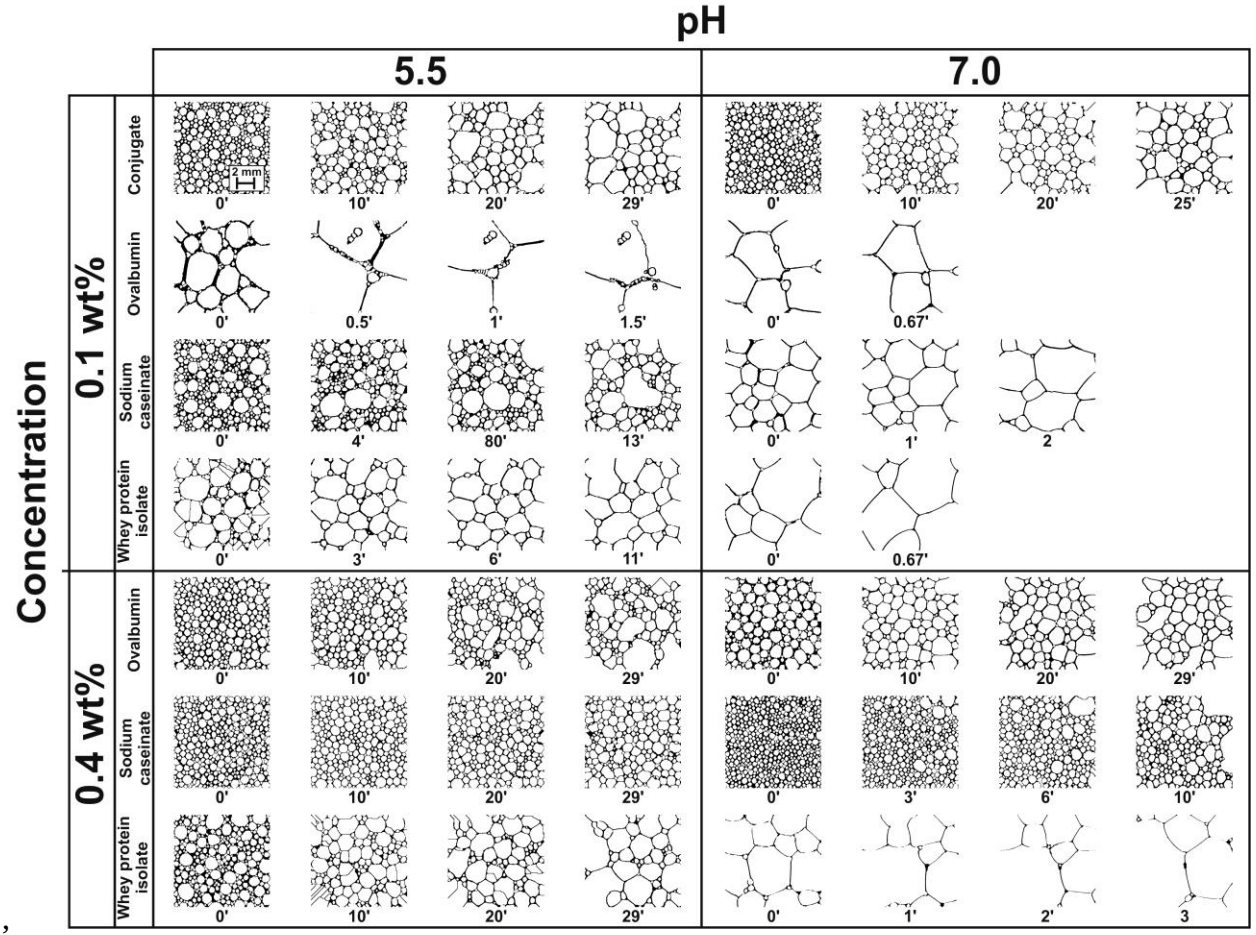

Figure 3.7: Gallery showing examples of resulting segmented binary images of foam structures. Pictures are grouped according to concentration and pH values of solutions used to prepare foams. Numbers under each image indicates the time in minutes at which the picture was taken, measured immediately after sparging was stopped.

foam structures. The broad scope of foam structures depicted in the figure is explained partially by the process proteins undergo at gas/liquid interfaces. In the general case molecules have to diffuse, adsorb, unfold and aggregate at the surface (Maldonado-Valderrama *et al.* 2005; de Jongh 2007). The rates at which these events occurs are modulated by the chemical nature and size of molecules, together with physical factors like pH, temperature, concentration viscosity, ionic strength, etc. Additional changes of the foam structure arise from the inherent unstable nature these systems (Weaire and Hutzler 1999). Foam structure stability is affected by three basic mechanisms: drainage, Oswald ripening and coalescence. Foam instabilities impact not only bubble sizes, but modifies as well spatial properties.

Figure 3.8 summarizes the results of the Minkowski analysis on real foams by plotting values of the four Euler characteristic parameters measured from foam images as a function of their corresponding mean D_{eq}. These plots allow direct evaluation of the relations existing between mean bubble sizes and bubble spatial distributions.

The relatively vertical dispersion on the values of χ_{max} shown in the first plot in Figure 3.8 indicates that for the real foams this parameter do not have a strong dependency on the mean bubble size. In the previous analysis it was shown that χ_{max} reflects compactness of the spatial arrangement. Because all images taken during the experiments shared the same dimensions and magnification, higher values of χ_{max} are therefore connected to higher packing degrees of bubbles in the foam structure. Data of χ_{max} in Figure 3.8 shows that in several cases foams that display similar mean D_{eq} have different values of χ_{max}. A direct example are data sets for foams prepared using 0.1 wt% SNC at pH 5.5 (χ_{max} ~ 475) and 0.5 wt% SNC at pH 7.0 (χ_{max} ~250).

Connectivity degree of foam structures characterized by values of χ_{min} displayed a peculiar dependence on the mean bubble size. The plot in Figure 3.8 indicates that the general tendency of this parameter was to steadily increase from around -200 to -10 between 400 μm and 1000 μm, remaining virtually constant at larger

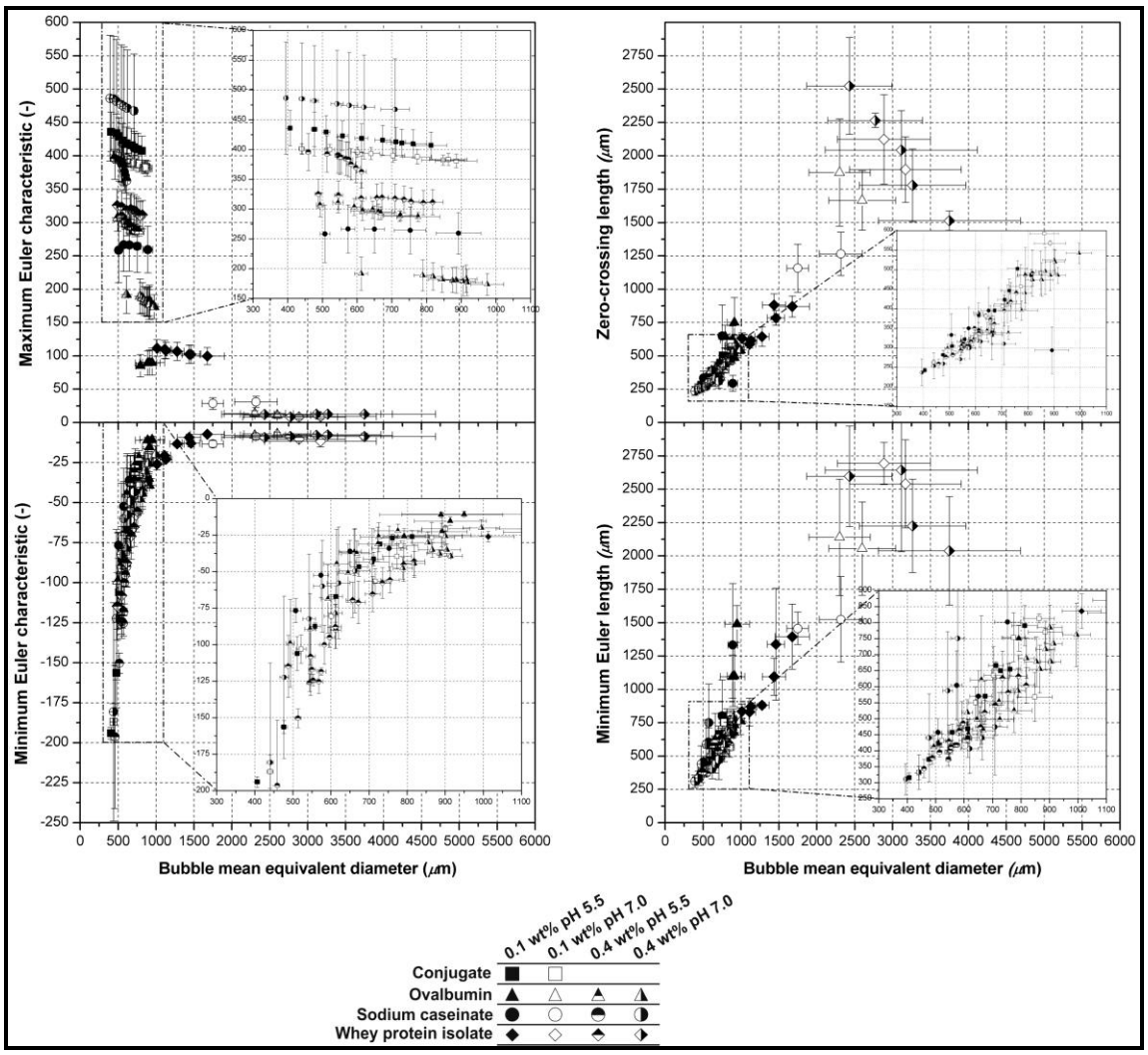

Figure 3.8: Results of size and spatial distribution measurements on real foam structures. Values of Euler characteristic parameters are plotted against corresponding mean equivalent diameters.

mean bubble sizes. The apparent limiting value reached by χ_{min} at larger mean sizes is explained by the second law of Plateau (1873). This law applies to foams in the dry limit and dictates that at the vertices of the foam structure no more than 4 intersection lines (or 6 surfaces) may meet. Thus, in dry foams when bubbles are no longer spherical connectivity is geometrically restricted. In relatively wet foams with spherically shaped bubbles connectivity can be higher as evidenced by the low values of χ_{min} reached in

Figure 3.8, particularly for foams prepared with 0.1 wt% CJG at pH 5.5 and 7.0 and 0.4 wt% SCN at pH 7.0. The plot insert shows that, despite the general correlation observed between χ_{min} and D_{eq}, the value of this Euler parameter varied between foams with equal mean sizes, thus complementing also the information given by size measurements.

Both Euler parameters related to distance measures, l_0 and l_{min}, show similar linear dependencies with D_{eq} (Figure 3.8). This correlation is not totally unexpected, since it is straightforward that separations between bubbles have a direct dependence with bubble sizes. Values of l_0 in Figure 3.8 can estimate the average thickness of the liquid films separating the bubbles at their closest point (between 80-110 μm for bubble with D_{eq} < 900 μm according to the data in Figure 3.8). However, it is not possible to conclude that l_0 gives any significant differences between samples at equal mean sizes as was before for χ_{max} and χ_{min}. The situation is different with the values of l_{min} as a function of D_{eq}. Data in Figure 3.8 shows that values of l_{min} disperse along the vertical axis at constant mean D_{eq}, indicating that part of the information in l_{min} is uncorrelated with the mean sizes and consequently provide further data on foam structure. It can be concluded therefore that, although in the experiments mean distances remain equal for structures of the same mean bubble sizes (equal values of l_0), values of l_{min} may differ because bubbles only change their relative positions and not their absolute separations.

3.4. Conclusions

New features of the complex structure of foams were elucidated by a novel approach, the Minkowski analysis. Complementary to the bubble size measurements, Euler characteristic parameters derived from this analysis were able to provide additional information related to spatial distributions of bubbles within foam structures. The four parameters used to describe the foams architectures in this work provided valuable information related to,

- Compactness degree of bubble arrangements (Maximum Euler characteristic)

- Average separating distances between adjacent bubbles (Zero-crossing length)

- Connectivity degree of bubble arrangements (Minimum Euler characteristic)

- Connectivity distances of between adjacent bubbles (Euler minimum length)

Material scientists and engineers work to unveil the connections between structure and ways products behave (Aguilera 2006). Concepts and tools like those presented in this work can help in closing gaps between the structure of foams and our understanding of their macroscopic physical properties.

3.5. References

Aguilera, J.M. (2006). Seligman Lecture 2005 - Food product engineering: Building the right structures. *Journal of the Science of Food and Agriculture*, 86(8), 1147-1155.

Aguilera JM. (2005). Why food microstructure*? Journal of Food Engineering*, 67(1-2), 3-11.

Aguilera, J.M. (2000). Microstructure and food product engineering. *Food Technology*, 54:56-58, 60, 62, 64, 66.

Aguilera, J.M. and Stanley, D.W. (1999). *Microstructural Principles of Food Processing and Engineering* (2nd. Ed.), Gaithersburg, MD, Aspen Publishers Inc.

Alavi, S.H., Gogoi, B.K., Khan, M., Bowman, B.J. and Rizvi, S.S.H. (1999). Structural properties of protein-stabilized starch-based supercritical fluid extrudates. *Food Research International*, 32(2), 107-118.

Arns, C., Knackstedt, M., Pinczewski, W. and Lindquist, W.B. (2001a). Accurate estimation of transport properties from microtomographic images. *Geophysical Research Letters*, 28(17), 3361-3364.

Arns, C., Knackstedt, M., Pinczewski, W. and Mecke, K. (2001b). Euler-Poincaré characteristics of classes of disordered media. *Physical Review E*, 63, 31112-1-31112-13.

Babin, P., Della Valle, G., Chiron, H., Cloetens, P., Hoszowska, J., Pernot, P., Réguerre, A.L., Salvo, L. and Dendievel, R. (2006). Fast X-ray tomography analysis of bubble growth and foam setting during bread making. *Journal of Cereal Science*, 43, 393-397.

Babin, P., Della Valle, G., Dendievel, R., Lassoued, N. and Salvo, L. (2005). Mechanical properties of bread crumbs from tomography based Finite Element simulations. *Journal of Materials Science*, 40(22), 5867-5873.

Bals, A. and Kulozik, U. (2003). Effect of pre-heating on the foaming properties of whey protein isolate using a membrane foaming apparatus. *International Dairy Journal*, 13(11), 903-908.

Campbell, G.M. and Mougeot, E. (1999). Creation and characterisation of aerated food products. *Trends in Food Science and Technology*, 10(9), 283-296.

Chang, Y. and Hartel, R.W. (2002). Measurement of air cell distributions in dairy foams. *International Dairy Journal*, 12(5), 463-472.

de Jongh, H.H.J. (2007). Proteins in food microstructure formation. In D.J. McClements (Ed.) *Understanding and controlling the microstructure of complex foods*, Woodhead Publishing Limited, Cambridge, England, pp. 40-66.

Dickinson, E. (2007). Colloidal systems in foods containing droplets and bubbles. In D. J. McClements (Ed.) *Understanding and controlling the microstructure of complex foods*. Woodhead Publishing Limited, Cambridge, UK, pp. 153-184.

Eisner, M.D., Wildmoser, H. and Windhab, E.J. (2005). Air cell microstructuring in a high viscous ice cream matrix. *Colloids and Surfaces A-Physicochemical and Engineering Aspects*, 263(1-3), 390-399.

Gloria-Hernández, H. (2006). *Formation of protein-polysaccharide conjugates ad study of their physicochemical and functional properties*. Unpublished Doctoral thesis, Universidad Politécnica de Valencia, Valencia, España.

Guillerme, C., Loisel, W., Bertrand, D. and Popineau, Y. (1993). Study of foam stability by video image analysis: relationship with the quantity of liquid in the foams. *Journal of Texture Studies*, 24, 287-302.

Haedelt, J., Pyle, D.L., Beckett, S.T. and Niranjan, K. (2005). Vacuum-induced bubble formation in liquid-tempered chocolate. *Journal of Food Science*, 70, E159-E164.

Hicsasmaz, Z., Yazgan, Y., Bozoglu, F. and Katnas, Z. (2003). Effect of polydextrose-substitution on the cell structure of the high-ratio cake system. *Lebensmittel-Wissenschaft Und-Technologie-Food Science and Technology*, 36(4), 441-450.

Jang, W., Nikolov, A., Wasan, D.T., Chen, K. and Campbell, B. (2005). Prediction of the bubble size distribution during aeration of food products. *Industrial & Engineering Chemistry Research*, 44(5), 1296-1308.

Kerscher, M. (2000). Statistical Analysis of Large-Scale Structure in the Universe. In K. Mecke and D. Stoyan (Eds.) *Statistical physics and spatial statistics: The art of analyzing and modelling spatial structures and pattern formation (Lecture notes in physics 554)*, Springer Verlag, Berlin.

Kerscher, M., Mecke, K., Schuecker, P., Böhringer, H., Guzzo, L., Collins, C.A., Schindler, S., De Grandi, S. and Cruddace, R. (2001). Non-Gaussian morphology on large scales: Minkowski functionals of the REFLEX cluster catalogue. *Astronomy and Astrophysics*, 377, 1-16.

Kulmyrzaev, A., Cancelliere, C. and McClements, D.J. (2000). Characterization of aerated foods using ultrasonic reflectance spectroscopy. *Journal of Food Engineering*, 46(4), 235-241.

Liang, B.M., Sebright, J.L., Shi, Y.P., Hartel, R.W. and Perepezko, J.H. (2006). Approaches to quantification of microstructure for model lipid systems. *Journal of the American Oil Chemists Society*, 83(5), 389-399.

Lim, K.S. and Barigou, M. (2004) X-ray micro-computed tomography of cellular food products. *Food Research International*, 37(10), 1001-1012.

Maldonado-Valderrama, J., Fainerman, V.B., Aksenenko, E.V., Gàlvez-Ruiz, M.J., Cabrerizo-Vílchez, M.A. and Miller, R. (2005). Dynamics of protein adsorption at the oil–water interface: comparison with a theoretical model. *Colloids and Surfaces A: Physicochemical and Engineering Aspects*, 261, 85-92.

Martinet, V., Valentini, C., Casalinho, J., Schorsch, C., Vaslin, S. and Courthaudon, J.-L. (2005). Composition of interfacial layers in complex food emulsions before and after aeration: effect of egg to milk protein ratio. *Journal of Dairy Science*, 88, 30-39.

Mecke, K. (2000). Additivity, Convexity, and Beyond: Applications of Minkowski Functionals in Statistical Physics. In K. Mecke and D. Stoyan (Eds.) *Statistical physics and spatial statistics: The art of analyzing and modelling spatial structures and pattern formation (Lecture notes in physics 554)*, Springer Verlag, Berlin.

Mecke, K.R. and Sofonea, V. (1997). Morphology of spinodal decomposition. *Physical Review E*, 56(4), R3761-R3764.

Michielsen, K. and De Raedt, H. (2001). Integral-geometry morphological image analysis. *Physics Reports*, 347, 461-538.

Plateau, J.A.F. (1873). *Statique Expérimentale et Théorique des Liquides soumis aux seules Forces Moléculaires*, Gauthier-Villars, Paris, France.

Richardson, G., Langton, M., Faldt, P. and Hermansson, A.M. (2002). Microstructure of alpha-crystalline emulsifiers and their influence on air incorporation in cake batter. *Cereal Chemistry*, 79(4), 546-552.

Russ, J.C. (2005). *Image Analysis of Food Microstructure*. Boca Raton, Florida, EE.UU.: CRC Press LLC.

Sahi, S.S. and Alava, J.M. (2003). Functionality of emulsifiers in sponge cake production. *Journal of the Science of Food and Agriculture*, 83(14), 1419-1429.

Schoonman, A., Mayor, G., Dillmann, M.L., Bisperink, C. and Ubbink, J. (2001). The microstructure of foamed maltodextrin/sodium caseinate powders: a comparative study by microscopy and physical techniques. *Food Research International*, 34(10), 913-929.

Serra, J. (1982). *Image Analysis and Mathematical Morphology*, London, UK: Academia Press.

Serra, J. (1986). Introduction to Mathematical Morphology. *Computer Vision, Graphics, and Image Processing*, 35, 283-305.

Trater, A.M., Alavi, S. and Rizvi, S.S.H. (2005). Use of non-invasive X-ray microtomography for characterizing microstructure of extruded biopolymer foams. *Food Research International*, 38(6), 709-719.

Weaire, D. and Hutzler, S. (1999). *The Physics of Foams*. Clarendon Press, Oxford, UK.

4. IDENTIFYING INDUSTRIAL FOOD FOAM STRUCTURES BY 2D SURFACE IMAGE ANALYSIS AND PATTERN RECOGNITION

4.1. Introduction

Incorporation of gas (most commonly air) bubbles into food structures is a simple and rather inexpensive way to significantly modify several product characteristics (Campbell and Mougeot, 1999). Among them is the remarkable alteration of rheological properties this process provokes. An illustrating example experienced everyday in kitchens worldwide is simply beating egg albumen to produce meringue. This process begins with a viscous fluid and ends with a system displaying completely different rheology with solid-like characteristics.

Understanding the quantitative relationships existing between inclusion of gas bubbles and physical transformations in food systems is of practical importance. This knowledge can be applied, for example, to engineer products with tailored properties. The link between aeration and physical properties can be partially realized when bubble containing foods (and all foods in general) are viewed as engineering materials similar to textiles, wood, clay, metal, ceramics and plastics (Aguilera and Lillford, 2008). Material properties are a direct consequence of the particular attributes of their constitutive elements (the building blocks) and their organization within the system (the structure). Physical properties of food foams and aerated products therefore can be regarded as a result of bubble characteristics (size) and their spatial arrangement.

In this work, foam structure refers to the size and shape of bubbles within foams and also to their spatial organization within the whole system. Bubble size is probably the most important and direct parameter to define foam structure. Examples of bubble size and size distribution measurements on numerous foamed products, using multiple techniques, abound in the literature (Niranjan and Silva, 2008; Germain and Aguilera, 2011). Bubble spatial organization in foam structures is however an aspect commonly overlooked. The complete description of foam structure requires not only information related to bubble size, but also accurate and objective quantitation of bubble

spatial organization in aerated systems. A number of methodologies can be applied to determine bubble spatial distribution, and particularly for foam structure characterization (Reed *et al.*, 1997; Torquato, 2002; Schabenberger and Gotway, 2005).

One suitable approach to describe the distribution of elements within structures is Minkowski functionals (MFs), a family of topological and geometrical descriptors belonging to methods of integral geometry (Michielsen and De Raedt, 2001). MFs allow quantitative characterization (time evolution of content, shape, and connectivity) of spatial patterns (Mecke and Sofonea, 1997). They embody information from every order of the correlation functions, are numerically robust even for small samples, and yield global as well as local morphological information (Kerscher *et al.*, 2001). Application of MFs in statistical physics and cosmology has been reviewed by Mecke (2000) and Kerscher (2000), respectively. These basic functionals (Serra, 1982) have been successfully applied to image analysis in many areas, including condensed matter physics (Mecke, 2000), geology (Arns *et al.*, 2001a,b), and general mathematical morphology (Serra, 1986). Within a two dimensional plane three MFs can be defined: covered area, boundary length, and Euler characteristic. Of particular interest is the latter parameter that contains information related to pattern connectivity. The microstructure of a model lipid system has been described using an image analysis method based on changes of the Euler characteristic (Liang *et al.*, 2006).

A second way to analyze food structure properties is fractal theory. Mandelbrot (1983) proposed the definition of fractal objects as a way to describe complex structures which cannot be properly characterized by Euclidean geometry. Since the limited initial application of fractal analysis in food science (Peleg, 1993; Barret and Peleg, 1995), the theory has gained increasing popularity and is used intensively for food structure analysis (Falcone *et al.*, 2006). Although foams and foods in general are not true fractals from a mathematical standpoint, they do have fractal-like properties. Non-periodic complex structures produced through random physical and biochemical processes like that of food foams may be well characterized by fractional dimensions (Liu and Scanlon, 2003).

Image texture analysis represents a third approach to study food structure properties. It is a method that basically describes visual perception of irregularities and variations over digital images (Aguilera and Germain, 2007). It relates both, pixel brightness values and spatial distributions over images, and represents an objective way to characterize complex food structures. To the best of our knowledge, Bertrand *et al.* (1992) were the first to use image texture analysis to describe foam-like structures. The authors proposed a method based on the two-dimensional Haar transform to describe bread crumb from digital images. Following studies by Guillerme *et al.* (1993), Fains *et al.* (1997), Hagolle *et al.* (2000), and Rahali and Gueguen (2000) used this approach to investigate protein-based liquid foams. Other image texture methodologies to analyze foam structures have also been described (Sarker *et al.*, 1998; Rouillé *et al.*, 2005). Zheng *et al.* (2006) have reviewed most of the recent applications of image texture analysis to food systems. Among the different alternatives, the gray level co-occurrence matrix (GLCM) appears as the most widely used technique for quality grading or classification in the food industry. GLCMs present the relative frequency distributions of gray levels and describe how often one gray level will appear in a specified spatial relationship to another gray level. They can be regarded as two-dimensional histograms containing important characteristics of the image texture. Haralick *et al.* (1973) proposed 14 textural features that can be derived from GLCMs, each one representing a specific image property. GLCMs have been used in the investigation of many different food products; nevertheless, the only application to foam-like structures is that of Gao and Tan (1996a,b).

This work presents the study of foam structures using different image analysis methodologies (Euler characteristic, Minkowski fractal and GLCM). For this purpose, images of liquid foams prepared by sparging aqueous solutions of three different proteins and a conjugated protein at different protein concentrations and pH levels were recorded and analyzed. The objective was to identify quantitative parameters that can be used to further describe the structural properties of foamed systems.

4.2. Materials and Methods

4.2.1. Foam sample preparation and structure imaging

Three commercially available protein sources and a synthesized conjugated protein were used to prepare foam samples with different structural characteristics. Sodium caseinate (SCN) was obtained from Sigma–Aldrich (Saint Louis, USA), lot 84H478; whey protein isolate (WPI) from Davisco Foods International (Minnesota, USA), lot 057–4-420; ovalbumin (OVB) from Fluka BioChemica (Buchs, Switzerland), lot 1143891. Conjugated protein (CJG) was the result of the chemical reaction between sodium caseinate (Emmi Suisse SA, Dagmersellen, Switzerland) and Glucidex 21 (Roquette Fréres, Lestrem, France), a dried glucose syrup obtained by starch hydrolysis with a dextrose equivalent of 20–23. The conjugation process is described in detail by Gloria-Hernández (2006). Aqueous solutions were prepared by carefully dispersing the protein or the conjugate in distilled water. The protein concentration was adjusted to low (0.1 wt.%) and high (0.4 wt.%) levels, except for the conjugate, which was only analyzed at a low concentration. These concentrations values were chosen based on dynamic tensiometry data (Section 2.3.3) indicating complete surface coverage at both conditions but faster protein adsorption at 0.4 wt.%. The conjugate was studied only at 0.1 wt.% because its foamability was already high at that concentration and comparable to 0.4 wt.%. The pH was adjusted by the addition of either 0.1 N HCl or 1 N NaOH when necessary to achieve a low (5.5) or neutral (7.0) pH. At these two different pH's the proteins have different surface charges, neutral at pH 5.5 and strongly charged at pH 7.0.

The experimental set-up of the foaming apparatus used for controlled preparation of foam samples has been detailed previously (Section 3.2.2). The device is based on the description of Guillerme *et al.* (1993) and allows imaging of foam structures produced by sparging gas inside an acrylic column with rectangular cross section illuminated using neon tubes (two vertically placed on the column sides, and a third illuminating from top). During each experiment, 120 mL of foam was prepared from 20 mL of solution (theoretical gas fraction of 83.3%) at a gas flow rate of 50

mL/min. In certain cases the foam volume achievable was lower because of low foamability of the solutions, particularly those containing proteins at low concentration and neutral pH. The experiments were conducted at room temperature, which ranged between 18–23 °C. Foam structure was recorded as uncompressed TIFF color images with frame size of 1392 × 1040 pixels and a calibration of 17 μm/pixel. To have a description of the initial foam structure, a first picture was taken immediately after sparging was stopped and a second record taken 10–60 s after, depending on the stability of the particular system. Both images shared very similar spatial parameters slightly altered by drainage and coalescence processes occurring between acquisition of the 2 frames.

In total, 14 combinations (referred henceforward as sample classes) were studied considering surface active molecule type, concentration and pH levels. Experiments were done in triplicate and each sample class was therefore described by 6 images. The only exception was foam prepared from 0.1 wt.% CJG at pH 7.0 which was only analysed in duplicate and hence only 4 images were recorded. A complete set of 82 foam images was processed in a semi-automatic mode to produce segmented binary images with isolated bubbles in Image Pro-Plus software (Media Cybernetics, Silver Spring, USA). Processing steps consisted of: selecting and cutting the center zone to produce images of 657 × 624 pixels; converting color images to grey scale maps; contrast enhancement through histogram equalization; highpass and sharpen filtering; separation of touching objects through morphological watershed filtering; binarization by global thresholding. At the end an opening filter was used to remove remaining noise, and segmentation errors were corrected manually by filling operations. Figure 4.1 compares the results of the processing protocol with the respective gray scale unprocessed images for two selected cases.

4.2.2. Structural parameters determination

The structural properties of foam samples were analyzed from segmented digital images using three methods: Euler characteristic, Minkowski fractal and image texture analyses. Descriptions of these methodologies are given below. In addition,

mean bubble size values of foam samples were also determined from the segmented digital images. The area of each bubble was calculated from the number of pixels and translated into equivalent bubble diameter (D_{eq}) values by:

$$D_{eq} = \sqrt{\frac{4}{\pi} area} \tag{4.1}$$

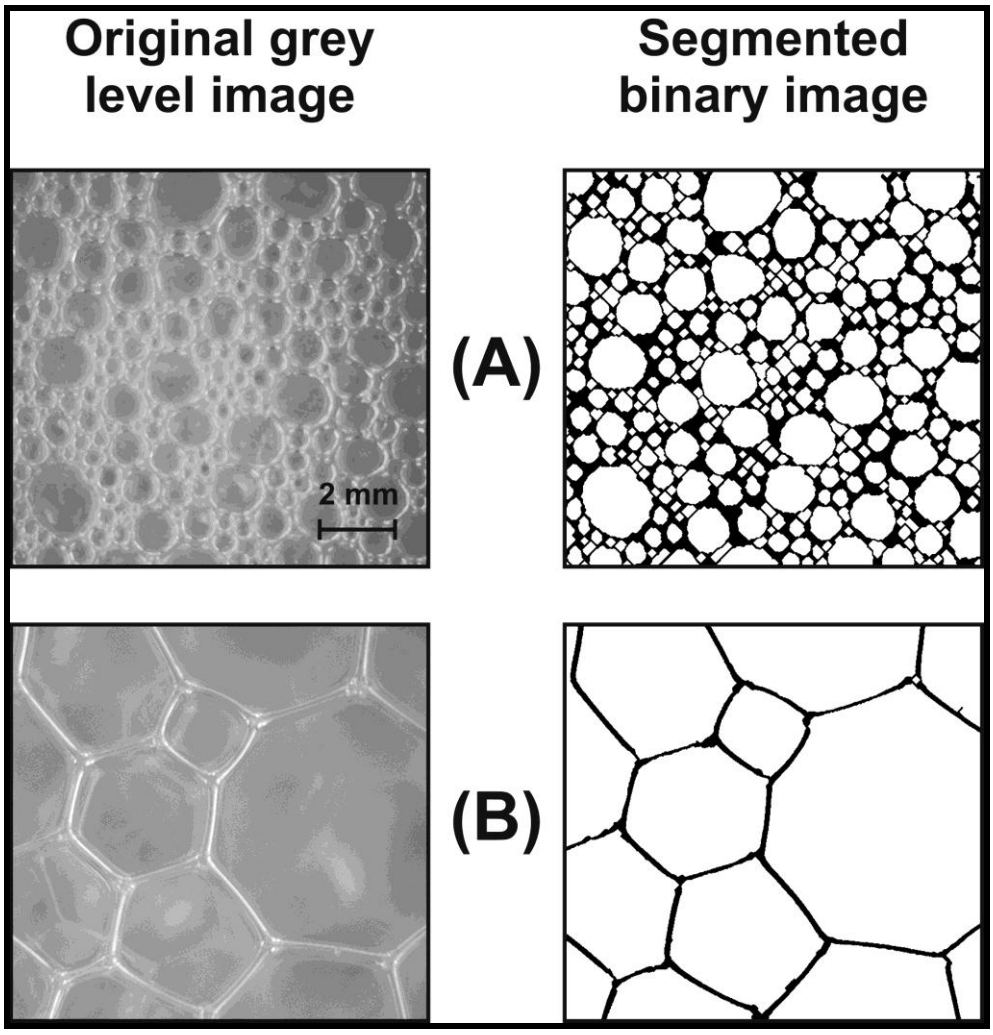

Figure 4.1: Comparison between original grey level images recorded during foaming experiments with their corresponding processed and binarized results. Images represent samples prepared with (A) 0.4 wt% whey protein isolate at pH 5.5 and (B) 0.1 wt% sodium caseinate at pH 7.0.

Mean D_{eq} values and statistical errors were computed using the data from all replicates for each system investigated. Analyses were performed using in-house codes implemented in MATLAB 7.10 (MathWorks, Massachusetts, USA).

Euler characteristic analysis

The Euler characteristic (χ) is a geometrical and topological descriptor belonging to integral geometry methods that describes the connectivity (topology) of a pattern in space (Michielsen and De Raedt, 2001). Values of this parameter represent the number of connected objects minus the number of holes between those objects. Foam structure image analysis using χ was performed as an iterative process carried out over binary images starting by finding bubble centroids in the image, dilating these centroids, and then calculating χ at each dilation step. Centroids were determined as the center of mass of the pixel regions defining each bubble in an image, but Delaunay triangulation may also be applied for this purpose. Furthermore, the analysis could be performed based on foam vertices determined by tessellation algorithms instead of bubble centroids. Plotting the χ values obtained versus dilation distance of bubble centroids produces a distinctive curve where the four parameters that describe the structure under analysis are identified. Maximum Euler characteristic (χ_{max}) indicates the number of objects in the original image (equal to the number of centroids). Minimum Euler characteristic ($\chi_{\min}$) and Euler minimum length (l_{min}) are measures of the size of the voids between the objects and are related to the nearest neighbor distance. Zero crossing length (l_0) incorporates both the number of objects and the distance between them. Liang *et al.* (2006) have used this methodology to describe microstructures of model lipid systems and in Chapter 3 it has been applied to bubble spatial distribution in foam structures.

Minkowski fractal analysis

Minkowski fractal dimensions (D_S) of foam structure images were calculated following the Bouligad-Minkowski protocol (Russ, 1995). Due to its mathematical definition, D_S can be obtained by iterative erosion and dilation image processing steps.

The method consists of producing a series of images displaying only the boundaries of the structure. Boundary images are formed by adding the complementary part of a dilated image (following the ‘‘OR’’ Boolean logic) to an eroded image of the same picture, and gradually increasing dilatation/erosion degrees as shown in Figure 4.2A. Dilation and erosion processes were defined with respect to the film phase (black pixels) and performed using a technique based on the Euclidean distance map, which has the advantage of being isotropic (Russ, 2005). To calculate D_S, the effective boundary width (defined as the area of the boundary, divided by the dilation/erosion degree and the number of iterative cycles) is calculated for each boundary image and plotted versus the number of dilation/erosion cycles on a log–log scale. Minkowski fractal dimensions are calculated from the slope of the curves as D_S = 1–slope.

Minkowski fractal dimensions were obtained by adjusting straight lines to each log–log plot by means of a robust linear regression, as exemplified in Figure 2B. However, plots obtained following the Bouligad-Minkowski protocol were generally not linear. Deviations from linearity give rise to two values for D_S, textural (D_{S1}) and structural (D_{S2}) fractal dimensions (Dathe *et al.*, 2001). Both values were also determined from each log–log plot by fitting two straight lines to the plot (Figure 4.2B). The crossing point (C_P) between both lines was determined minimizing the combined mean quadratic error of both regressions.

Image texture analysis

Image texture measures are based on two sources of information: pixel brightness and spatial locations. Therefore, images containing intensity information (gray levels) are required to calculate textural features. Intensity images were obtained using segmented binary foam structure images. Each binary image was cropped to 512 × 512 pixels and divided into $2^{2\times n}$ (n = 1. . .7) square sections. Average pixel intensities were calculated for each section and the resulting values taken to represent pixel intensities for building 7 intensity images describing foam structure as shown in Figure 4.3.

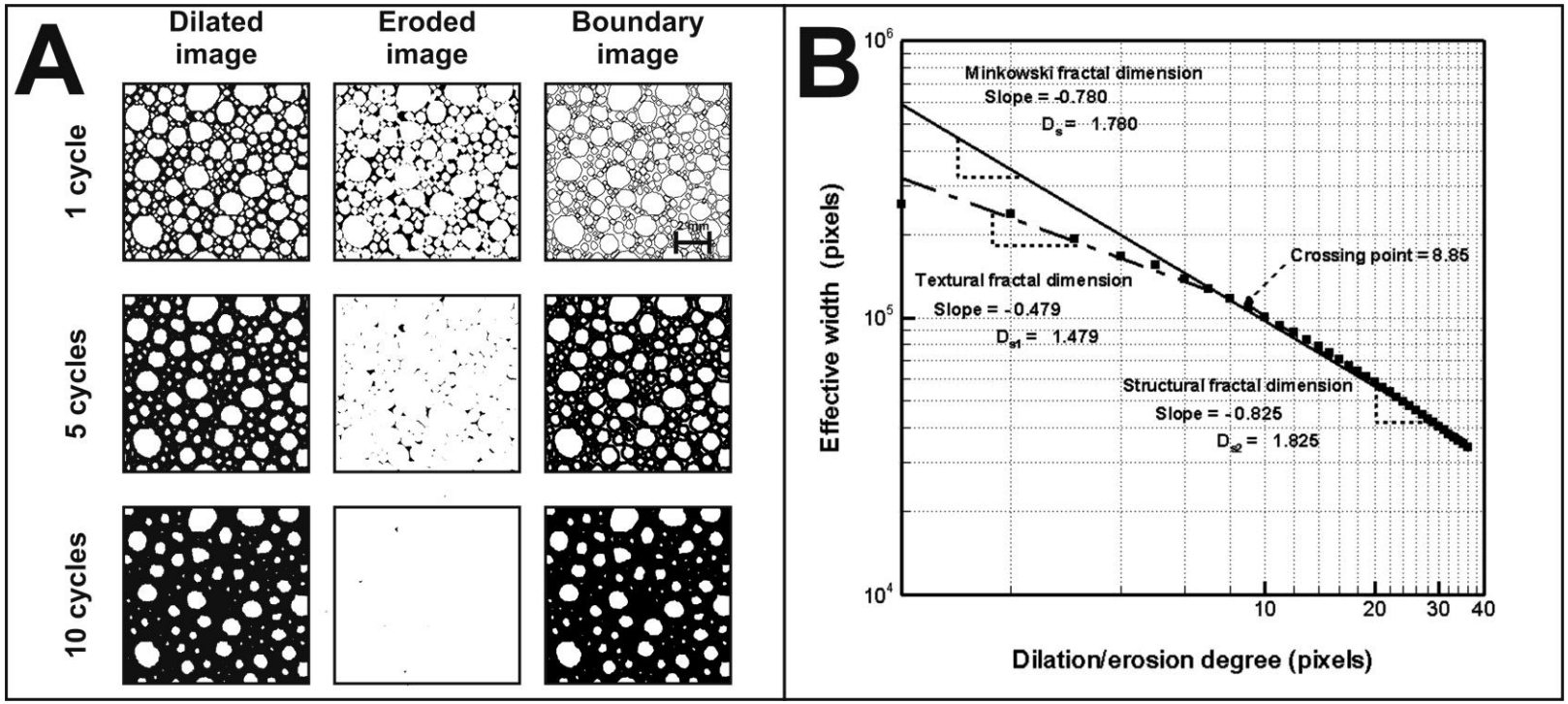

Figure 4.2: (A) Demonstration of iterative erosion and dilation image processing to determine Minkowski fractal dimensions. Boundary images are built from the segmented binary image shown in Figure 4.1A. (B) Double logarithmic plot of effective width versus number of dilating/eroding cycles resulting from processing shown in A. The linear regressions are adjusted to the data to determine Minkowski fractal parameters.

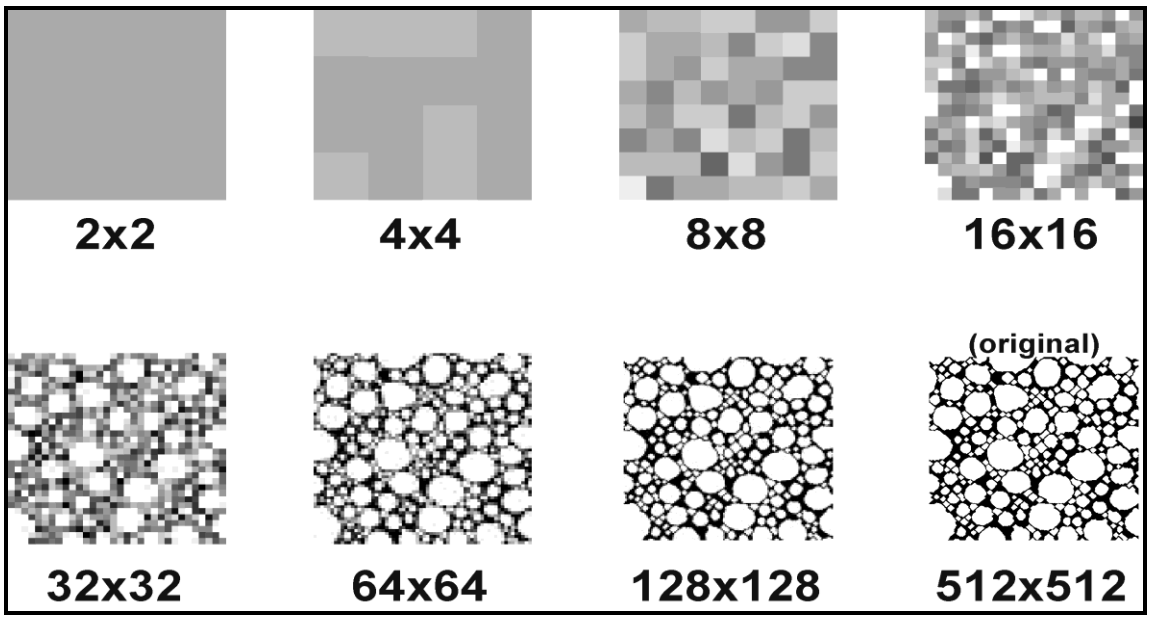

Figure 4.3: Intensity images made from the segmented binary image shown in Figure 4.1A. Each intensity image was obtained by dividing the original image into 2^{2xn} (n=1...7) square sections and replacing the value in each one with its corresponding average grey level.

Texture image analysis based on GLCM was applied to the seven intensity images made from each binary foam structure image. GLCM calculations were scaled down to only 32 gray levels rather than the original 256. Using a lower number of gray levels reduces the number of cells filled with zeros in the GLCM (combinations of gray levels that do not occur), improving statistical validity and speeding-up calculation. Therefore, GLCM were 32 × 32 square matrixes normalized by the following function:

$$p(i, j, d, \theta) = \frac{P(i, j, d, \theta)}{R} \tag{4.2}$$

where *R* is the normalized function, usually set as the sum of the elements in the GLCM (Zheng *et al.*, 2006). Depending on the selected distance and direction, several GLCM can be derived from a single image. Each distance and angle value employed are usually selected according to the spatial resolution and anisotropy of the sample studied,

respectively. For simplicity, in this work only one distance d = 1 and direction θ = 0° were used. Among the various textural features that are calculated from GLCM, seven were selected to describe structural properties of foam samples; Angular second moment (ASM), Contrast (CT), Sum of squares (SOS), Correlation (CR), Inverse difference moment (IDM), Entropy (ET), and Homogeneity (HM). Definitions of these parameters can be found elsewhere (Zheng *et al.*, 2006).

4.2.3. Foam structure identification according to structural parameters

For each image of foam structure included in this work, 57 structural parameters were calculated, 4 from Euler characteristic analysis (χ_{max}, l_0, χ_{min}, and l_{min}), 4 from Minkowski fractal analysis (D_S, D_{S1}, D_{S2}, C_P), and 49 from image texture analysis (ASM, CT, SOS, CR, IDM, ET, HM for the seven intensity images). These parameters were used to first perform an independent classification for each experimental condition (concentration and pH combination) and then an overall classification including experimental conditions and samples altogether.

Identification of foam structure images belonging to the same sample class was done using the following approach. The first objective was to extensively reduce the number of structural parameters by finding those that most effectively discriminated the different foam classes. Seven different feature groups were built for each foam structure image by combining the 8 parameters obtained from Euler characteristic and Minkowski fractal analyses together with 7 textural features calculated from intensity images of different size. Every foam structure image was therefore described by seven feature groups, each containing 15 structural parameters. The classification performance of these different feature groups was evaluated by canonical discriminant analysis (CDA) done using Statgraphics software Version 4.0 (Manugistic Inc. Rockville, MD, USA). All 6 (or 4) images from each sample class were used in CDA as the training set. For a given a set of independent variables, CDA attempts to find linear combinations of those variables that best separate samples. These combinations are called canonical discriminant functions. CDA was done with sequential forward selection (SFS) method. SFS is a common search method in image classification that proceeds by adding one

feature at a time to a current suboptimal feature set (Aha and Bankert, 1996; Dash and Liu, 1997). At the end of this analysis, the four concentration and pH combinations and the case when considering all samples simultaneously could be described by just 3 structural parameters, selected based on the percent of sample images correctly classified as the performance criteria.

Reduced groups of structural parameters that resulted from CDA were finally used to perform a Bayesian discriminant analysis (BDA). BDA is a probabilistic approach of pattern recognition. According to this method it is possible to derive a classification that is optimal in the sense that, on average, it yields the lowest probability of committing classification errors (Gonzalez and Woods, 1992). An advantage of BDA over CDA is that calculated discriminant functions are non-linear, allowing boundary definitions that improve the separation of different classes (Aguilera and Briones, 2005).

4.3. Results and Discussion

4.3.1. Foam structure images

Foam structure images resulting from foaming experiments of protein and conjugate samples prepared at different concentration/pH combinations are shown in Figure 4.4. For simplicity, the figure shows only one picture for each sample class investigated. The work was based on two-dimensional images because of technical feasibility. However, it must be noted that real foams are true three-dimensional objects with complex structures and using only two-dimensional projections will not provide reliable data on real bubble size and shape. For a more accurate and complete structure characterization it would be desirable to extend the analysis towards foam volume investigations, either by projection methods like optical projection imaging (Monnereau and Vignes-Adler, 1998) and X-ray radiography (Myagotin *et al.*, 2009), or using three-dimensional tomographic techniques (Lim and Barigou, 2004; Trater *et al.*, 2005; Babin *et al.*, 2006).

Inspection of the foam structures depicted in Figure 4.4 indicates that two general cases are easily recognizable: (1) Kugelschaum or sphere foams with small

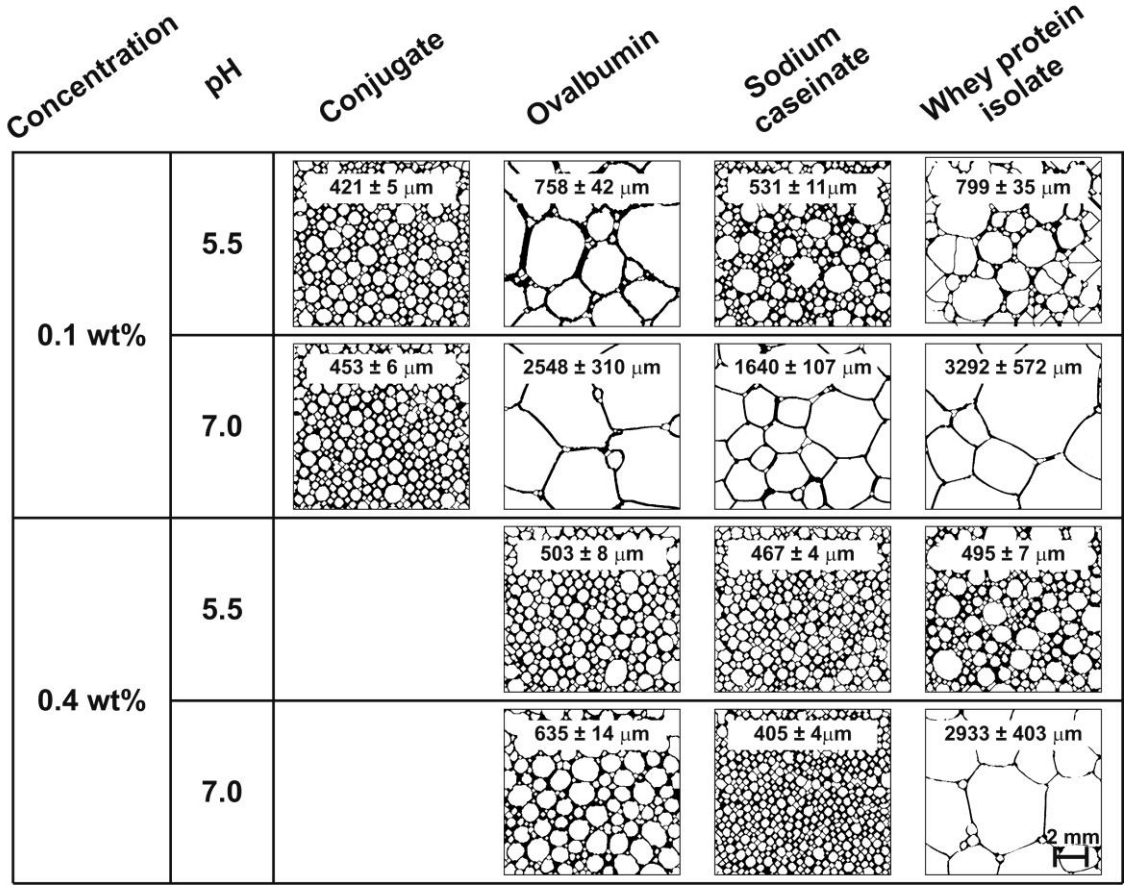

Figure 4.4: Pictures showing the resulting foam structure segmented binary images obtained from sparing experiments of protein/conjugate aqueous solutions at four concentration/pH combinations. The individual images shown are representative of image sets describing each experimental condition. Values indicate mean bubble sizes and standard errors for each sample class.

roughly spherical bubbles separated by thick films and (2) polyederschaum with polyhedral gas cells and thin flat walls (Pugh, 2005). However finer distinction of foam structures within these two cases is not straightforward and requires quantitative analysis. Bubble size measures are most frequently used to compare foam structures. Mean bubble D_{eq} values determined for each sample class are also given in Figure 4.4. Nonetheless, this size data gives no information associated to bubble spatial distribution. Foams with similar bubble sizes can have different bubble spatial arrangements and therefore different structural attributes, as discussed in Chapter 3. Comparing the range of foam structures produced during sparging experiments of aqueous solutions illustrated in Figure 4.4 requires additional quantitative structural information besides bubble size measurements to account for the entire foam architecture.

4.3.2. Structural parameters selected by canonical discriminant analysis

The structure of foams coming from the different sample classes described in Figure 4.4 was analyzed using the techniques detailed previously. CDA with SFS was performed as described previously using the 57 structural parameters determined for each image. A series of reduced groups containing only 3 key structural parameters that could successfully identify structures belonging to each sample class were determined for each concentration/pH combination independently and for all sample classes simultaneously. Results of the analysis expressed as a percentage of foam structure images assigned to their correct sample class are shown in Table 4.1. Values in bold indicate parameter sets that yielded maximum identification performance. In those cases where multiple maxima were found, the set formed using the smaller intensity image was selected. Parameter groups determined by SFS and that gave the maximum values highlighted in Table 4.1 for each case are given in Table 4.2.

The data in Tables 4.1 and 4.2 shows that optimal parameter combinations for identifying the structure of different sample classes depended on the particular sample group analyzed and that unfortunately no single combination could be used ubiquitously. The CDA classification protocol employed focuses only on finding parameter

Table 4.1: Percentage of foam structure images correctly classified using the canonical discriminant analysis with sequential forward selection for each concentration/pH combination and when considering all samples simultaneously. Calculations done for feature groups including parameters from Euler characteristic and Minkowski fractal analyses together with textural features calculated from intensity images of different sizes.

Experimental conditions (concentration (wt%)/pH)		0.1 / 5.5	0.1 / 7.0	0.4 / 5.5	0.4 / 7.0	All
Feature group formed with the textural parameters calculated from the 2^n x 2^n (n=1…7) intensity image:	2 x 2	*	*	*	*	*
	4 x 4	83.3%	72.7%	**94.4%**	94.4%	52.44%
	8 x 8	91.7%	**86.4%**	77.8%	**100.0%**	59.8%
	16 x 16	91.7%	72.7%	77.8%	94.4%	62.2%
	32 x 32	**100.0%**	81.8%	83.3%	94.4%	**
	64 x 64	92.0%	68.2%	88.9%	88.9%	**65.9%**
	128 x 128	100.0%	72.7%	94.4%	**	65.9%

* Variables are linearly dependent
** Insufficient tolerance to perform test

combinations that yield maximum percentage of systems correctly classified from a purely mathematical standpoint. More adequate/general parameter groups might be obtained if in the classification analysis information accounting for the particularities of the foam structure could be incorporated beforehand. Nevertheless, Table 4.2 shows that at least one parameter, χ_{max}, was consistently chosen among the group of discriminating features. Euler characteristic analysis states that χ_{max} represents the number of objects within the systems under analysis, the number of bubbles within each foam structure image in this particular case. According to previous work χ_{max} can be interpreted as the compactness degree of bubble arrangements (Chapter 3). No other structural parameter

besides χ_{max} appeared as a general foam structure attribute for identifying different systems. Only in the last case when all sample classes were analysed simultaneously, could the group of descriptors (ASM, CR and χ_{max}) be considered a more general descriptors of the foam structure. However, these results indicate that each individual case might require determination of its own optimum set of discriminating variables.

Table 4.2: Selected structural parameters determined by canonical discriminant analysis with sequential forward selection for each concentration/pH combination and when considering all samples simultaneously. Parameters correspond to those giving highest percentage of foam structure images correctly classified indicated in Table 4.1.

Experimental conditions (concentration (wt%)/pH)	Selected group of discriminating features
0.1 / 5.5	$\chi_{min,}$ CR, χ_{max}
0.1 / 7.0	$\chi_{max,}$ HM, D_{s2}
0.4 / 5.5	$\chi_{max,}$ SOS, ET
0.4 / 7.0	CP, CT, χ_{max}
All	ASM, CR, χ_{max}

4.3.3. Foam structures indentified by Bayesian discriminant analysis

Even though a unique set of structural attributes could not be determined, analysis of the parameters resulting from CDA provides interesting information about the particular structural attributes that distinguish one sample class from another. BDA was applied to the experimental data to determine non-linear discriminant functions for each individual sample class analyzed based on the parameters reported in Table 4.2. These functions define a set of boundaries for each sample class and provide improved foam structure identification compared to CDA. Table 4.3 shows the results of BDA

classification expressed as a percentage of foam structure images assigned to their correct sample class. Flawless classifications were obtained for foam samples prepared at 0.1 wt.% and pH 5.5 and 0.4 wt.% and pH 7.0, results that correspond to classifications obtained earlier by CDA. In the other three cases, incorporating the non-linear BDA approach either kept or increased classification performance compared to results from CDA (Table 4.1). The outcome was remarkably better particularly when all sample classes were analyzed simultaneously.

Table 4.3: Percentage of foam structure images correctly classified using structural parameters indicated in Table 4.2 and determined by non-linear Bayesian discriminant analysis for each concentration/pH combination and when considering all samples simultaneously.

Experimental conditions (concentration (wt%)/pH)	Percent of images correctly classified
0.1 / 5.5	100.0%
0.1 / 7.0	95.5%
0.4 / 5.5	94.4%
0.4 / 7.0	100.0%
All	87.8%

Graphical representations of foam structure identification results obtained by BDA are depicted in the three dimensional plots shown in Figures 4.5–4.9. Each figure shows experimental data points representing single foam images plotted against the structural parameters determined by CDA together with the corresponding class boundaries determined by BDA. Two dimensional projections of experimental points and class boundaries are also represented in these figures to aid data reading and interpretation.

The values of χ_{max} were different between wet foams of CJG and SCN prepared at 0.1 wt.% and pH 5.5 as shown in Figure 4.5, but could not separate the dry foam structures produced by OVB and WPI. This parameter can be interpreted as foam structure compactness or the number of bubbles per unit area, meaning that higher values indicate smaller bubbles and/or bubbles which are closer together in a more compact arrangement. Incorporation of χ_{min} mostly enhanced differentiation of CJG foams from the other samples. Values of χ_{min} describe connectivity of foam structure and lower values specify situations where bubbles can establish a higher number of direct interconnections with others in the structure (Chapter 3). CJG foam structures were described by much lower values of χ_{min} because in this case bubbles were surrounded by a larger number of immediate neighbors compared to the other three systems. Good differentiation between OVB and WPI samples was only achieved by including CR. This parameter measures pixel linear dependencies (Zheng *et al.*, 2006), meaning that images with more regular pixel intensity differences have higher CR than noisier images with uncorrelated intensities. OVB foams which had a more regular structure compared to WPI foams were characterized by higher CR.

The conjugate sample was easily separated from the other three protein foams prepared at 0.1 wt.% and pH 5.5 using just χ_{max} (Figure 4.6). However, the three protein systems had χ_{max} values within the same range (0–50) and thus required additional structural data for further identification. Separating WPI samples from SCN and OVB foams was done by D_{S2}. D_{S2} can be interpreted as a measure of interbubble space tortuosity with larger values of the parameter representing more meandering liquid film paths, and thus WPI foams were characterized by lower values this parameter. Finally, HM allowed almost perfect discrimination between OVB and SCN foam structures. Only a single OVB sample was wrongly assigned to SCN class. HM measures closeness of the distribution of elements in the GLCM to the matrix diagonal. High HM values indicate that neighboring pixels in the image share identical or very similar intensities. Cases like WPI foams with very thin lamellae compared to bubble sizes are described by high HM values closer to 1. The tendency of HM values was to decrease as the bubbles became more comparable in size to film thicknesses.

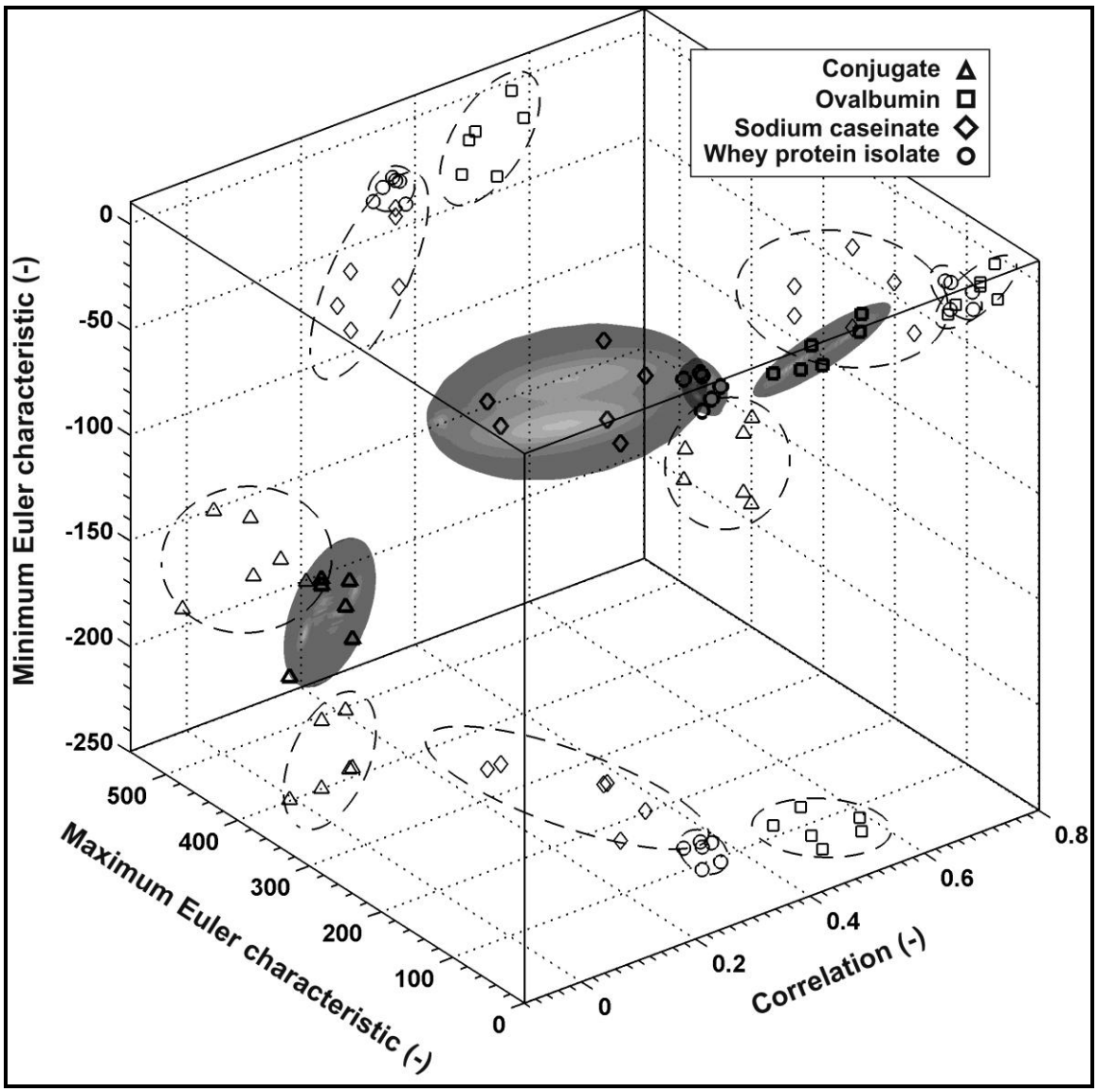

Figure 4.5: Three dimensional plot of non-linear functions determined by Bayesian discriminant analysis used to classify structure images of foams formed by sparging 0.1 wt% protein/conjugate aqueous solutions at pH 5.5. Data points and discriminant functions are projected onto x-y, x-z and y-z axis to visualize the ability of selected structural parameters to separate different foam sample classes.

Figure 4.7 depicts results of protein foams prepared at 0.4 wt.% and pH 5.5. Although structures were very similar (Figure 4.4) only a single WPI picture was

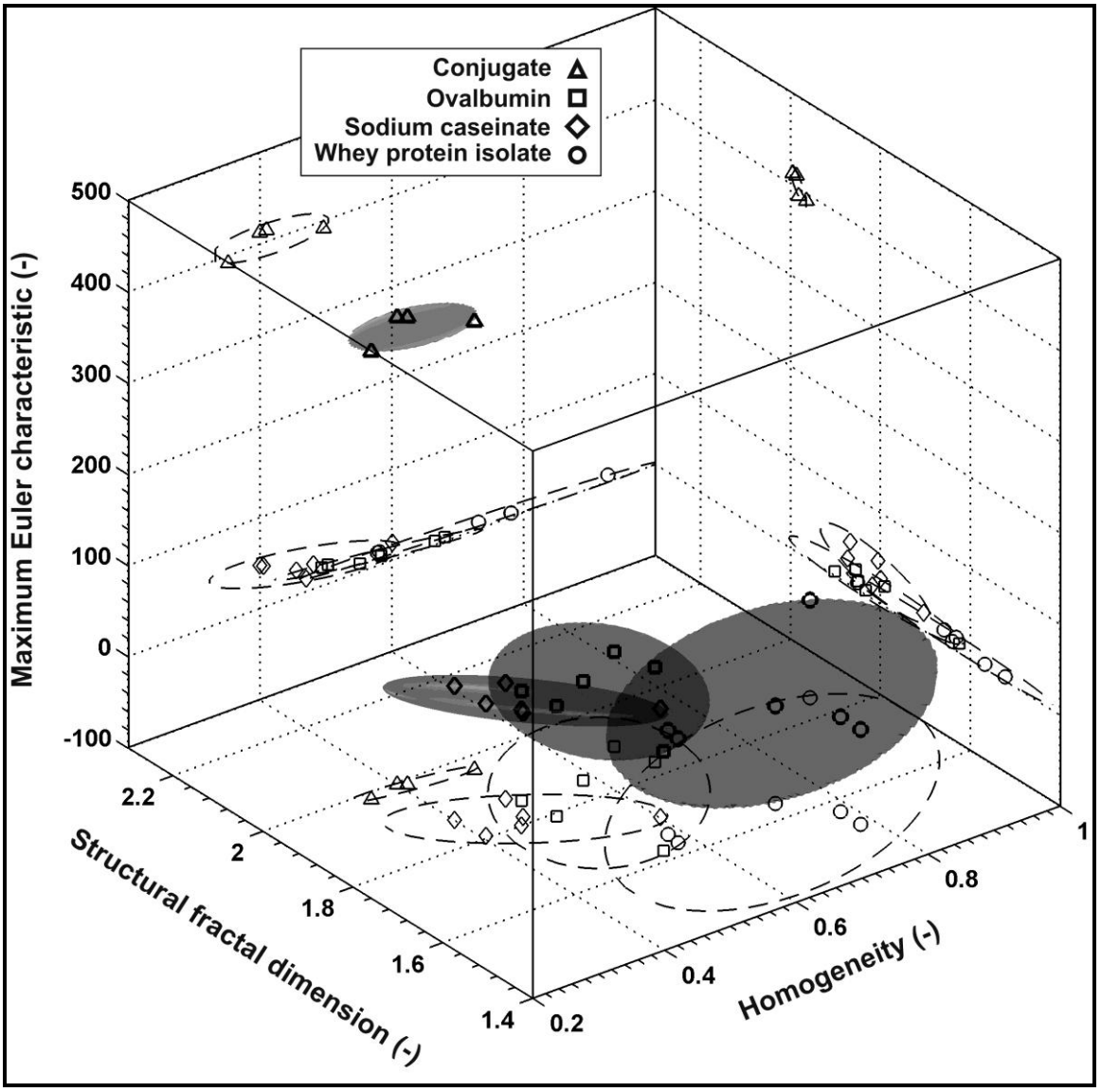

Figure 4.6: Three dimensional plot of non-linear functions determined by Bayesian discriminant analysis used to classify structure images of foams formed by sparging 0.1 wt% protein/conjugate aqueous solutions at pH 7.0. Data points and discriminant functions are projected onto x-y, x-z and y-z axis to visualize the ability of selected structural parameters to separate different foam sample classes.

misclassified as belonging to OVB group. Neither χ_{max}, SOS or ET alone could provide clear separation between each sample classes. Proper foam structure identification in this

case depended equally on the 3 structural parameters. Foam compactness (χ_{max}) was somehow higher for SCN, mainly because bubbles were smaller and had a narrower size range. Textural parameters, ET and SOS, measure the amount of order in images and image roughness respectively. Lower ET and SOS values should designate cases where the foam structure is better organized with narrower bubble and liquid-film-thickness size distributions. ET values were on average slightly higher for OVB followed by SCN and WPI as the order of the structure seems to decrease. SOS values were within the same range for the 3 sample classes.

The structure identification results for foams prepared at 0.4 wt.% and pH 7.0 are shown in Figure 4.8. In this particular case sample class separation was simple due to the very different structural attributes of each foam (Figure 4.4). Values of χ_{max} alone could completely discriminate between the 3 sample classes. Complementary CT and C_P data was only needed to define compact boundaries between sample classes. CT is used to describe local variations in images and did not vary greatly among samples. Only OVB foams show slightly larger CT values, but a direct interpretation seems not straightforward in this case. OVB and SCN foams showed similar C_P values while those for WPI were higher. C_P is a distance measure that reflects transition between textural and structural fractal dimensions. Since length scales in dry foams were longer in our samples they are described by higher C_P values than wet foams.

The final plot in Figure 4.9 shows results of foam structure identification analysis using all sample classes simultaneously. Table 4.2 indicates that 87.8% of sample images in this figure were correctly assigned to their class (10 of the 82 images included were misclassified). Due the amount of data and crowding in Figure 4.9 it is not possible to have clear graphical impression of the separation level achieved. However, general guidelines about the foam structure attributes can be derived from the two dimensional projections. Compactness degree remained low ($\chi_{max} < 50$) for dry foam structures but increased rapidly as foams become wet and bubbles spherical. In wet foam the bubbles are mobile and can more easily reorganize whereas in dry foam the geometry is determined by equilibrium laws (Plateau, 1873). As mentioned above, CR

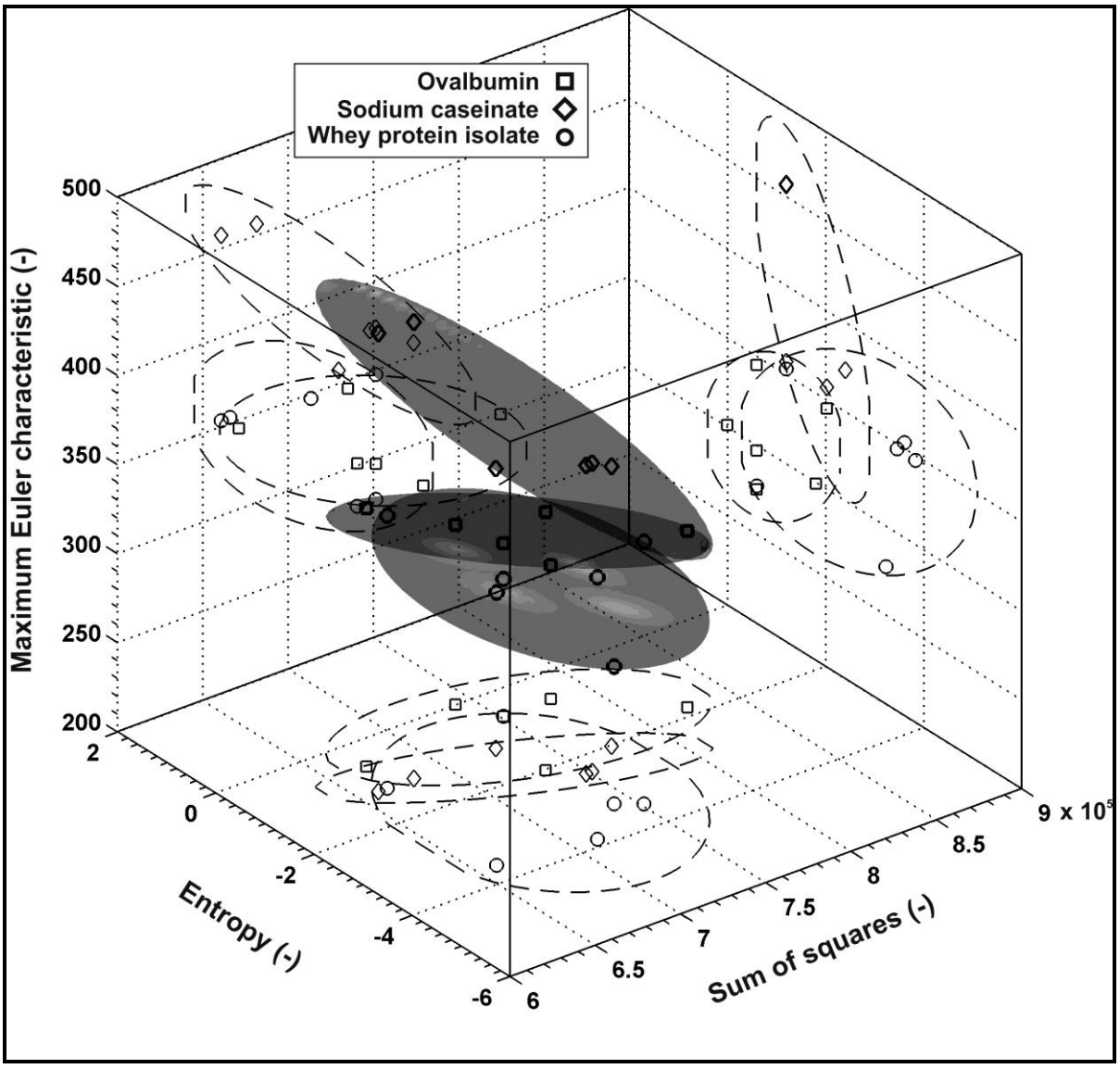

Figure 4.7: Three dimensional plot of non-linear functions determined by Bayesian discriminant analysis used to classify structure images of foams formed by sparging 0.4 wt% protein aqueous solutions at pH 5.5. Data points and discriminant functions are projected onto x-y, x-z and y-z axis to visualize the ability of selected structural parameters to separate different foam sample classes.

measures pixel linear dependencies and values remain fairly constant for dry foams (0.4 < CR < 0.6), but rapidly decrease for wet foams (CR < 0.4). Textural parameter ASM,

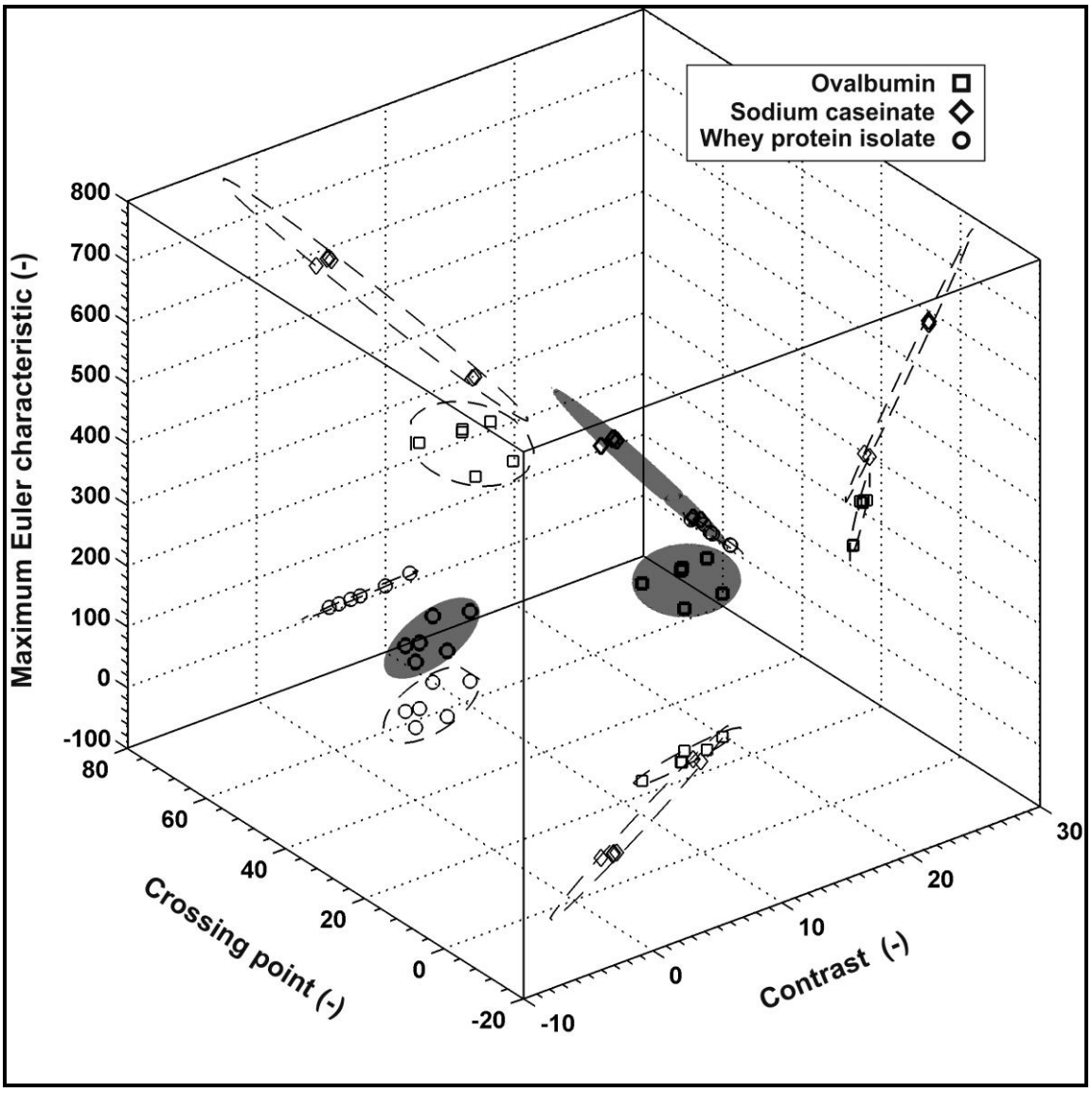

Figure 4.8: Three dimensional plot of non-linear functions determined by Bayesian discriminant analysis used to classify structure images of foams formed by sparging 0.4 wt% protein aqueous solutions at pH 7.0. Data points and discriminant functions are projected onto x-y, x-z and y-z axis to visualize the ability of selected structural parameters to separate different foam sample classes.

which describes image uniformity, appeared also as a significant discriminant of structural attributes. If all image pixels have the same value, ASM is one and decreases

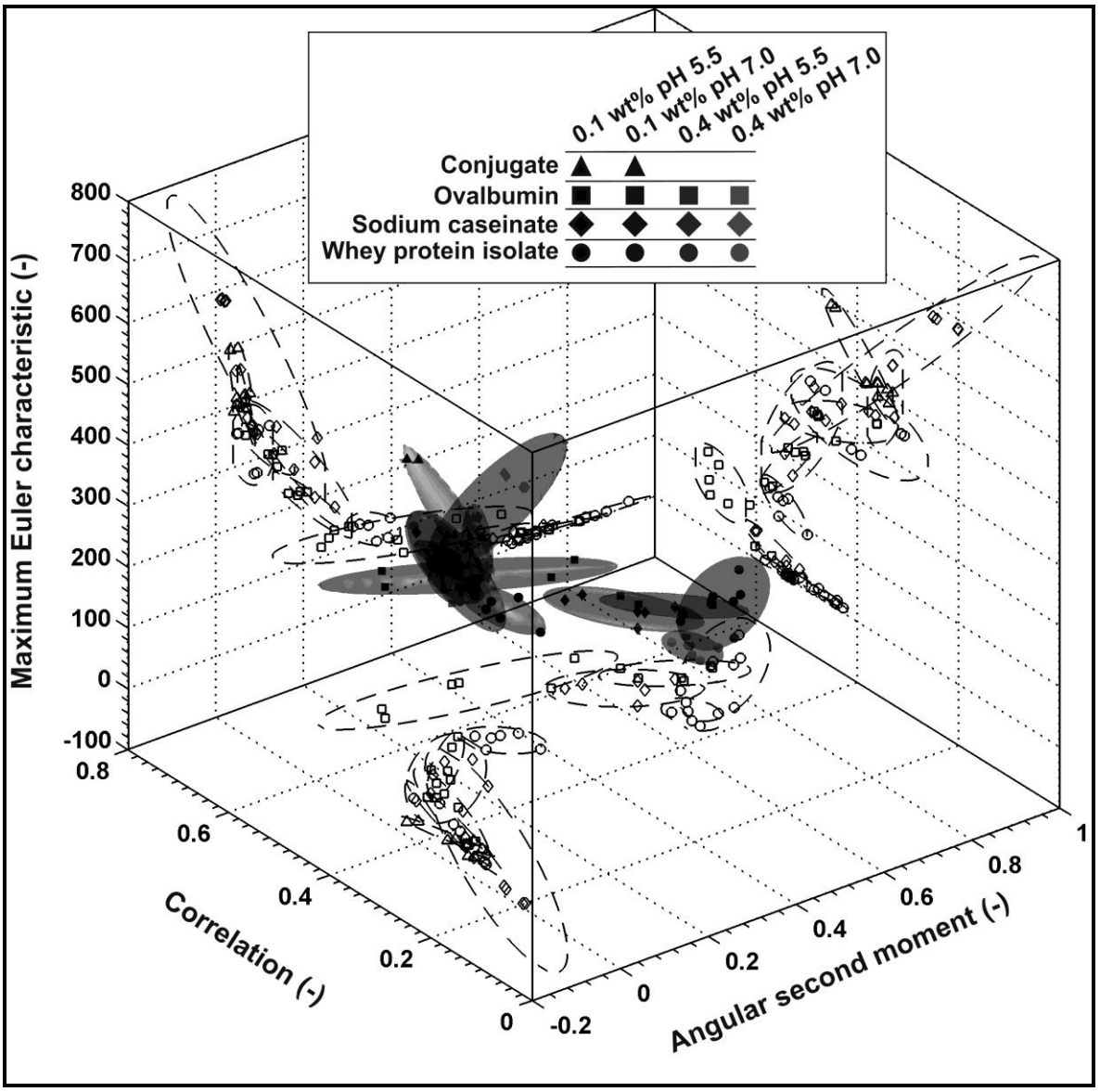

Figure 4.9: Three dimensional plot of non-linear functions determined by Bayesian discriminant analysis used to classify structure images of foams formed by sparging protein/conjugate aqueous solutions at 4 concentration/pH combinations. Data points and discriminant functions are projected onto x-y, x-z and y-z axis to visualize the ability of selected structural parameters to separate different foam sample classes.

as the number of intensity levels pixels adopt increases. Dry foams were described by ASM values close to one, whereas wet foams values were much closer to zero.

4.4. Conclusions

Foams and aerated food products are complex structures that cannot be solely described by parameters like bubble size and size distributions. The results in this work have showed that Euler characteristic, Minkowski fractal and GLCM analysis methods can be applied to also describe the spatial attributes of foam structures. The parameters derived from these methodologies were able to successfully discriminate between foam samples produced by sparging aqueous solutions of different proteins at varying conditions (concentration and pH), even though in certain cases samples shared very similar bubble size characteristics. Measures that describe foam structure spatial properties have also to be taken into consideration together with bubble size and size distribution data to provide a more comprehensive description of these types of systems.

The food industry is showing an ever increasing interest to exploit bubbles as an ingredient in products. Design and control of aerated systems needs better understanding of bubble containing structures and how they impact food properties. Methods to describe quantitatively the complex nature of foam structures like the ones shown here will provide information that may lead in the future to the design and production of foods with tailored and improved characteristics.

4.5. References

Aguilera, J.M. and Briones, V. (2005). Computer vision and food quality. *Food Australia*, 57(3), 79-87.

Aguilera, J.M. and Germain, J.C. (2007). Advances in image analysis for the study of food microstructure. In D.J. McClements (Ed.) *Understanding and controlling the microstructure of complex foods*, Woodhead Publishing Limited, Cambridge, England, pp.261-287.

Aguilera, J.M. and Lillford, P.J. (2008). Preface. In J.M. Aguilera and P.J. Lillford (Eds.) *Food Material Science*. Springer Science+Business Media LLC, New York, USA.

Aha, D.W., Bankert, R.L.A. (1996). Comparative evaluation of sequential feature selection algorithms. In D. Fisher and J.H. Lenz (Eds.), *Artificial intelligence and statistics*. Springer, New York, pp. 199-206.

Arns, C., Knackstedt, M., Pinczewski, W. and Mecke, K. (2001a). Euler-Poincaré characteristics of classes of disordered media. *Physical Review E*, 63, 31112-1-31112-13.

Arns, C., Knackstedt, M., Pinczewski, W. and Mecke, K. (2001b). Accurate estimation of transport properties from microtomographic images. *Geophysical Research Letters*, 28(17), 3361-3364.

Babin, P., Della Valle, G., Chiron, H., Cloetens, P., Hoszowska, J., Pernot, P., Réguerre, A.L., Salvo, L., Dendievel, R. (2006). Fast X-ray tomography analysis of bubble growth and foam setting during breadmaking. *Journal of Cereal Science* 43, 393-397.

Barret, A.H. and Peleg, M. (1995). Applications of fractal analysis to food structure. *LWT - Food Science and Technology*, 28(6), 553-563.

Bertrand, D., Le Guerneve, C., Marion, D., Devaux, M.F. and Robert, P. (1992). Description of the textural appearance of bread crumb by video image analysis. *Cereal Chemistry*, 69, 257-261.

Campbell, G.M. and Mougeot E. (1999). Creation and characterisation of aerated food products. *Trends in Food Science and Technology*, 10(9), 283-296.

Dash, M., Liu, H. (1997). Feature selection methods for classification. *Intelligent Data Analysis, An International Journal*, 1(3), 131-156.

Dathe, A., Eins, S., Niemeyer, J. and Gerold, G. (2001). The surface fractal dimension of the soil-pore interface as measured by image analysis. *Geoderma*, 103, 203-229.

Fains, A., Bertrand, D., Baniel A. and Popineau, Y. (1997). Stability and texture of protein foams: a study by video image analysis. *Food Hydrocolloids*, 11(1), 63-69.

Falcone, P.M., Baiano, A., Conte, A., Mancini, L., Tromba, G., Zanini, F. and Del Nobile, M.A. (2006). Imaging techniques for the study of food microstructure: a review. *Advances in Food and Nutrition Research*, 51, 205-263.

Gao, X. and Tan, J. (1996a). Analysis of expended-food texture by image processing part I: Geometric properties. *Journal of Food Processing Engineering*, 19, 425-444.

Gao, X. and Tan, J. (1996b). Analysis of expended-food texture by image processing part II: Mechanical properties. *Journal of Food Processing Engineering*, 19, 445-456.

Germain, J.C. and Aguilera, J.M. (2008). Quantification of the structural changes in foams stabilized by proteins via image analysis. In G. Campbell, M. Scanlon and L. Pyle (Eds.) *Bubbles in Food 2: Novelty, Health and Luxury*. Eagan Press, St. Paul, USA, pp. 83-87.

Gloria-Hernández, H. (2006). Formation of Protein-Polysaccharide Conjugates and Study of their Physicochemical and Functional Properties. [DPhil dissertation]. Valencia, España: Universidad Politécnica de Valencia 218 p.

Gonzalez, R.C. and Woods, R. E. (1992). *Digital image processing (2nd ed.)*. Addison-Wesley Longman Publishing Co. Inc, Boston, MA.

Guillerme, C., Loisel, W., Bertrand, D. and Popineau, Y. (1993). Study of foam stability by video image analysis: relationship with the quantity of liquid in the foams. *Journal of Texture Studies*, 24, 287-302.

Hagolle, N., Relkin, P., Popineau Y. and Bertrand, D. (2000). Study of the stability of egg white protein-based foams: Effect of heating protein solution. *Journal of the Science of Food and Agriculture*, 80(8), 1245-1252.

Haralick, R.M., Shanmugam, K. and Dinstein, I. (1973). Textural features for image classification. *IEEE Transactions on Systems, Man, and Cybernetics*, 6, 610-621.

Kerscher, M. (2000). Statistical Analysis of Large-Scale Structure in the Universe. In K. Mecke and D. Stoyan (Eds.) *Statistical physics and spatial statistics: The art of analyzing and modelling spatial structures and pattern formation (Lecture notes in physics 554)*, Springer Verlag, Berlin.

Kerscher, M., Mecke, K., Schuecker, P., Böhringer, H., Guzzo, L., Collins, C.A., Schindler, S., De Grandi, S. and Cruddace, R. (2001). Non-Gaussian morphology on large scales: Minkowski functionals of the REFLEX cluster catalogue. *Astronomy and Astrophysics*, 377, 1-16.

Liang, B.M., Sebright, J.L., Shi, Y.P., Hartel, R.W. and Perepezko, J.H. (2006). Approaches to quantification of microstructure for model lipid systems. *Journal of the American Oil Chemists Society*, 83(5), 389-399.

Lim, K.S., Barigou, M. (2004). X-ray micro-computed tomography of cellular food products. Food Research International, 37(10), 1001-1012

Liu, Z. and Scanlon, M.G. (2003). Predicting mechanical properties of bread crumb. *Food and Bioproducts Processing: Transactions of the Institution of Chemical Engineers*, *Part C*, 81(3), 224-238.

Mandelbrot, B.B. (1983). *The Fractal Geometry of Nature*, New York, W.H. Freeman & Co.

Mecke, K. (2000). Additivity, Convexity, and Beyond: Applications of Minkowski Functionals in Statistical Physics. In K. Mecke and D. Stoyan (Eds.) *Statistical physics and spatial statistics: The art of analyzing and modelling spatial structures and pattern formation (Lecture notes in physics 554)*, Springer Verlag, Berlin.

Mecke, K.R. and Sofonea, V. (1997). Morphology of spinodal decomposition. *Physical Review E*, 56(4), R3761-R3764.

Michielsen, K. and De Raedt, H. (2001). Integral-geometry morphological image analysis. *Physics Reports*, 347, 461-538.

Monnereau, C., Vignes-Adler, M. (1998). Optical tomography of real three dimensional foams. *Journal of Colloid and Interface Science*, 202(1), 45-53.

Myagotin, A., Helfen, L. and Baumbach, T. (2009). Coalescence measurements for evolving foams monitored by real-time projection imaging. *Measurement Science and Technology*, 20(5), art. no. 055703.

Niranjan, K., Silva, S.F.J. (2008). Bubble-Containing Foods. In J.M Aguilera and P.J. Lillford (Eds.), *Food Material Science*. Springer Science+Business Media LLC, New York, USA, pp. 281-303.

Peleg, M. (1993). Fractals in foods. *Critical Reviews in Food Science and Nutrition*, 33, 179-164.

Plateau, J.A.F. (1873). *Statique Expérimentale et Théorique des Liquides soumis aux seules Forces Moléculaires*, Gauthier-Villars, Paris, France.

Pugh, R.J. (2005). Experimental techniques for studying the structure of foams and froths. *Advances in Colloid and Interface Science*, 114, 239-251.

Rahali, V. and Gueguen, J. (2000). Foaming characteristics of chemical and enzymatic hydrolysates of bovine beta-lactoglobulin. *Nahrung*, 44(5), 309-317.

Reed, M.G., Howard, C.V., Shelton, C.G. (1997). Confocal imaging and second-order stereological analysis of liquid foam. *Journal of Microscopy*, 185, 313-320.

Rouillé, J., Della Valle, G., Devaux, M.F., Marion, D. and Dubreil, L. (2005). French bread loaf volume variations and digital image analysis of crumb grain changes induced by the minor components of wheat flour. *Cereal Chemistry*, 82(1), 20-27.

Russ, J. C. (1995). *The Image Processing Handbook*. CRC Press LLC, Boca Raton, Florida, USA.

Russ, J.C. (2005). *Image Analysis of Food Microstructure*. CRC Press LLC, Boca Raton, Florida, USA.

Sarker, D.K., Bertrand, D., Chtioui, Y. and Popineau, Y. (1998). Characterisation of foam properties using image analysis. *Journal of Texture Studies*, 29, 15-42.

Schabenberger, O., Gotway, C.A. (2005). *Statistical methods for spatial data analysis*. Chapman & Hall/CRC, Boca Raton, Florida, USA.

Serra, J. (1982). *Image Analysis and Mathematical Morphology*. Academia Press, London, UK.

Serra, J. (1986). Introduction to mathematical morphology. *Computer Vision, Graphics, and Image Processing*, 35, 283-305.

Torquato, S. (2002). Statistical description of microstructures. *Annual Review of Materials Research*, 32, 77-111.

Trater, A.M., Alavi, S., Rizvi, S.S.H. (2005). Use of non-invasive X-ray microtomography for characterizing microstructure of extruded biopolymer foams. *Food Research International*, 38(6), 709-719.

Zheng, C.X., Sun, D.W., Zheng, L.Y. (2006). Recent applications of image texture for evaluation of food qualities - a review. *Trends in Food Science and Technology*, 17(3), 113-128.

5. GENERAL CONCLUSIONS AND FUTURE PROSPECTS

Bubbles are gaining importance as industry seeks to exploit their novelty and versatility as food ingredient, while Food Science faces an increasing awareness about the relevance that air has as part of our everyday foods. As the emphasis in food developments shifts from process engineering to product engineering, opportunities appear to give novel uses to gases in our foods and for the design of new products.

As it has been mentioned, incorporation of air is an important way to influence food product textures. A challenge and opportunity is use bubbles to design products with tailored characteristics. This requires an in depth understanding and control over raw materials and manufacturing processes, but also having proper and reliable methods to access and measure food foam properties, identifying most relevant and desirable attributes, and finding mechanisms to reproduce and optimize them.

Main purpose of this thesis was to show that the study of food foams and of protein stabilized liquid foams spans along a wide length-scale from the molecular the macroscopical. As the physical and chemical phenomena affecting foams intermingle on these various length-scales, their study requires a multidisciplinary approach and a variety of scientific talents.

Emphasis was placed in that quantitative information is needed at each level to understand and eventually control formation of protein stabilized foams. Specific and reliable methods and tools are required to seek this purpose. For future studies it will be of interest to extend the image analysis method developed in the thesis to volumetric data and use them to derive the associations existing between structures at all scales and foam properties.

6. REFERENCES

Adachi, M., Ho, C.Y. and Utsumi, S. (2004). Effects of designed sulfhydryl groups and disulfide bonds into soybean proglycinin on its structural stability and heat induced gelation. *Journal of Agricultural and Food Chemistry*, 52, 5717-5723.

Aguilera J.M. (2006). Seligman Lecture 2005 - Food product engineering: Building the right structures. *Journal of the Science of Food and Agriculture*, 86(8), 1147-1155.

Aguilera JM. (2005). Why food microstructure*? Journal of Food Engineering*, 67(1-2), 3-11.

Aguilera, J.M. (2000). Microstructure and food product engineering. *Food Technology*, 54:56-58, 60, 62, 64, 66.

Aguilera, J.M. and Briones, V. (2005). Computer vision and food quality. *Food Australia*, 57(3), 79-87.

Aguilera, J.M. and Germain, J.C. (2007). Advances in image analysis for the study of food microstructure. In D.J. McClements (Ed.) *Understanding and controlling the microstructure of complex foods*, Woodhead Publishing Limited, Cambridge, England, pp. 261-287.

Aguilera, J.M. and Lillford, P.J. (2008). Preface. In J.M. Aguilera and P.J. Lillford (Eds.) *Food Material Science*. Springer Science+Business Media LLC, New York, USA.

Aguilera, J.M. and Stanley, D.W. (1999). *Microstructural Principles of Food Processing and Engineering* (2nd. Ed.), Gaithersburg, MD, Aspen Publishers Inc.

Aha, D.W., Bankert, R.L.A. (1996). Comparative evaluation of sequential feature selection algorithms. In D. Fisher and J.H. Lenz (Eds.), *Artificial intelligence and statistics*. Springer, New York, pp. 199-206.

Aksenenko, E.V. (2001). Software tools to interpret the thermodynamics and kinetics of surfactant adsorption. In V.B. Fainerman, D. Möbius and R. Miller (Eds.) *Surfactants: Chemistry, Interfacial Properties, Applications*, Elsevier Science B.V., Amsterdam, The Netherlands, pp. 619-649.

Alavi, S.H., Gogoi, B.K., Khan, M., Bowman, B.J. and Rizvi, S.S.H. (1999). Structural properties of protein-stabilized starch-based supercritical fluid extrudates. *Food Research International*, 32(2), 107-118.

Andreas. J.M., Hauser, E.A. and Tucker, W.B. (1938). Boundary tension by pendant drops. *Journal of Physical Chemistry*, 42, 1001-1019.

Arns, C., Knackstedt, M., Pinczewski, W. and Lindquist, W.B. (2001a). Accurate estimation of transport properties from microtomographic images. *Geophysical Research Letters*, 28(17), 3361-3364.

Arns, C., Knackstedt, M., Pinczewski, W. and Mecke, K. (2001b). Accurate estimation of transport properties from microtomographic images. *Geophysical Research Letters*, 28(17), 3361-3364.

Babin, P., Della Valle, G., Chiron, H., Cloetens, P., Hoszowska, J., Pernot, P., Réguerre, A.L., Salvo, L. and Dendievel R. (2006). Fast X-ray tomography analysis of bubble growth and foam setting during bread making. *Journal of Cereal Science*, 43, 393-397.

Babin, P., Della Valle, G., Dendievel, R., Lassoued, N. and Salvo, L. (2005). Mechanical properties of bread crumbs from tomography based Finite Element simulations. *Journal of Materials Science*, 40(22), 5867-5873.

Bals, A. and Kulozik, U. (2003). Effect of pre-heating on the foaming properties of whey protein isolate using a membrane foaming apparatus. *International Dairy Journal*, 13(11), 903-908.

Baniel, A., Fains, A., and Popineau, Y. (1997). Foaming properties of egg albumen with a bubbling apparatus compared with whipping. *Journal of Food Science*, 62, 377-381.

Barret, A.H. and Peleg, M. (1995). Applications of fractal analysis to food structure. *LWT - Food Science and Technology*, 28(6), 553-563.

Beneventi, D., Pugh, R.J., Carré, B. and Gandini A. (2003). Surface rheology and foaming properties of sodium oleate and C12(EO)6 aqueous solutions. *Journal of Colloid and Interface Science*, 268, 221-229.

Benjamins, J. and Lucassen-Reynders, E.H. (1998). Surface dilational rheology of proteins adsorbed at air/water and oil/water interfaces. In D. Möbius and R. Miller (Eds.) *Proteins at Liquid Interfaces*. Elsevier Science B.V., Amsterdam, The Netherlands, pp. 341-384.

Bertrand, D., Le Guerneve, C., Marion, D., Devaux, M.F. and Robert, P. (1992). Description of the textural appearance of bread crumb by video image analysis. *Cereal Chemistry*, 69, 257-261.

Bisperink, C.G.J. , Akkerman, J.C., Prins, A. and Ronteltap, A.D. (1992). A moving optical fibre technique for structure analysis of heterogeneous products: application to the determination of the bubble-size distribution in liquid foams. *Food Structure*, 11, 101-108.

Bos, M.A. and Van Vliet, T. (2001). Interfacial rheological properties of adsorbed proteins layer and surfactants: a review. *Advances in Colloid Interface Science*, 91, 437-471.

Branden, C. and Tooze, J. (1991). *Introduction to protein structure*. Garland Publishing Inc., New York, USA.

Cagna, A., Esposito, G., Rivière, C., Housset, S. and Verger, R. (1992). *3rd International Conference on the Biochemistry of Lipids*, Lyon.

Campbell, G.M. and Mougeot E. (1999). Creation and characterisation of aerated food products. *Trends in Food Science and Technology*, 10(9), 283-296.

Carrera Sánchez, C. and Rodríguez Patino, J.M. (2005). Interfacial, foaming and emulsifying characteristics of sodium caseinate as influenced by protein concentration in solution. *Food Hydrocolloids*, 19, 407-416.

Carrera Sánchez, C., Rodríguez Niño M.R., Caro, A.L. and Rodríguez Patino, J.M. (2005). Biopolymers and emulsifiers at the air–water interface. Implications in food colloid formulations. *Journal of Food Engineering*, 67, 225-234.

Cauvain, S.P. (2003). Inside the cell structures of bakery products. *The World of Food Ingredients*, 2, 24-28.

Chang, Y. and Hartel, R.W. (2002). Measurement of air cell distributions in dairy foams. *International Dairy Journal*, 12(5), 463-472.

Cohen-Addad, S., Hoballah, H. and Höler, R. (1998). Viscoelastic response of a coarsening foam. *Physical Review E*, 57(6), 6897-6901.

Creighton, T.E. (1993). *Proteins: Structure and Molecular Properties* (2nd edition). W.H. Freeman and Company, New York, USA.

Damodaran, S. (2005). Protein stabilization of emulsions and foams. *Journal of Food Science*, 70(3), R54-R66.

Dash, M., Liu, H. (1997). Feature selection methods for classification. *Intelligent Data Analysis, An International Journal*, 1(3), 131-156.

Dathe, A., Eins, S., Niemeyer, J. and Gerold, G. (2001). The surface fractal dimension of the soil-pore interface as measured by image analysis. *Geoderma*, 103, 203-229.

de Gennes, P.-G., Brochard-Wyart, F. and Quéré, D. (2004). *Capillarity and wetting phenomena. Drops, bubbles, pearls, waves*. Springer-Verlag New York, Inc., New York, USA.

de Jongh, H.H.J. (2007). Proteins in food microstructure formation. In D.J. McClements (Ed.) *Understanding and controlling the microstructure of complex foods*, Woodhead Publishing Limited, Cambridge, England, pp. 40-66.

Dickinson, E. (1992). *An Introduction to Food Colloids*, Oxford University Press, Oxford, UK.

Dickinson, E. (2007). Colloidal systems in foods containing droplets and bubbles. In D. J. McClements (Ed.) *Understanding and controlling the microstructure of complex foods*. Woodhead Publishing Limited, Cambridge, UK, pp. 153-184.

Dickinson, E., Ettelaine, R., Murray, B.S. and Du, Z. (2002). Kinetics of disproportionation of air bubbles beneath the planar air-water interface stabilized by food proteins. *Journal of Colloid and Interface Science*, 252, 202-213.

Douillard, R., Daoud, M. and Aguié-Béghin, V. (2003). Polymer thermodynamics of adsorbed protein layers. *Current Opinion in Colloid and Interface Science*, 8, 380-386.

Duce, S.L., Amin, M.H.G., Horsfield, M.A., Tyszka, M. and Hall, L.D. (1995). Nuclear-magnetic-resonance imaging of dairy-products in 2-dimensions and 3-dimensions. *International Dairy Journal*, 5(4), 311-319.

Dukhin, S.S., Kretzschmar, G. and Miller, R. (1995). The dynamics of adsorption at liquid interfaces. In D. Möbius and R. Miller (Eds.) *Dynamics of Adsorption at Liquid*

Interfaces: Theory, Experiment, Application. Elsevier Science B.V., Amsterdam, The Netherlands, pp 100-139.

Dutta, A., Chengara, A., Nikolov, A., Wasan, D. T., Chen, K., and Campbell, B. (2004). Texture and stability of aerated food emulsions—effects of buoyancy and Ostwald ripening. *Journal of Food Engineering*, 62, 169-175.

Eisner, M.D., Wildmoser, H. and Windhab, E.J. (2005). Air cell microstructuring in a high viscous ice cream matrix. *Colloids and Surfaces A-Physicochemical and Engineering Aspects*, 263(1-3), 390-399.

Fainerman, V.B. and Miller, R. (1999). Equation of state for concentrated protein surface layers at the water/air interface. *Langmuir*, 15, 1812-1816

Fainerman, V.B., Lucassen-Reynders, E.H. and Miller, R. (2003). Description of the adsorption behaviour of protein at water/fluid interfaces in the framework of a two-dimensional solution model. *Advances in Colloid Interface Science*, 106, 237-259.

Fains, A., Bertrand, D., Baniel A. and Popineau Y. (1997). Stability and texture of protein foams: a study by video image analysis. *Food Hydrocolloids*, 11(1), 63-69.

Falcone, P.M., Baiano, A., Conte, A., Mancini, L., Tromba, G., Zanini, F. and Del Nobile, M.A. (2006). Imaging techniques for the study of food microstructure: a review. *Advances in Food and Nutrition Research*, 51, 205-263.

Fernández, L., Castillero C. and Aguilera, J.M. (2005). An application of image analysis to dehydration of apple discs. *Journal of Food Engineering*, 67(1-2), 185-193.

Fox, P., Smith, P.P. and Sahi, S. (2004). Ultrasound measurements to monitor the specific gravity of food batters. *Journal of Food Engineering*, 65, 317-324.

Gao, X. and Tan, J. (1996a). Analysis of expended-food texture by image processing part I: Geometric properties. *Journal of Food Processing Engineering*, 19, 425-444.

Gao, X. and Tan, J. (1996b). Analysis of expended-food texture by image processing part II: Mechanical properties. *Journal of Food Processing Engineering*, 19, 445-456.

Gardiner, B.S., Dlugogorski, B.Z., Jameson, G.J. and Chhabra R.P. (1998). Yield stress measurements of aqueous foams in the dry limit. *Journal of Rheology*, 42, 1437-1450.

Germain, J.C. and Aguilera, J.M. (2008). Quantification of the structural changes in foams stabilized by proteins via image analysis. In G. Campbell, M. Scanlon and L. Pyle (Eds.) *Bubbles in Food 2: Novelty, Health and Luxury*. Eagan Press, St. Paul, USA, pp. 83-87.

German, J.B. and McCarthy, M.J. (1989). Stability of aqueous foams - Analysis using magnetic-resonance imaging. *Journal of Agricultural and Food Chemistry*, 37(5), 1321-1324.

Gloria-Hernández, H. (2006). Formation of Protein-Polysaccharide Conjugates and Study of their Physicochemical and Functional Properties. [DPhil dissertation]. Valencia, España: Universidad Politécnica de Valencia 218 p.

Golding, M. and Sein, A. (2004). Surface rheology of aqueous casein-monoglyceride dispersions. *Food Hydrocolloids*, 18, 451-461.

Gonzalez, R.C. and Woods, R. E. (1992). *Digital image processing (2nd ed.)*. Addison-Wesley Longman Publishing Co. Inc, Boston, MA.

Gopal, A.D. and Durian, D.J. (2003). Relaxing in foam. *Physical Review Letters*, 91, 2051-2054.

Grigoriev, D.O., Fainerman, V.B., Makievski, A.V., Krägel, J.,Wüstneck, R. and Miller, R. (2002). β-casein bilayer adsorption at the solution/air interface: experimental evidences and theoretical description. *Journal of Colloid and Interface Science*, 253, 257-264.

Guillerme, C., Loisel, W., Bertrand, D. and Popineau, Y. (1993). Study of foam stability by video image analysis: relationship with the quantity of liquid in the foams. *Journal of Texture Studies*, 24, 287-302.

Gunning, P.A., Mackie, A.R., Gunning, A.P., Wilde, P.J., Woodward, N.C. and Morris, V.J (2004). The effect of surfactant type on protein displacement from the air-water interface. *Food Hydrocolloids,* 18, 509-515.

Haedelt, J., Pyle, D.L., Beckett, S.T. and Niranjan, K. (2005). Vacuum-induced bubble formation in liquid-tempered chocolate. *Journal of Food Science*, 70, E159-E164.

Hagolle, N., Relkin, P., Popineau Y. and Bertrand, D. (2000). Study of the stability of egg white protein-based foams: Effect of heating protein solution. *Journal of the Science of Food and Agriculture*, 80(8), 1245-1252.

Haralick, R.M., Shanmugam, K. and Dinstein, I. (1973). Textural features for image classification. *IEEE Transactions on Systems, Man, and Cybernetics*, 6, 610-621.

Hicsasmaz, Z., Yazgan, Y., Bozoglu, F. and Katnas, Z. (2003). Effect of polydextrose-substitution on the cell structure of the high-ratio cake system. *Lebensmittel-Wissenschaft Und-Technologie-Food Science and Technology*, 36(4), 441-450.

Hoballah, H., Höler, R. and Cohen-Addad, S. (1997). Time evolution of the elastic properties of aqueous foam. *Journal de Physique II*, 7, 1215-1224.

Höler, R. and Cohen-Addad, S. (2005). Rheology of liquid foam. *Journal of Physics: Condensed Matter*, 17, R1041-R1069.

Jang, W., Nikolov, A., Wasan, D.T., Chen, K. and Campbell, B. (2005). Prediction of the bubble size distribution during aeration of food products. *Industrial and Engineering Chemistry Research*, 44(5), 1296-1308.

Joos, P. and Serrien, G.J. (1991). The principle of Braun-Le Châtelier at surfaces. *Journal of Colloid and Interface Science*, 145, 291-294.

Kampf, N., Martinez, C.G., Corradini, M.G. and Peleg, M. (2003). Effect of two gums on the development, rheological properties and stability of egg albumen foams. *Rheologica Acta*, 42(3), 259-268.

Kato, A., Osako, Y., Matsudomi, N. and Kobayashi, K. (1983). Changes in emulsifying and foaming properties of proteins during heat denaturation. *Agricultural and Biological Chemistry*, 47, 33-38.

Kerscher, M. (2000). Statistical Analysis of Large-Scale Structure in the Universe. In K. Mecke and D. Stoyan (Eds.) *Statistical physics and spatial statistics: The art of analyzing and modelling spatial structures and pattern formation (Lecture notes in physics 554)*, Springer Verlag, Berlin.

Kerscher, M., Mecke, K., Schuecker, P., Böhringer, H., Guzzo, L., Collins, C.A., Schindler, S., De Grandi, S. and Cruddace, R. (2001). Non-Gaussian morphology on large scales: Minkowski functionals of the REFLEX cluster catalogue. *Astronomy and Astrophysics*, 377, 1-16.

Khan, S.A., Schnepper, C.A. and Armstrong, R.C. (1988). Foam rheology: III. Measurement of shear flow properties. *Journal of Rheology*, 32, 69-92.

Kloek W., van Vliet T. and Meinders M. (2001). Effect of bulk and interfacial rheological properties on bubble dissolution. *Journal of Colloid and Interface Science*, 237, 158-166.

Krishnan, A., Wilson, A., Sturgeon J., Siedlecki, C.A. and Vogler, E.A. (2005). Liquid–vapour interfacial tension of blood plasma, serum and purified protein constituents thereof. *Biomaterials*, 26, 3445-3453.

Krustev, R., Platikanov D. and Nedyalkov, M. (1996). Temperature dependence of gas permeability of Newton black films. *Langmuir*, 12, 1688-1689.

Kulmyrzaev, A., Cancelliere, C. and McClements, D.J. (2000). Characterization of aerated foods using ultrasonic reflectance spectroscopy. *Journal of Food Engineering*, 46(4), 235-241.

Labourdenne, S., Gaudry-Rolland, N., Letellier, S., Lin, M., Cagna, A., Esposito, G., Verger, R. and Riviere, C. (1996). The oil-drop tensiometer: potential applications for studying the kinetics of (phospho)lipase action. *Chemistry and Physics of Lipids*, 71, 163-173.

Larson R.G. (1999). *The Structure and Rheology of Complex Fluids*. Oxford University Press, New York, USA.

Lau, C.K. and Dickinson, E. (2005). Instability and structural change in an aerated system containing egg albumen and invert sugar. *Food Hydrocolloids*, 19, 111-121.

Liang, B.M., Sebright, J.L., Shi, Y.P., Hartel, R.W. and Perepezko, J.H. (2006). Approaches to quantification of microstructure for model lipid systems. *Journal of the American Oil Chemists Society*, 83(5), 389-399.

Lim, K.S. and Barigou, M. (2004) X-ray micro-computed tomography of cellular food products. *Food Research International*, 37(10), 1001-1012.

Liu, M. and Damodaran, S. (1999). Effect of transglutaminase-catalyzed polymerization of β-casein on its emulsifying properties. *Journal of Agricultural and Food Chemistry*, 47, 1514-1519.

Liu, Z. and Scanlon, M.G. (2003). Predicting mechanical properties of bread crumb. *Food and Bioproducts Processing: Transactions of the Institution of Chemical Engineers, Part C,* 81(3), 224-238.

Llewellin, E.W., Mader, H.M. and Wilson, S.D.R. (2002). The constitutive equation and flow dynamics of bubbly magmas. *Geophysical Research Letters*, 29(24), 2170.

Logley, W.R. and Van Name, R.G. (1928). *The Collected Works of J. Willard Gibbs, I: Thermodynamics*. Longmans, Green, and Company, New York, USA.

Lucassen, J. and van den Tempel, M. (1972). Dynamic measurements of dilational properties of a liquid interface. *Chemical Engineering Science*, 27, 1283-1291.

Lucassen-Reynders, E.H, Fainerman, V.B. and Miler, R. (2004). Surface dilational modulus or Gibbs' elasticity of protein adsorption layers. *Journal of Physical Chemistry*, 108, 9173-9176.

Lucassen-Reynders, E.H. (1993). Interfacial viscoelasticity in emulsions and foams. *Food Structure*, 12(1), 1-12.

Maldonado-Valderrama, J., Fainerman, V.B., Aksenenko, E.V., Gàlvez-Ruiz, M.J., Cabrerizo-Vílchez, M.A. and Miller, R. (2005). Dynamics of protein adsorption at the oil–water interface: comparison with a theoretical model. *Colloids and Surfaces A: Physicochemical and Engineering Aspects*, 261, 85-92.

Mandelbrot, B.B. (1983). *The Fractal Geometry of Nature*, New York, W.H. Freeman & Co.

Martinet, V., Valentini, C., Casalinho, J., Schorsch, C., Vaslin, S. and Courthaudon, J.-L. (2005). Composition of interfacial layers in complex food emulsions before and after aeration: effect of egg to milk protein ratio. *Journal of Dairy Science*, 88, 30-39.

Mason, T.G., Bibette, J. and Weitz, D. A. (1995). Elasticity of compressed emulsions. *Physical Review Letters*, 75, 2051-2054.

Mecke, K. (2000). Additivity, Convexity, and Beyond: Applications of Minkowski Functionals in Statistical Physics. In K. Mecke and D. Stoyan (Eds.) *Statistical physics and spatial statistics: The art of analyzing and modelling spatial structures and pattern formation (Lecture notes in physics 554)*, Springer Verlag, Berlin.

Mecke, K.R. and Sofonea, V. (1997). Morphology of spinodal decomposition. *Physical Review E*, 56(4), R3761-R3764.

Michielsen, K. and De Raedt, H. (2001). Integral-geometry morphological image analysis. *Physics Reports*, 347, 461-538.

Miller, R., Fainerman, V.B., Aksenenko, E.V., Leser, M. E. and Michel, M. (2004). Dynamic surface tension and adsorption kinetics of β-casein at the solution/air interface. *Langmuir*, 20, 771-777.

Miller, R., Fainerman, V.B., Makievski, A.V., Krägel, J., Grigoriev, D.O., Kazakov. V.N. and Sinyachenko, O.V. (2000). Dynamics of protein and mixed protein/surfactant adsorption layers at the water/fluid interface. *Advances in Colloid Interface Science*, 86, 39-82.

Möbius, D. and Miller, R. (1998). *Drops and Bubbles in Interfacial Research*, Elsevier, Amsterdam.

Monnereau, C., Vignes-Adler, M. (1998). Optical tomography of real three dimensional foams. *Journal of Colloid and Interface Science*, 202(1), 45-53.

Morris, G.A., Sims I.M., Robertson, A.J. and Furneaux, R.H. (2004). Investigation into the physical and chemical properties of sodium caseinate-maltodextrin glyco-conjugates. *Food Hydrocolloids*, 18, 1007-1014.

Myagotin, A., Helfen, L. and Baumbach, T. (2009). Coalescence measurements for evolving foams monitored by real-time projection imaging. *Measurement Science and Technology*, 20(5), art. no. 055703.

Nedyalkov, M., Krustev, R., Kashchiev, D., Platikanov, D. and Exerowa, D. (1988). Permeability of Newtonian black foam films to gas. *Colloid Polymer Science*, 266, 291-296.

Nedyalkov, M., Krustev, R., Stankova, A. and Platikanov, D. (1992). Mechanism of permeation of gas through Newton black films at different temperatures. *Langmuir*, 8, 3142-3144.

Niranjan, K. and Silva, S.F.J. (2008). Bubble-Containing Foods. In J.M. Aguilera and P.J. Lillford (Eds.) *Food Material Science*. Springer Science+Business Media LLC, New York, USA, pp. 281-303.

Onwulata, C.I., Konstance, R.P., Cooke, P.H. and Farrell, H.M.Jr. (2003). Functionality of extrusion-texturized whey proteins. *Journal of Dairy Science*, 86, 3775-3782.

Peleg, M. (1993). Fractals in foods. *Critical Reviews in Food Science and Nutrition*, 33, 179-164.

Petkova, V., Sultanem, C., Nedyalkov, M., Benattar, J., Leser, M.E. and Schmitt, C. (2003). Structure of a freestanding film of *β*-lactoglobulin. *Langmuir*, 19, 6942-6949.

Pizones Ruíz-Henestrosa V., Carrera Sánchez, C. and Rodríguez Patino. J.M. (2007). Formulation engineering can improve the interfacial and foaming properties of soy globulins. *Journal of Agricultural and Food Chemistry*, 55, 6339-6348.

Plateau, J.A.F. (1873). *Statique Expérimentale et Théorique des Liquides soumis aux seules Forces Moléculaires*, Gauthier-Villars, Paris, France.

Platikanov, D., Nedyalkov, M. and Nasteva, V. (1980). Line tension of Newton black films II. Determination by the diminishing bubble method. *Journal of Colloid and Interface Science*, 75(2), 620-6289.

Prins, A., Bos, M.A., Boerboom, F.J.G. and Van Kalsbeek, H.K.A.I. (1998). Relation between surface rheology and foaming behaviour. In D. Möbius and R. Miller (Eds.) *Proteins at Liquid Interfaces*. Elsevier Science B.V., Amsterdam, The Netherlands, pp. 221-265.

Pugh, R.J. (2005). Experimental techniques for studying the structure of foams and froths. *Advances in Colloid and Interface Science*, 114, 239-251.

Rahali, V. and Gueguen, J. (2000). Foaming characteristics of chemical and enzymatic hydrolysates of bovine beta-lactoglobulin. *Nahrung*, 44(5), 309-317.

Raharitsifa, N., Genovese, D.B. and Ratti, C. (2006). Characterization of apple juice foams for foam-mat drying prepared with egg white protein and methylcellulose. *Journal of Food Science*, 71(3), E142-E151.

Ralet, M.C. and Guéguen J. (2001). Foaming properties of potato raw proteins and isolated fractions. *Lebensmittel Wissenschaft und Technologie*, 34, 266-269.

Razumovsky, L. and Damodaran, S. (1999). Surface activity-Compressibility relationship of proteins. *Langmuir*, 15, 1392-1399.

Reed, M.G., Howard, C.V. and Shelton, C.G. (1997). Confocal imaging and second-order stereological analysis of liquid foam. *Journal of Microscopy*, 185, 313-320.

Reinelt, D.A. and Kraynik, A.M. (2000). Simple shearing flow of dry soap foams with tetrahedrally close-packed structure. *Journal of Rheology*, 44, 453-471.

Richardson, G., Langton, M., Faldt, P. and Hermansson, A.M. (2002). Microstructure of alpha-crystalline emulsifiers and their influence on air incorporation in cake batter. *Cereal Chemistry*, 79(4), 546-552.

Rodriguez Patino, J.M., Rodríguez Nino, R. and Alvarez Gomez, J.M. (1997). Interfacial and foaming characteristics of protein-lipid systems. *Food Hydrocolloids*, 11(1), 49-58.

Rouillé, J., Della Valle, G., Devaux, M.F., Marion, D. and Dubreil, L. (2005). French bread loaf volume variations and digital image analysis of crumb grain changes induced by the minor components of wheat flour. *Cereal Chemistry*, 82(1), 20-27.

Rouimi, S., Schorsch, C., Valentini, C. and Vaslin, S. (2005). Foam stability and interfacial properties of milk protein–surfactant systems. *Food Hydrocolloids*, 19, 467-478.

Rouyer, F.R, Cohen-Addad, S. and Höler, R. (2005). Is the yield stress of aqueous foams a well defined quantity? *Colloids and Surfaces A: Physicochemical and Engineering Aspects*, 263, 111-116.

Russ, J. C. (1995). *The Image Processing Handbook*. CRC Press LLC, Boca Raton, Florida, USA.

Russ, J.C. (2005). *Image Analysis of Food Microstructure*. CRC Press LLC, Boca Raton, Florida, USA.

Russo, C. (2000). Food foams. *Industrie Alimentari*, 39(391), 425-443.

Sahi, S.S. and Alava, J.M. (2003). Functionality of emulsifiers in sponge cake production. *Journal of the Science of Food and Agriculture*, 83(14), 1419-1429.

Saint-Jalmes, A. and Durian, D.J. (1999). Vanishing elasticity for wet foams: Equivalence with emulsions and role of polydispersity. *Journal of Rheology*, 43, 1411-1432.

Sarker, D.K., Bertrand, D., Chtioui, Y. and Popineau, Y. (1998). Characterisation of foam properties using image analysis. *Journal of Texture Studies*, 29, 15-42.

Schabenberger, O. and Gotway, C.A. (2005). *Statistical methods for spatial data analysis*. Chapman & Hall/CRC, Boca Raton, Florida, USA.

Schmitt, C., Bovay, C, Rouvet, M., Shojaei-Rami, S., and Kolodziejczyk, E. (2007). Whey protein soluble aggregates from heating with nacl: physicochemical, interfacial, and foaming properties. *Langmuir*, 23, 4155-4166.

Schmitt, C., Palma Da Silva, T., Bovay, C, Rami-Shojaei, S., Frossard, P, Kolodziejczyk, E. and Leser, M.E. (2005). Effect of time on the interfacial and foaming properties of β-lactoglobulin/acacia gum electrostatic complexes and coacervates at pH 4.2. *Langmuir*, 21, 7786-7795.

Schoonman, A., Mayor, G., Dillmann, M.L., Bisperink, C. and Ubbink, J. (2001). The microstructure of foamed maltodextrin/sodium caseinate powders: a comparative study by microscopy and physical techniques. *Food Research International*, 34(10), 913-929.

Serra, J. (1982). *Image Analysis and Mathematical Morphology*. Academia Press, London, UK.

Serra, J. (1986). Introduction to mathematical morphology. *Computer Vision, Graphics, and Image Processing*, 35, 283-305.

Sitohy, M., Chobert, J.M., Popineau, Y. and Haertle, T. (1995). Functional properties of β-lactoglobulin phosphorylated in the presence of different aliphatic amines. *Lait*, 75, 503-512.

Stauffer, C.E. (1965). The measurement of surface tension by the pendant drop technique. *Journal of Physical Chemistry*, 69, 1933-1938.

Torquato, S. (2002). Statistical description of microstructures. *Annual Review of Materials Research*, 32, 77-111.

Tranchant, J.F., Bonté, F., Leroy, S., Nedyalkov, M., Platikanov, D., Javierre, I. and Jean-Benattar, J.J. (2002). Black foam films from aqueous solutions of a mixture of phospholipids and a permeation enhancer. *Journal of Colloid and Interface Science*, 249, 398-404.

Trater, A.M., Alavi, S. and Rizvi, S.S.H. (2005). Use of non-invasive X-ray microtomography for characterizing microstructure of extruded biopolymer foams. *Food Research International*, 38(6), 709-719.

Utsumi, S., Maruyama, N., Satoh, R. and Adachi, M. (2002). Structure-function relationships of soybean proteins revealed by using recombinant systems. *Enzyme and Microbial Technology*, 30, 284-288.

Vischer, N. (2001). Object Image, version 2.07. Available from: http://simon.bio.uva.nl/object-image.html.

Walstra, P. and Smulders, I. (1997). Making emulsions and foams: an overview. In E. Dickinson and B. Bergenståhl (Eds.) *Food Colloids – Proteins, Lipids and Polysaccharides*. Woodhead Publishing Limited, Cambridge, UK, pp. 367-381.

Weaire, D. and Hutzler, S. (1999). *The Physics of Foams*. Clarendon Press, Oxford, UK.

Weaire, D., Fortes, M.A. and Portugal, L. (1994). Stress and strain in liquid and solid foams. *Advances in Physics*, 43(6), 685-738.

Wilde, P.J. (2000). Interfaces: their role in foam and emulsion behaviour. *Current Opinion in Colloid & Interface Science*, 5,176-181.

Xu, S. and Damodaran, S. (1993). Comparative adsorption of native and denatured egg-white, human, and T_4 phage lysozymes at the air/water interface. *Journal of Colloid and Interface Science*, 159, 124-133.

Yu, M.-A. and Damodaran, S. (1991). Kinetics of protein foam destabilization: Evaluation of a method using bovine serum albumin. *Journal of Agricultural and Food Chemistry*, 39, 1555-1562.

Zheng, C.X., Sun, D.W. and Zheng, L.Y. (2006). Recent applications of image texture for evaluation of food qualities - a review. *Trends in Food Science and Technology*, 17(3), 113-128.

Zhu, H. and Damodaran, S. (1994). Heat-induced conformational changes in whey protein isolate and its relation to foaming properties. *Journal of Agricultural and Food Chemistry*, 42, 846-855.

7. NOMENCLATURE

Acronyms

ASM	Angular second moment
BDA	Bayesian discriminant analysis
CDA	canonical discriminant analysis
CJG	Conjugated protein
CLSM	Confocal laser scanning microscopy
CMC	Critical micelle concentrations
CR	Correlation
CT	Contrast
DB	Diminishing bubble
ET	Entropy
G-function	Nearest-neighbor distribution function
GLCM	Gray level co-occurrence matrix
HM	Homogeneity
IDM	Inverse difference moment
ITA	Image texture analysis
K-function	Second-moment distribution function
LM	Light microscopy
MF	Minkowski functional
MRI	Magnetic resonance imaging
OVB	Ovalbumin
SCN	Sodium caseinate
SEM	Scanning electron microscopy
SFS	Sequential forward selection
SOS	Sum of squares
WPI	Whey protein isolate

Notation

a(t)	scaling factor in Eq. 1.20, dimensionless
a	Frumkin-type intermolecular interaction parameter, dimensionless
A	interfacial area in Eq. 1.1, m^2
A	Total area in Eq. 3.2, m^2
A_0	initial film area at the top of the bubble, m^2
A_f	film area at the top of the bubble, m^2
b(t)	scaling factor in Eq. 1.20, dimensionless
b	experimental fitting parameter
b	radius of curvature of the drop/bubble apex in Eq 1.3, m^{-1}
b_i	equilibrium adsorption constant for the protein in state i
c^*	critical protein concentration, mol/L
c	capillary constant in Eq 1.3, m^{-2}
c	protein bulk concentration, mol/L
c_0	initial bulk protein concentration, mol/L
C_d	dynamic capillary number
C_P	crossing point, m
d	distance, pixels
D	protein diffusion coefficient in the bulk, m^2/s
D_{eq}	equivalent bubble diameters, m
D_S	Minkowski fractal dimension, dimensionless
D_{S1}	Textural fractal dimension, dimensionless
D_{S2}	Structural fractal dimension, dimensionless
G^*	complex shear modulus, Pa
g	acceleration of gravity, 9.81 m/s^2.
G’	storage modulus, Pa
G’’	loss modulus, Pa
G_0	elastic modulus, Pa
G_{surf}	surface free energy, J
h	distance, m

h_i	distance of a point i to its nearest neighbor, m
I	indicator function, dimensionless
i	intensity level of a pixel within an image
j	intensity level of a pixel within an image
K	film permeability coefficient, cm/s
l_0	Zero crossing length, m
l_{min}	Euler minimum length, m
m_c	weight of the continuous phase, kg
m_f	weight of the foamed dispersion, kg
n	number of protein states during adsorption, dimensionless
n	total number of point in a pattern, dimensionless
n_e	Total number of edges, dimensionless
n_s	Total number of pixels, dimensionless
n_v	Total number of vertices, dimensionless
P_{atm}	atmospheric pressure, atm
R	bubble radius, m
r	film radius, m
R	ideal gas law constant,
R	normalized function in Eq 4.2, dimensionless
R_0	bubble radius at $t = 0$, m
R_{32}	Sauter mean bubble radius, m
R_t	bubble radius at $t = t$, m
$\bar{R}$	mean bubble radius, m
T	temperature, ºC
t	time, s
t'	dummy integration variable
t_0	arbitrary reference time, s
U	Total perimeter, m
x	Cartesian coordinates, m
z	Cartesian coordinates, m

***Greek* letters**

ϵ'	elastic modulus, N/m
ϵ_0	limiting Gibbs' elasticity, N/m
ϕ	phase angle, rad
$\dot{\varepsilon}$	shear strain rate, 1/s
ϵ	surface dilatational modulus, N/m
ϵ'	viscous modulus, N/m
μ	bulk viscosity, Pa s
μ_{eff}	effective viscosity, Pa s
$\emptyset$	Gas hold-up or volume fraction of the dispersed phase, dimensionless
$\emptyset_c$	critical volume fraction of the dispersed phase, dimensionless
α	dimensionless prefactor in Eq. 1.17
γ	interfacial (surface) tension, N/m
Γ	total protein adsorption in all n states, mg/m^2
γ_0	interfacial (surface) tension of the pure solvent, N/m
ΔP	pressure difference, Pa
$\Delta\rho$	difference between the volumetric masses of two fluids, kg/m^3
ε	shear strain, dimensionless
θ	angle of the tangent to the drop/bubble profile in Eq. 1.3, rad
θ	direction defining the GLCM
λ	bubble relaxation time, s
ξ	empirical parameter on Eq. 1.24
Π	surface pressure, N/m
Π^*	critical surface pressure at c=c^*, N/m
X	Euler characteristic, dimensionless
χ_{max}	maximum Euler characteristic, dimensionless
χ_{min}	minimum Euler characteristic, dimensionless
ω	angular frequency, 1/s
ω	mean molar area defined as the weighted average over all protein states in the interfacial layer, m^2/mol

ω_0	partial molar area of the solvent molecules, m^2/mol
ω_{max}	maximum partial molar area of the protein molecules, m^2/mol
ω_{min}	minimum partial molar area of the protein molecules, m^2/mol
Γ	protein adsorption, mg/m^2
Γ^*	critical protein adsorption, mg/m^2
β	factor in Eq. 1.21, dimensionless
σ	shear stress, Pa
σ_y	yield stress, Pa